The Dissertation Committee for Brian Philip Osborn
certifies that this is the approved version of the following dissertation:

VACUUM ULTRAVIOLET DIRECTED DESIGN, SYNTHESIS AND

DEVELOPMENT OF 157 nm PHOTORESIST MATERIALS

Committee:

_____
C. Grant Willson, Supervisor

_____
Michael J. Krische

_____
Brian L. Pagenkopf

_____
David A. Vanden Bout

_____
Jeffrey D. Byers

VACUUM ULTRAVIOLET DIRECTED DESIGN, SYNTHESIS AND DEVELOPMENT OF 157 nm PHOTORESIST MATERIALS

by

Brian Philip Osborn, B.S., M.S.

Dissertation

Presented to the Faculty of the Graduate School of

the University of Texas at Austin

in Partial Fulfillment

of the Requirements

for the Degree of

Doctor of Philosophy

The University of Texas at Austin
December 2004

Dedicated to my parents Robert and Elia

e

alla mia bella Silvia per tutto.

Acknowledgements

My stay in the Willson research group has been long and entirely enjoyable, and my indebtedness extends to an array of good people. First and foremost, I want to profess my deepest gratefulness to Professor Grant Willson, without whom I would not be here writing this document. He is an outstanding advisor and I will not forget his contributions to my life and career. Thank you.

The work I participated in during the 157 nm project would simply not have been possible without the help of Dr. Ryan Callahan, Charles Chambers, Matthew Pinnow, Dr. Raymond Hung, Takashi Chiba, Dr. Brian Trinque and, last but by no means least, Daniel Sanders of CalTech. Their help in the lab was invaluable and I learned a great deal from each of them. The vacuum UV spectroscopic work was due in large part to the skills of Dr. Colin Brodsky, Dr. Hoang Vi Tran, Dr. Leslie Carpenter, Guen Su Lee and Prof. David Dixon.

The imaging work done at International SEMATECH was made possible by the help and assistance of Dr. Kyle Patterson and Dr. Andrew Jamieson in our group, and Will Conley, Danny Miller, Vicki Graffenberg, Shashikant Patel, Georgia Rich, Mike Rodriguez, Jordan Owens and Tony Vander Heyden of SEMATECH. It was great fun and a remarkable learning experience working with the SEMATECH crew, giving me many lessons I will take with me on my

foray into industry.

I was fortunate enough to work with two talented undergraduates who did outstanding work in the lab, Daniel Hall and Janelle Stickney. It was my good fortune to work with them both.

My years of both undergraduate and graduate work in the Willson group were made possible by Dr. Uzodinma Okoroanyanwu, Dr. Christopher McAdams, Dr. Mark Somervell, Dr. Peter "Tatts" Tattersall, Heather Meiring, William Heath and Stephan Caporale. Best of luck to Jacob Adams, Brian Long and Kristina Winters as they begin to take on the mantle of chemistry in our group. I will fondly remember the banter with Chris Taylor, Dr. Robert "Lithowoman" LeSeur, Jason Meiring, the Burns brothers (Drs. Sean and Ryan), Dr. Scott Grayson, Tim "T-Bone" Michaelson, Eui Kyoon Kim, Frank Palmieri, Elizabeth Collister, Mikey Lin, Kane Jen, Alok Vasudev, Ben Noyes, Dr. Tsutomu Shimokawa, Mikio Yamachika, Shiro Kusumoto and Yukio Nishimura.

Many thanks are also due to Margaret "the Vicar" Rodgers who made the red tape of graduate school less a challenge and more of a (fun) assault course.

MJ, Chaci and Sally—thanks for the friendship and fun, see y'all around.

Finally, I owe much gratitude to Kathleen Sparks for her assistance and congeniality: in long years—kind, dedicated, helpful.

VACUUM ULTRAVIOLET DIRECTED DESIGN, SYNTHESIS AND DEVELOPMENT OF 157 nm PHOTORESIST MATERIALS

Publication No._____

Brian Philip Osborn, Ph.D.

The University of Texas at Austin, 2004

Supervisor: C. Grant Willson

The design of 157 nm materials for photolithography presented many challenges, stemming from the inherently strong absorbance of the majority of organic compounds in the vacuum ultraviolet (V-UV). A spectrophotometer designed to operate in the vacuum was utilized to screen a multitude of materials for high transparency at 157 nm. These hydrogenated monomers served as model compounds for the repeat units in polymers. A variety of fluorinated, hydrogenated norbornanes were found to be transparent for use at 157 nm, and empirical evidence showed that the position and amount of fluorine incorporation mattered significantly in norbornene systems. The best of these are geminally substituted but, unfortunately, geminally disubstituted norbornenes do not polymerize to any significant degree using transition metal addition catalysts such

as palladium or nickel.

A variety of different methods were used to incorporate fluorinated and transparent monomers into polymers. Dinorbornene monomers were used in conjunction with the Grubbs second-generation catalyst to produce polymers using ring-opening metathesis polymerization (ROMP), but these compounds were found to be too strongly absorbing for use at 157 nm. Tricyclononene analogues of the norbornene materials were synthesized, found to be transparent in the V-UV and can be polymerized via addition polymerization. The absorbance of these materials matched the absorbance trends first seen in the gas phase spectra of the monomers, which bolstered the case for screening materials in the vacuum UV first. Vicinal *cis*-*exo*-norbornane diols were also synthesized of these fluorinated, geminally disubstituted norbornenes for use as condensation polymer precursors. Attempts to form polycarbonates and polyethers from these diols proved unsuccessful, because of the propensity for the *cis*-*exo*-norbornane diols to form cyclic carbonates.

The final, optimized photoresist that gave the best results in imaging experiments at 157 nm employed poly(2-(3,3,3-trifluoro-2-trifuoromethyl-2-hydroxypropyl)bicyclo[2.2.1]heptane-5-ene) (PNBHFA) or the Asahi Glass RS001 fluoropolymer in conjunction with a variety of oligomeric dissolution inhibitors. These formulations allowed us to print high resolution, high aspect ratio images at 157 nm. The vacuum ultraviolet spectroscopy, polymer synthesis and imaging of 157 nm materials are presented.

Table of Contents

List of Figures

CHAPTER 1 — Introduction to Photolithography

The Age of the Transistor

Arguably the most important discovery of the 20th century was the transistor, invented in 1947 at Bell Telephone Laboratories. This seemly simple semiconductor-based device, acting as both an electronic switch and as an amplifier, had several advantages over its predecessor, the vacuum tube. These advantages included smaller size, lower power consumption, less heat during use and superior reliability. Although transistors were used in analog systems such as radio and stereo systems, transistors found their ultimate use in the digital computer age.

Transistors were first built into integrated circuits (ICs) in 1959, by Jack Kirby (Texas Instruments) and Robert Noyce (Fairchild Semiconductor). Integrated circuits, coupled with the power of digital logic, enabled the production of the first computer systems using memory and central processing units (CPUs). The transistor gained more ground by virtue of the ability to mass-produce them using silicon wafer substrates, along with the requisite capacitors, resistors, inductors, diodes, etc., that make up a microelectronic device. The technology, engineering and science behind transistor miniaturization and mass production drove the fabrication of increasingly smaller ICs, accelerating the world into the information age at a rapid pace.

By the end of the 20th century, barely fifty years after the transistor's invention, its utility and importance are difficult to rival. Integrated circuits and computer chips have proliferated such that without the transistor there would be no internet, space travel or

cell phones as we know them today. The advent of the transistor has enabled the remarkable communication, networking and computing advances of the past 50 years, and is responsible for the massive proliferation of the multitude of compact and powerful computation devices that are utilized today.

The Miniaturization Race

The remarkable success of the semiconductor industry has been due to a variety of different innovations and breakthroughs, although there is one yardstick that has kept the industry at its rapid pace of improvement in engineering and scientific feats. Moore's Law is the *de facto* standard by which the semiconductor industry measures its own rate of technical progress and economic growth. Gordon Moore, co-founder and former CEO of Intel, Corp., wrote his famous 1965 paper describing his prescient forecast for the semiconductor industry that the fabricated transistor density for integrated devices would double every 18-24 months (Moore 1994). Hidden in this assessment are the other criteria that the industry must also address to find the optimum balance between yield and performance: wafer size increases, defect density decreases and component packaging must be reduced accordingly (Moore 1965).

Moore's Law states that device performance will increase at a predictable but very fast pace, driven in large part by the packing of more and more transistors within a given area (**Figure 1.1**). This has been accomplished by continually shrinking the size of individual transistors, thereby leading the semiconductor companies into a frenzied competition to see who can manufacture devices using the smallest feature sizes. What began with transistor gates being manufactured at size regimes of 1-5 microns in *ca*. 1980

has led to present day gate widths of 60-90 nm. This is an approximately hundred-fold reduction in size in the span of just over 20 years!

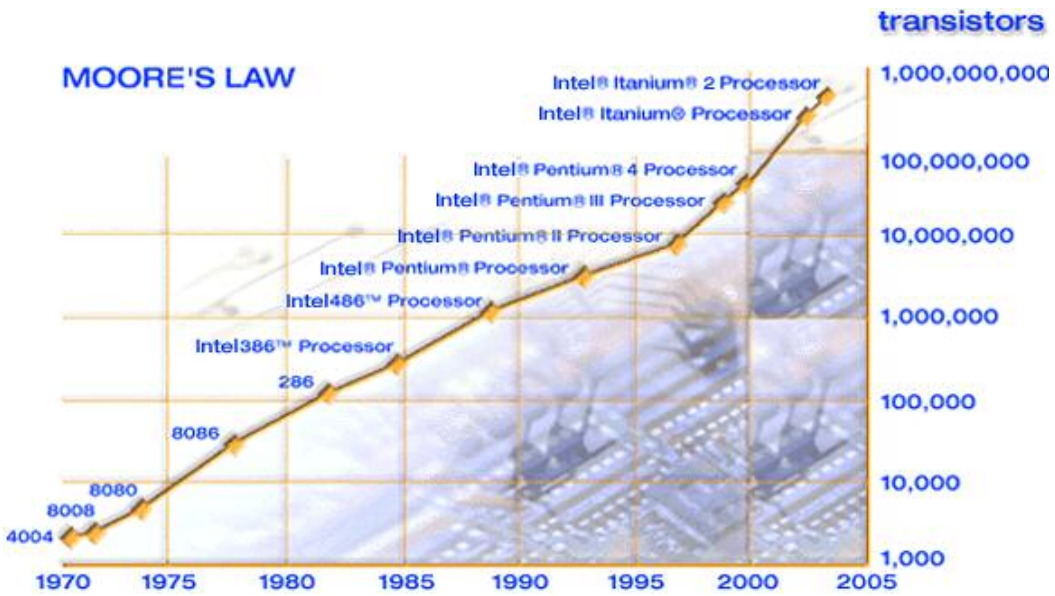

Figure 1.1: Moore's Law as shown through Intel microprocessor development. Note the transistor count increases over time (http://www.intel.com/research/silicon/mooreslaw.htm).

Moore's "law," which originally began as an empirical observation rather than a scientific law, has nevertheless become the metric the semiconductor industry follows with relentless fervor. "Moore's Law" is a critically important standard rather than a law. It has allowed companies to keep a measure of how high their product device performance must be in order to remain competitive. Moore's Law drives the development of novel methods to allow feature size reductions, while trying to keep the ever-increasing costs of device fabrication at a minimum.

It is in this pursuit of continually decreasing features sizes for device components, which leads to an area where chemistry, physics and engineering converge to enable this industry's growth. This area is known as photolithography.

Photolithography

The primary method used to pattern silicon wafer substrates is the multistep process termed *photolithography*. The *photo-* part of the term stems from the fact that the materials used for patterning are light sensitive; *-lithography* (Greek for "stone drawing") is a term that originated from the printing invention of the German, Alois Senefelder in 1798 (Willson 1994). Lithography at its inception consisted of applying a pattern of greasy material to limestone; ink was subsequently rolled over the limestone plate and was attracted and bound to the hydrophobic, greased areas. This produced contrast between areas that absorbed the ink and areas which did not; such that transfer of the ink patterns, via a roller to paper provided a printing process that could reproduce writing and artistic renderings.

Lithography as it is today is practiced much the same, as engineers seek to resolve smaller and smaller device features, accomplished by selectively modifying parts of a silicon substrate while leaving other areas unaffected (**Figure 1.2**). Photolithography uses polymeric resins that undergo a solubility switch upon irradiation. Exposed areas with selective solubilities can either be selectively developed away in the exposed regions or rendered insoluble, depending on the type of material used. This leaves a relief image of the desired pattern that can be transferred into the substrate using a subsequent etching

step. By repeating lithographic imaging several times, a semiconductor device can be fabricated layer by layer. It is in this manner that modern CPUs and memory devices are built in cleanroom manufacturing facilities around the world.

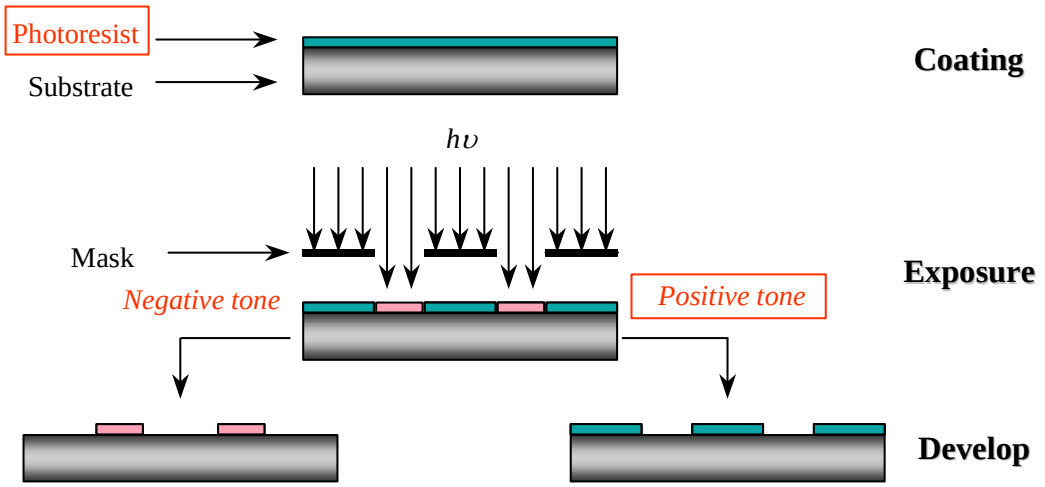

Figure 1.2: The photolithographic process—irradiation initiates photochemistry that changes the photoresist solubility in aqueous base, the method by which the desired image is transferred.

The polymeric material that is responsible for this image transfer is known as photoresist, so named for the dual roles of photosensitivity and etch resistance it plays during lithographic processing. As previously stated, the photoresist, also known simply as "resist," must be photosensitive at the wavelength used for exposure and the following step requires that it be stable to the etching liquid or gas such that selective etching of the silicon substrate or other underlying layer can be accomplished. If the resist material becomes more soluble in basic aqueous developer after exposure, it is known as a positive tone resist. Conversely, if the resist becomes base insoluble after exposure, it is

known as a negative tone resist. The bulk of modern day devices are built using positive tone resists.

A photoresist is a formulation of a polymer resin mixed in with various compounds to provide the material properties required. The polymer itself has several requirements that it must fulfill, such as transparency at the exposure wavelength, photosensitivity or an added photoactive component, high contrast between exposed and unexposed dissolution rates and etch resistance. In chemically amplified resists (CARs), a photosensitive component, known as a photoacid generator (PAG), is added. Such resist systems are called "amplified" due to the catalytic regeneration of acid as the resist undergoes the solubility switching reaction. Other components that may be added are dissolution rate modifiers in the form of molecular, oligomeric and/or polymeric additives. Small amounts of base quenchers, typically in the form of quaternary amines or, sometimes, ionic bases, are also added to limit undesired acid diffusion into unexposed areas of the film after exposure.

The photolithographic process, in principle, sounds simple and straightforward, but its complexity grows with every generation of new materials, exposure wavelength and modifications of the processing steps. Finally, the demands of the processing steps that must occur before and after the lithography (etch, deposition, ion implanting, metallization: see below) further increase the demands on the materials (**Figure 1.3**).

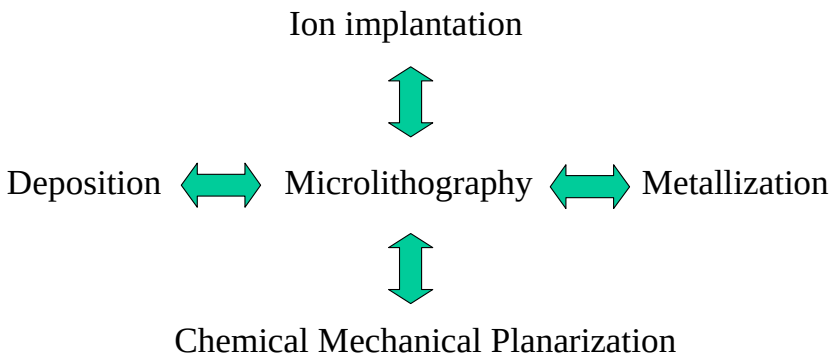

Figure 1.3: Photolithography is central to the many key processes involved in the layer-by-layer construction of a semiconductor device (Hung 2001).

Lithographic Processing

The multitudes of steps that make up one lithography level during device fabrication deserve individual treatment. This analysis will serve to illustrate the multitude of demands that a resist must satisfy, which makes lithography materials science highly challenging. The majority of resists used today are positive tone; therefore the following examples are based on positive tone photoresists.

— Substrate Treatment

The wafer is treated before resist is spin coated. There are a number of different ways to prepare a wafer, but the primary methods involve either treating the bare silicon surface itself or coating the silicon substrate with an underlying organic material that the photoresist is then coated onto in order to control adhesion and reflection. The former method involves silating the surface of the wafer using hexamethyldisilazane ($((CH_3)_3SiSi(CH_3)_3)$ (HMDS), which aids in polymer adhesion by reducing the

hydrophilicity of the silicon substrate. Scattered and reflected light from the silicon substrate can often become a problem, so another substrate treatment process is sometimes used, in which the wafer is spin coated with a specific thickness of polymeric solution that is highly absorbing at the irradiation wavelength. This layer is known as a bottom anti-reflective coating, or BARC. When the bare wafer has either undergone a surface treatment or been coated with an ARC layer, it is ready for resist deposition via spin coating.

— Photoresist Formulation and Spin Coating

Photoresists come pre-mixed from vendors. Typical formulations consist of polymer (90+%), PAG (2-6%), with dissolution inhibitors and base quenchers making up the remaining formulation. The individual resist components can be mixed independently, allowing one to generate a range of formulations, which allows for easy resist formulation modification, making studies of PAG and base loadings, varying the amount of inhibitors, etc., very easy for the experimenter.

All of the components are dissolved in an appropriate casting solvent, one that has high solubility for all the resist components, is easily removed using a bake step and is also safe to handle or use in a cleanroom environment. Spin coating is typically accomplished with solvents such as propylene glycol methyl ether acetate (PGMEA), ethyl lactate, or 2-heptanone. Resists are diluted to between 10-25% in the casting solvent of choice to adjust viscosity and provide the target casting thickness.

The resist solution is then spin coated onto the silicon wafer to a target thickness. This is accomplished by varying the dilution level of the resist solution and the spin

speed at which the wafer is coated. Keeping precise control of these two variables, allows the control of resist film thickness to within nanometer variability across the wafer.

— **Post-application Bake**

The next processing step after spin coating is known as the post-application bake (PAB) or the soft bake. The goal is to drive off the residual casting solvent in the thin film, as well as promoting better resist adhesion to the substrate. The soft bake is done, but well below the temperature at which any thermal degradation or deprotection occurs in resist components, but high enough to solidify the film before exposure. Typical temperatures are 90-130 °C for 30-90 s.

— **Exposure**

After the soft bake, the wafer is taken to an exposure tool known as a stepper, where it is precisely aligned and exposed to different doses and focal lengths. In a positive tone chemically amplified resist this leads to the generation of acid in the irradiated areas of the resist. This is also when the sensitivity of the resist comes into play, as more sensitive resists require lower dosage to generate the requisite amount of acid necessary to induce a solubility change. Lower doses result in shorter exposure times, which increases the overall throughput of the process. The exposure step creates the so-called latent image within the resist film, which is simply the distribution of photoproducts generate upon exposure, as shown below (**Figure 1.4**).

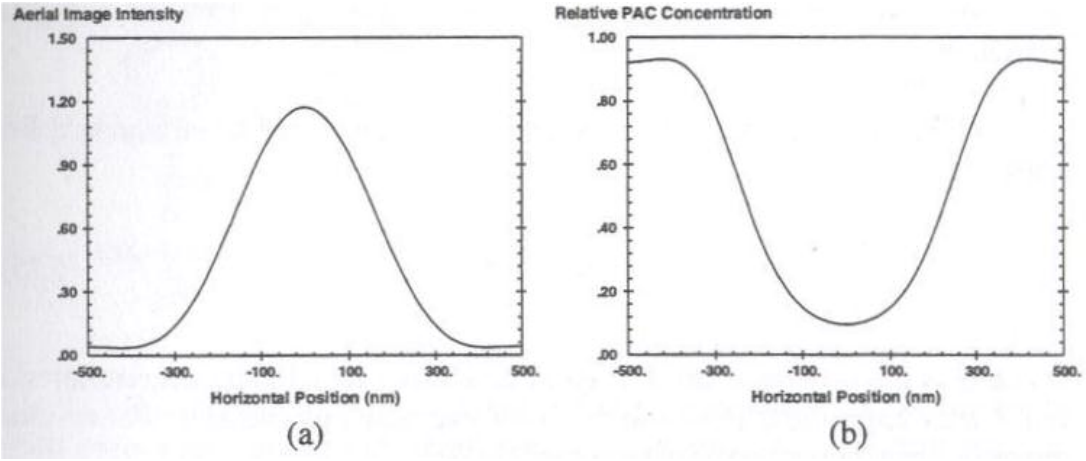

Figure 1.4: The photolysis of the photoactive compound (PAC) relative to the incident light intensity distribution creates the latent image (Mack 1997).

— Post-exposure Bake

Following exposure comes the post-exposure bake (PEB), or hard bake, which drives the acid-catalyzed thermolysis of protecting groups on the resist polymer. This is also the step that induces acid diffusion, which aids in the deprotection reactions that promote dissolution. This same diffusion, however, leads to resist bias and chemical blur, a topic that will be discussed later. The bake temperature and time can heavily influence the extent of intrinsic bias. Finally, the bake temperatures used are also related to the type of protecting groups used in the resist polymer. Low activation energy protecting groups such as acetals are typically baked around 90 °C, whereas *t*-BOC and t-butyl ester containing polymers require bake temperatures between 110-130 °C.

— **Development**

Once thermolysis is complete via the PEB, the wafer is pretreated with a water rinse. Then 0.26 N tetramethylammonium hydroxide (TMAH) is applied to the wafer for 20-60 s. For some resists, surfactants must be added to the developer to achieve wetting, to prevent feature collapse and decrease the roughness of the feature edges. Then the wafer is rinsed and spun at high speeds to remove all of the developer and water. This development step is followed by another hard bake to completely remove all remaining solvents, developer or water, and to prepare for the subsequent etching step.

— **Reactive Ion Etch and Resist Stripping**

During this stage the wafer is placed within a reactive ion etch chamber, which uses plasma to etch away the exposed areas of the silicon substrate. Applying a high electric field over a large volume of a fluorine containing gas at low pressure generates the ions (and, in concert, electrons) that will be used to etch the silicon. The ions are directed in an anisotropic fashion (that is, with a high degree of directionality), by the same applied electric field, towards the lower potential energy surface of the wafer. Ion bombardment results in the breaking of bonds within the silicon substrate, effectively etching through the solid lattice structure to produce nonvolatile products that are pumped away. This is where the etch resistance of the resist polymer becomes of paramount importance.

Once the silicon has been etched to a target depth, the wafer is taken to the final step of the lithography process: resist stripping. This involves the use of more plasma treatment, usually an oxygen-based gas type, to remove the remaining resist layer off of

the substrate while not attacking the silicon, thereby exposing the underlying three-dimensional relief structure now formed on the wafer.

The Resolution "Limit"

There are several different wavelengths of electromagnetic radiation that can be used to image resists. Sources such as electron beams, X-rays, ion beams and ultraviolet radiation have all been used in some way for performing materials fabrication. Electron beam writing is used for mask creation; X-rays have found little use due to high cost of generating power for the X-ray radiation; ion beam has likewise found few uses in device fabrication due to slow writing speeds. Of all the sources discussed here, ultraviolet radiation has found the most widespread and common usage, due to the various lamp and laser sources that are available.

There is a direct relationship between the wavelength of irradiation used and the minimum feature size that can be resolved in a resist. As shorter wavelengths of light are used, the resolving power of the lithographic process increases. In an optical projection system, this relationship is described as the Rayleigh equation (**Eqn. 1.1**) (Mack 1997):

$$R = \frac{k_1 \lambda}{NA} \quad (NA = \mathrm{n} \sin \theta) \qquad (1.1)$$

Equation 1.1: The Rayleigh criterion, which relates resolution, *R*, and wavelength. As wavelength decreases, resolution increases proportionally.

Where R is the resolution of the system; k_1 is referred to as the "k-factor," a dimensionless value intrinsic to each photoresist; *NA* is termed the numerical aperture of the lens system; *n* is the index of refraction of the medium (in most cases, air, $n = 1.00$); and θ is the maximum half of the angle of light that can pass through the lens.

From this relationship, one can see that decreasing the irradiation wavelength will translate into higher resolution. Lithographers have concentrated on modifying resist chemistries to maintain transparency, etch resistance and other constraints with each new generation of imaging technology while adapting the materials for use at even shorter exposure wavelengths.

Optics engineers have strived to create lens systems that have higher NA while maintaining maximum transparency and resistance to degradation during the printing process. The main drawback to larger lens NA is that the depth of focus, or DOF, the depth at which out-of-focus errors begins to degrade the resist feature quality. Unfortunately, DOF is inversely proportional to the square of the NA increase (**Eqn. 1.2**) (Mack 1997).

$$DOF = \frac{k_2 \lambda}{NA^2} \quad (NA = \mathrm{n} \sin \theta) \qquad (1.2)$$

Equation 1.2: Depth of focus (DOF) increases with decreasing numerical aperture, making reductions in the exposure wavelength more attractive for higher resolution.

As lithography technology advances to print ever-smaller features on silicon, the challenge has been finding new materials and systems that maintain the other required resist characteristics while enabling their use with shorter wavelengths of light. The

physical limit for high-resolution resist imaging has yet to reached. There have been several papers published throughout the history of the semiconductor industry that forecasted the end of photolithography, but none have proven true as of yet. Current state-of-the-art technologies are pushing image resolution down to 45 nm and lower, using projection printing. There is little consensus on when and where photolithography will reach its technical or economic limit. It will surely persist for several more years.

Early Photoresist Chemistry

Early photoresists were based on the novolac-diazonaphthoquinone (DNQ) system originally developed by the Kalle Corporation in Germany (Kawabe 1996). This two component resist system benefited from the base solubility characteristics of novolac polymer, a resin that can be dissolved in numerous organic solvents and spin coated to form high quality, glassy films. In its native state, novolac is highly base soluble due to its low pK_a, phenolic functional groups. However, it was found that adding in sufficient amounts of functionalized diazonaphthoquinones, one could effectively halt all dissolution of a novolac film in aqueous developer.

Upon irradiation with ultraviolet light, the diazonaphthoquinone undergoes photolysis to produce a carbene, which undergoes a Wolff rearrangement, forming a ketene and releasing nitrogen gas (Willson 1994). With the addition of water, this ketene then readily forms the final indenecarboxylic acid product, which is highly base soluble. The indenecarboxylic acid and novolac resin blend is base soluble in aqueous developer (**Figure 1.5**). Development of an exposed DNQ resist system results in a positive tone image.

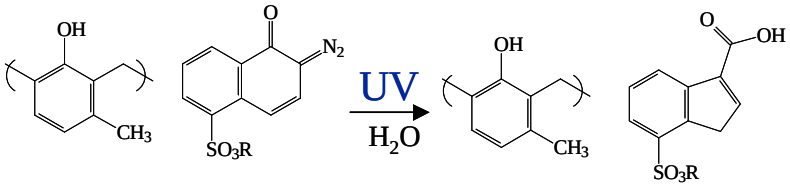

Figure 1.5: Deep UV Novolac-diazonaphthoquinone (DNQ) system and its photochemistry products.

The DNQ photoresist system served the semiconductor industry extremely well for decades. As a resist workhorse, it enabled the fabrication of devices using mercury arc lamps as the emission source. Properly filtered, strong illumination from a mercury arc lamp comes at 365 or 436 nm, wavelengths at which DNQ resists had few rivals for bulk volume device production. This continued for many years at the cutting edge of technology, until it became necessary to move to the next lower wavelength of UV light.

Unfortunately, below 250 nm in the deep-ultraviolet (DUV) region, problems developed for DNQ resist systems. DNQ is too absorbing below 300 nm, resulting in poor conversion of the diazonaphthoquinone inhibitor into its photoproduct and resulting in abysmal imaging performance. The photoefficiency of the Wolff Rearrangement has a quantum yield of approximately 0.1-0.3. This was acceptable for mercury arc lamp imaging, where the imaging dose (power) at the wafer plane was very high. In order to move to lower emission wavelengths, however, excimer lasers were employed in place of arc lamps. While having a much higher output power, the projection optics in excimer exposure systems is such that very little energy arrived at the wafer itself. A new resist system was needed that was highly transparent at the new 248 and 193 nm excimer laser wavelengths, as well having a far higher sensitivity to the incident radiation. The

solution to this materials issue helped propel the semiconductor industry to a highly productive generation of lithographic technology.

Chemically Amplified Resists

The primary obstacle to overcome regarding DNQ-type photoresists is that each absorbed photon only culminates in, at best, one photoevent, *i.e.*, the initiation of the Wolff Rearrangement. In order to create a more sensitive photoresist, it was necessary to find a way to build a catalytic solubility change into the polymer resin. One way in which this was accomplished (Ito 1982; Frechet 1983; Willson 1986), was by incorporating an acid labile protecting group, *tert*-butyloxycarbonyl, or *t*-BOC, onto poly(*p*-hydroxystyrene) (PHS). In this case, the presence of acid deprotects the *t*-BOC group, releasing the volatile by-products isobutylene and carbon dioxide, as well as regenerating acid after reaction completion. This regenerated acid can then proceed to catalyze yet another deprotection reaction, and so on, until some critical fraction of the total sites on the polymer have been deprotected, at which point the polymer chain is now base soluble (**Figure 1.6**).

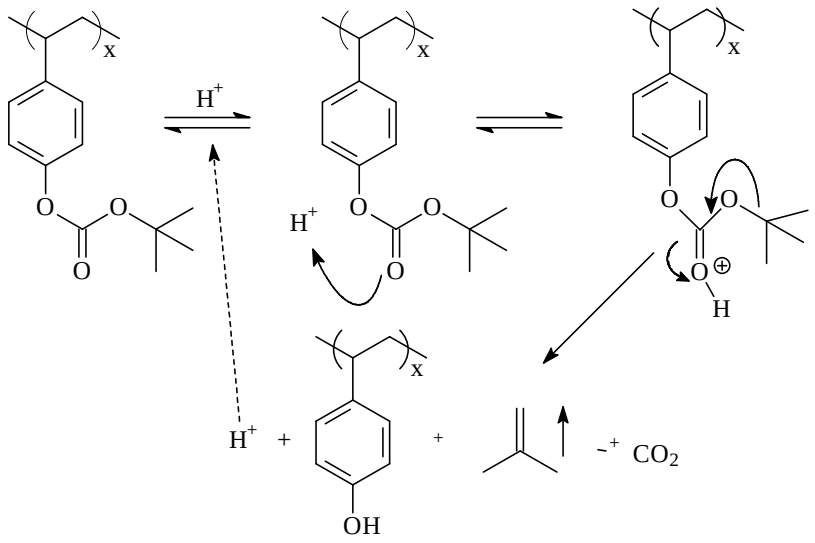

Figure 1.6: Chemically amplified resist chemistry—the catalytic acid deprotection mechanism in *t*-BOC protected PHS makes resists like these more photosensitive than DNQ-type counterparts.

The major benefit of the *t*-BOC-protected PHS system is its high transparency at 248 nm, thus making it a prime candidate for a DUV resist. The acid source is typically from a sulfonium or iodonium salt, which generates the conjugate acid of the anion upon exposure. This is usually a "super" acidic species such as perfluorosulfonic acid (Crivello 1980). Finally, as the deprotection is catalytic in nature, the sensitivity of this type of resist system is much higher than that of the DNQ-type systems.

Chemically amplified resist (CAR) systems have found great use at both 248 and 193 nm exposure technology. The former had great use with systems similar to the *t*-BOC PHS described above, but at 193 nm this system was again too opaque for the shorter wavelength (Allen 1997). The absorbance solution was found in combinations of acrylate and norbornene polymer systems, with protected carboxylic acid functionalities

instead of the phenolic groups of the DNQ and PHS systems. Again at 193 nm, chemically amplified resist systems provided the framework for producing transparent, high sensitivity, etch resistant and high-resolution resist systems for DUV technologies. To date, 248 and 193 nm CARs continue to be used in the fabrication of modern, cutting edge technology semiconductor devices. As those devices continue to increase in transistor density and decrease in feature sizes, the industry was looking ahead for next generation materials in yet another shorter wavelength regime.

Designing Photoresists for 157 nm Lithography

The focus of this thesis is the development of materials for use with the next generation of imaging technology—157 nm irradiation. As seen in previous emission source shifts, resist materials need to change to meet transparency and sensitivity demands, while still meeting the wide range of material requirements for use as a photoresist. Recall the primary requirements for an acceptable resist polymer: transparency, sensitivity at wavelength of irradiation, high dissolution rate contrast between exposed and dark regions of the resist and sufficient etch resistance.

The most daunting aspect of creating materials for use at such a low emission wavelength is the fact that a great many of materials are strongly absorbing at 157 nm. This includes such compounds as oxygen, water and carbon dioxide. Even simple polymers such as polyethylene are opaque.

Kunz, *et al* surveyed readily available materials, and reported the absorbance of a series of compounds in the vacuum ultraviolet (V-UV) (Kunz 199). Out of the litany of compounds surveyed, two classes of materials were found that had potential for use at

157 nm: fluoropolymers and silicon-containing polymers, such as siloxanes and silsequioxanes. This thesis project investigates the potential use of fluoropolymers at 157 nm.

To quickly and efficiently design a transparent 157 nm polymer, the minimum required properties for the photoresist were divided into four modules (**Figure 1.7**): 1) the polymer backbone, which tethers functionalized repeat units and provides the requisite mechanical properties, 2) an etch resistant unit for any subsequent wet or dry transfer processes, 3) an acidic group, which provides solubility in standard developers, such as tetramethylammonium hydroxide (TMAH) and 4) the acid-labile protecting group, which controls overall polymer solubility and wettability. All four modules must be as transparent as possible at 157 nm so that complete pattern transfer can occur (**Figure 1.8**) (Hung 2001).

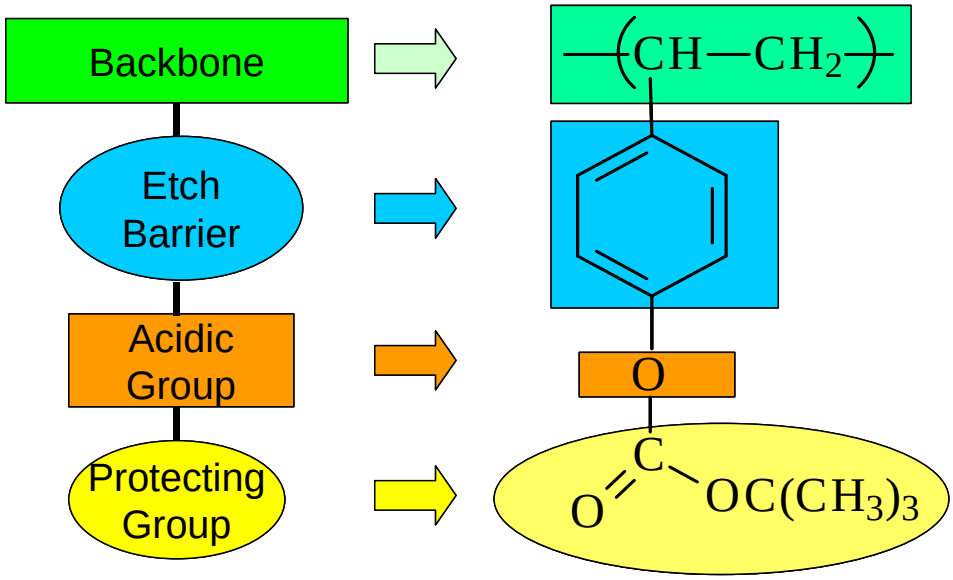

Figure 1.7: The modular approach to designing a 157 nm photoresist, using *t*-BOC protected poly(hydroxystyrene) as an example of a common commercial resist polymer.

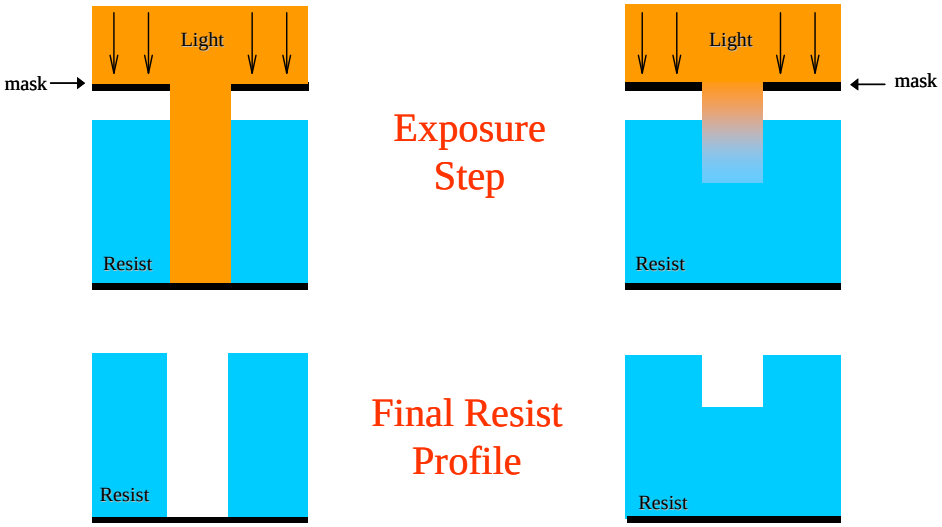

Figure 1.8: Resists must be as transparent as possible for complete photochemistry to occur down to the substrate surface; transparency will be a constant effort for synthesizing 157 nm materials.

The first challenge was to find materials transparent in this wavelength regime by screening potential monomer candidate materials using a vacuum UV spectrophotometer. The means were then sought to incorporate compounds that showed high transparency at 157 nm into a polymer system. Once polymers were synthesized, they were imaged at 248 nm using a simple contact printing experimental setup to ensure that the photochemistry and solubility switching in the resist system worked. The materials were then imaged on a prototype 157 nm Microstepper exposure system at SEMATECH, Intl.

Several polymer systems emerged from this approach and were successfully imaged, although the lack of transparent materials at 157 nm would continue to be an issue that plagued the project. However, the approach of systemically breaking the photoresist into components (Hung 2001) and then screening candidate materials through

the V-UV spectrophotometer would ultimately be borne out as an effective, rapid and efficient process for focusing resist research at 157 nm.

Modern Challenges for Semiconductor Device Fabrication

Today's semiconductor industry faces the ever-present challenge of making processor and memory devices smaller, faster and cheaper (both the consumer and the device maker, as well). Manufacturers have considered 157 nm lithography as an eventual successor to the current, state-of-the-art 193 nm lithography that produces the most technologically advanced devices today.

There is also consideration for more "radical" changes to the conventional photolithographic process that would have been considered impractical or unrealistic just a few years ago. There is a movement to use immersion lithography for future generations of device fabrication. Immersion lithography uses a liquid layer, in this case water, between the final lens element of the exposure system and the wafer itself. Water has a higher index of refraction than air (1.4 versus 1.00, respectively), and can increase the depth of focus for the resist and exposure system.

There are also movements to return to contact printing instead of proximity projection lithography as described here (**Figure 1.9**). Such imprinting techniques are hardly new in fact; they existed well before the advent of optical projection systems, but had several drawbacks that made them unattractive in lieu of today's exposure systems at that time. However, recent advances have made modernized imprint systems attractive once again. There is also a strong interest in some areas of the industry to the use of extreme ultraviolet (EUV) light to perform advanced lithography. EUV sources have an

emission wavelength of 13.5 nm, making them highly attractive for high resolution imaging, although the throughput of a EUV system is currently low relative to UV systems and the cost is very high.

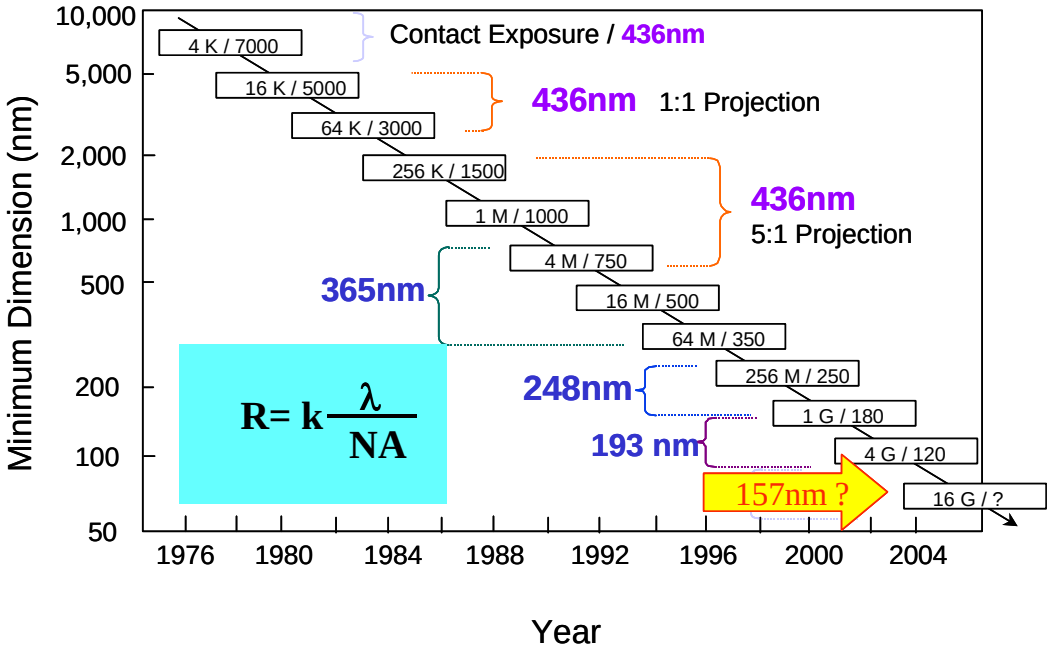

Figure 1.9: Changing photolithography systems in order to produce smaller printed features.

Finally, chemically amplified resists themselves, a mainstay of the semiconductor industry for decades now, are reaching their physical limit. It has been found (Stewart 2000, Schmid 2002) that the use of sulfonium or iodonium salts as the photoacid generator (PAG) component in resists results in an intrinsic "blur" or bias when printing high-resolution images. The diffusion of these PAGs during the post-exposure bake (PEB) causes deviations in the width of printed features and limits the ultimate resolution of these types of resists. There is also an inordinately large amount of so-called line edge

roughness (LER) inherent to 193 nm resists (to a degree not seen in 248 nm CARs) that is making imaging even more difficult for the most critical dimensions.

However, wherever there is difficulty and challenge, there lies opportunity, and the possibility of new breakthroughs in science and engineering. This is the state of the semiconductor industry—not so different from when Gordon Moore made his prescient forecast for the growth of device fabrication: rife with challenges, but also replete with researchers and technologists eager and willing to overcome those issues. So the never-ending quest to print smaller features to make faster and cheaper technology continues, as one will see in the discussion of 157 nm research and development here.

Dissertation Structure

Screening of materials was an absolute necessity considering the many possible materials that could be transparent enough for 157 nm imaging experiments. Chapter 2 details this process of rigorously purifying fluorinated compounds typically hydrogenated norbornanes that serve as models for the repeat units in possible polymers. Those compounds that demonstrated high transparency at 157 nm were used as monomers, although some were did not polymerize using conventional metal addition catalysts. Chapters 3, 4 and 5 describe the use of different monomer structures (tricyclononenes, dinorbornenes) and polymerization techniques (ROMP, condensation) as methods to incorporate those materials unable to be polymerized with addition initiators. Finally, the process development for 157 nm photoresist materials is described in Chapter 6, in an effort to find the most transparent combination of polymer, dissolution inhibitor(s) and

photoacid generator (PAG). This culminates in a final set of imaging experiments to print high resolution, high aspect ratio features using 157 nm lithography.

CHAPTER 2 — Vacuum Ultraviolet Spectroscopy of 157 nm Materials

Materials Challenge for 157 nm Photoresists

Materials development for 157 nm photoresists is challenging. The fundamental problem is that the majority of organic compounds, including simple hydrocarbons have very strong absorbance at 157 nm. This problem is magnified by the fact that many of the components of air such as O_2, CO_2 and H_2O are also highly absorbing at 157 nm. Even simple polymers such as polyethylene also have a strong absorbance (Patterson 2000). Thus, to evaluate the transparency of potential 157 nm materials, a V-UV spectrophotometer was modified and adapted to perform gas phase measurements and a series of model compounds was studied in an attempt to identify the structural elements that could be incorporated into monomers. These monomers would provide polymers that are sufficiently transparent at 157 nm to be considered for resist materials design.

Typical photoresists have an absorbance of approximately 0.4-0.7 μm^{-1} at their wavelength of irradiation (365 nm, 248 nm and 193 nm). The goal of the 157 nm project was similar: finding resist materials that would yield similarly low absorbance at this short wavelength, in this case absorbance at least below 1.0 μm^{-1}. The polymer makes up the majority of a typical photoresist formulation and so focus began on finding monomeric materials transparent at 157 nm.

Early research showed that the majority of typical photoresist polymers have strong absorbance at 157 nm (Kunz 1999). These polymers include polynorbornene, poly(methyl methacrylate) and polystyrene. The only promising platforms were

hydrogen silsesquioxane and fluorinated hydrocarbons, such as poly(tetrafluoroethylene) (Teflon). This preliminary information inspired exploration of the impact of fluorine incorporation on the V-UV absorbance of a variety of different monomers.

Through use of the V-UV tool, it was found that selective fluorination of norbornanes provided significantly reduced absorbance at 157 nm (Trinque 2003). Due to their utility in resist design, a wide range of fluorinated bicyclo[2.2.1]heptane monomers were synthesized and evaluated for their transparency at 157 nm. The norbornene monomers were then hydrogenated to simulate the repeat units in the intended polymer systems. In addition, various other compounds were measured and some were found to be surprisingly transparent at 157 nm, including the synthetically useful tricyclononanes as well as certain sulfur-containing compounds.

In conjunction with this experimental work on novel compounds, collaboration began with Pacific Northwest National Laboratories, and now with the University of Alabama, to do TD-DFT calculations of model compounds. It was hoped that by correlating the experimental data to the DFT results, that the calculations, by nature of their speed versus synthesis, characterization and spectroscopy, would accelerate progress in materials development for 157 nm. Therefore, several model compounds and sets of materials were compared to DFT calculated spectra, and found to not only correlate, but also follow similar trends as those seen in the absorbance data collected from the V-UV tool.

The final link necessary to make both V-UV spectroscopy and DFT calculations invaluable would be to see how the gas phase spectra of monomers compared to

polymers made from those same compounds. This type of comparison between gas phase monomeric material and the corresponding polymer is not without precedent. It was shown (Partridge 1966) that the gas phase absorbance of *n*-alkanes quickly approached that of thin film polyethylene (**Figure 2.1**).

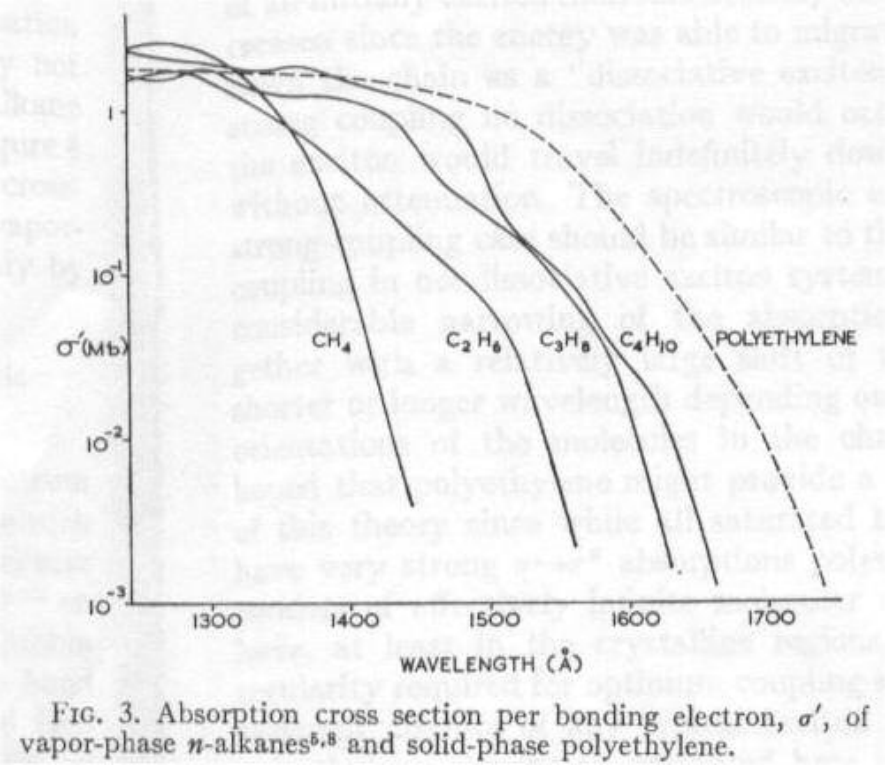

FIG. 3. Absorption cross section per bonding electron, σ', of vapor-phase *n*-alkanes[5,8] and solid-phase polyethylene.

Figure 2.1: Early studies of the correlation between gas phase and polymer absorbance in the V-UV; the spectrum for butane strongly resembles that of polyethylene, an "infinite-length" *n*-alkane.

In fact, through study of the series: methane, ethane, propane and butane, it is clear that the vapor phase and the polyethylene thin film spectra are very similar in form. The blue shifting differential between butane and polyethylene is in fact relatively minor, and the trend is clear that polyethylene does in fact resemble what could be expected of

an “infinite-length” *n*-alkane. This correlation strengthened our rationale for using the V-UV spectrometer as a monomer-screening tool.

Polymers made from transparent, fluorinated monomers were examined for absorbance when cast as a thin film on a silicon substrate using a technique known as variable angle scattering ellipsometry, or VASE. This polymer absorbance data was compared to that of the analogous precursor monomer gas phase spectra. Many of the resulting polymers displayed the same trends of absorbance as their representative monomers, enabling a well-defined methodology for screening potential 157 nm monomer candidates.

Once the V-UV analysis process provided a suitable monomer candidate, the monomer was incorporated into a polymer, cast as a thin film on a silicon wafer and then measured for absorbance using the variable angle scattering ellipsometer (VASE) technique. The absorbance trends of the monomeric materials correlated very well with the measured absorbances of the corresponding polymers. This strong correlation between saturated monomer absorbance and the corresponding polymer transparency provided confidence in the V-UV monomer screening process as a viable tool for polymer material development.

Rationale for 157 nm V-UV Spectrophotometer Use

We chose to use gas phase spectroscopy of model compounds to screen for potential monomers because it is possible to acquire very accurate measurements in this way. The purity of the compounds can be obtained by standard analytical methods and

the spectrometer can be calibrated with standards. Measuring polymers is more difficult, as small amounts of residual casting solvent or impurities can lead to an incorrect measurement of the absorbance of that structure. The absorbance coefficients for some organics (and polymer endgroups) are so high that very miniscule amounts of these substances in a sample could lead to dismissal of polymers that had good potential usage.

Fluorinated Benzenes and Phenols

Among the first set of compounds investigated were fluorinated benzenes and phenols. Aromatic compounds are a mainstay in the design of photoresist polymers that are used in 365 nm and 248 nm lithography. However, aromatic compounds are too absorbing for use at 193 nm (Willson 1999). Fluorinated aromatic compounds have been proposed for use at 157 nm (Bae 2002). The spectral data (**Figure 2.2**) from this survey indicates that increasing amounts of fluorine incorporation affect the molecules absorbance at 157 nm. Unfortunately, perfluorination of the benzene ring increases the monomer's absorbance. Benzene has been measured many times and is used in this study as a standard to ensure that the spectrophotometer is calibrated.

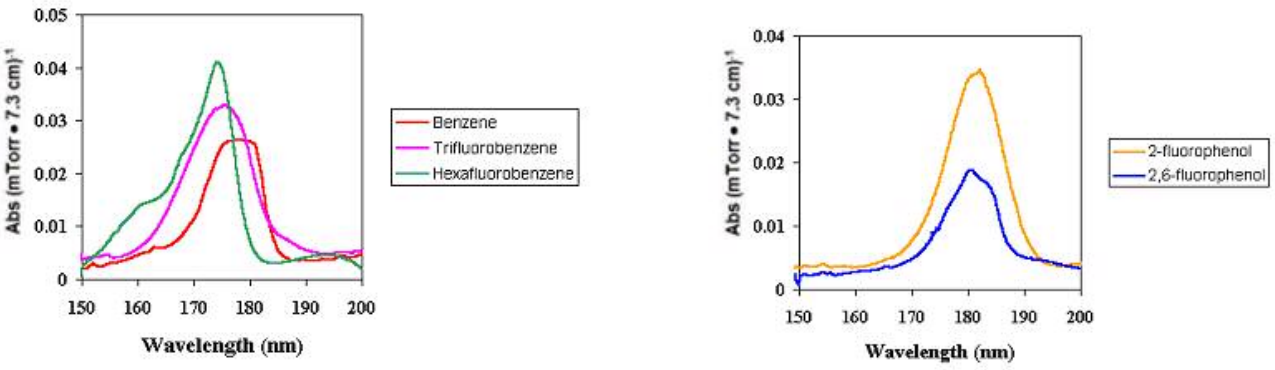

Figure 2.2: Fluorination and the effect on benzene and phenol at low wavelengths.

Fluorinated Esters as Representative Acrylates

One of the first resist systems examined for 157 nm uses was acrylates. Polyacrylates find heavy use in the semiconductor industry, particularly at 193 nm. Unfortunately, acrylate-based polymers are also strongly absorbing in the vacuum UV. The spectra of several fluorinated esters were examined in the gas phase to see if there was an impact on absorbance; fortunately, there was a strong impact of fluorination on the esters shown below (**Figure 2.3**). Trifluoroethyl trifluropropionate is far more transparent than its hydrocarbon analogue, and this inspired designs for fluorinated acrylates to polymerize and act as base photoresist resins at 157 nm.

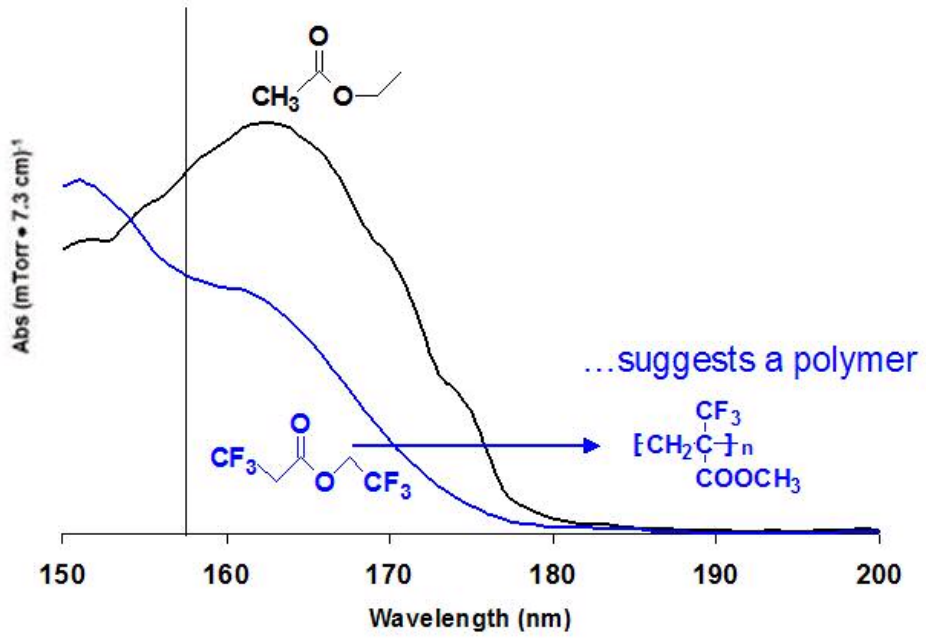

Figure 2.3: The absorbance of fluorinated esters suggested fluorinated acrylate polymers for 157 nm.

Fluorinated Norbornanes

Early work on the design of 157 nm resists identified hexafluoroisopropanol and/or α-trifluoromethylcarboxylic acid as viable acidic groups. The protecting group could be an acetal, *tert*-butoxycarbonyloxy (*t*-BOC), or *tert*-butyl group (Chiba 2000). Early studies for the development 193 nm photoresists found that the bicyclo[2.2.1]heptane system provides good etch resistance and 193 nm transparency. However, norbornane-based materials are too opaque for use at 157 nm (Kunz 1999a, Kunz 1999b). The most promising materials were either fluorinated aliphatics, or siloxanes. Initial focus for 157 nm materials development was therefore on the synthesis of various partially fluorinated bicyclo[2.2.1]heptane monomers, in hope that we could render the alicyclics transparent without perfluorination.

A systematic replacement of hydrogen atoms with fluorine was carried out to gain a better understanding of the effect that fluorine substitution has on the absorbance of the norbornane at 157 nm. Difluoro-substitution at the 2 and 7 positions (**1** and **2**, respectively, **Figure 2.4**) of norbornane provided spectroscopic model compounds. The V-UV absorbance of 2-fluoro- (**3**) and 7-fluoronorbornane (**4**), was previously reported.[4] This study demonstrated that V-UV absorbance depends strongly on both the number and position of the fluorine substituent(s) on the norbornane ring. As seen in **Figure 2.4**, disubstitution of hydrogen with fluorine gives better transparency at 157 nm than monofluorosubstitution. The VUV spectra also show that geminal fluorine substitution on the two-carbon bridge, rather than the single-carbon bridge, is the more effective substitution pattern. This information led to the conclusion that sufficient transparency at

157 nm can be achieved by synthesizing monomers with geminal fluorination at the 2-carbon bridge of norbornane.

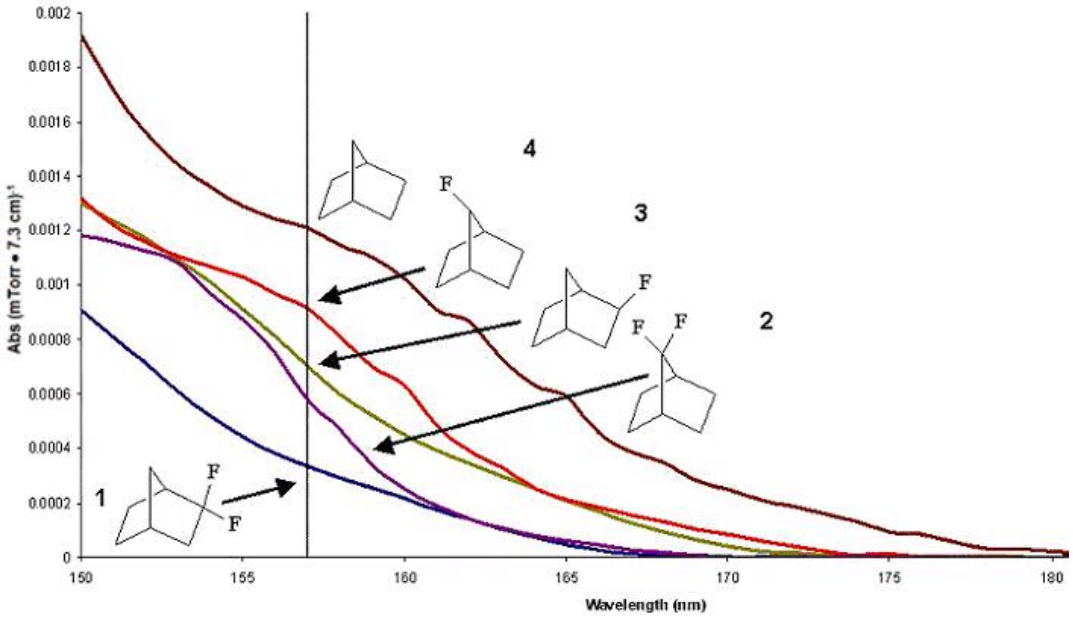

Figure 2.4: Mono- and difluoronorbornanes reveal that amount and position of fluorine has a direct impact on absorbance.

Functionalized Fluoronorbornanes

The next step required to design a monomer for use in a 157 nm photoresist was to functionalize the norbornane skeleton with the acidic group. One of the first monomers tested at 157 nm was bicyclo[2.2.1]heptane-2-(1,1,1-trifluoro-2-trifluoromethylpropan-2-ol) (NBHFA), which, while only monosubstituted, has surprising transparency in the gas phase (**Figure 2.5**), possesses the required acidic group and has the potential for providing etch resistance in the corresponding polymer.

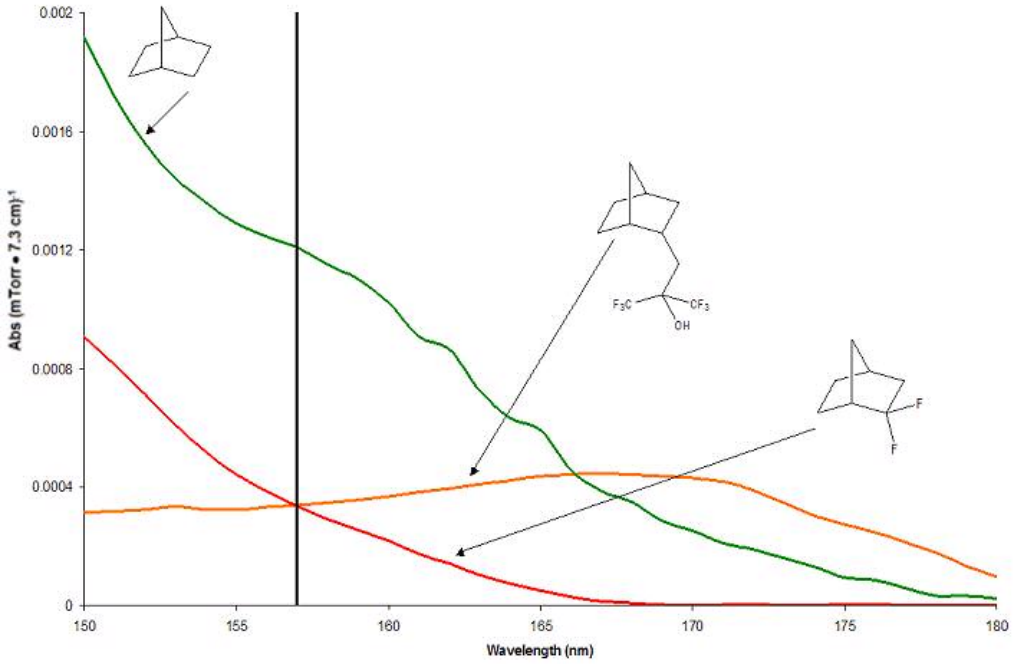

Figure 2.5: NBHFA shows surprisingly high transparency at 157 nm even with functionalization.

The immediate question was what impact carbonyl-containing protecting groups, such as *t*-BOC, have on the transparency of NBHFA. Therefore, the acetal and *t*-BOC protected versions of the model compound 1,1,1,3,3,3-hexafluoro-2-methyl-2-propanol (HMP) (**Figure 2.6**) were synthesized. There is an increase in absorbance with the incorporation of the *t*-BOC group, but the increase is not as significant as we expected when compared to an acetal-protecting group.

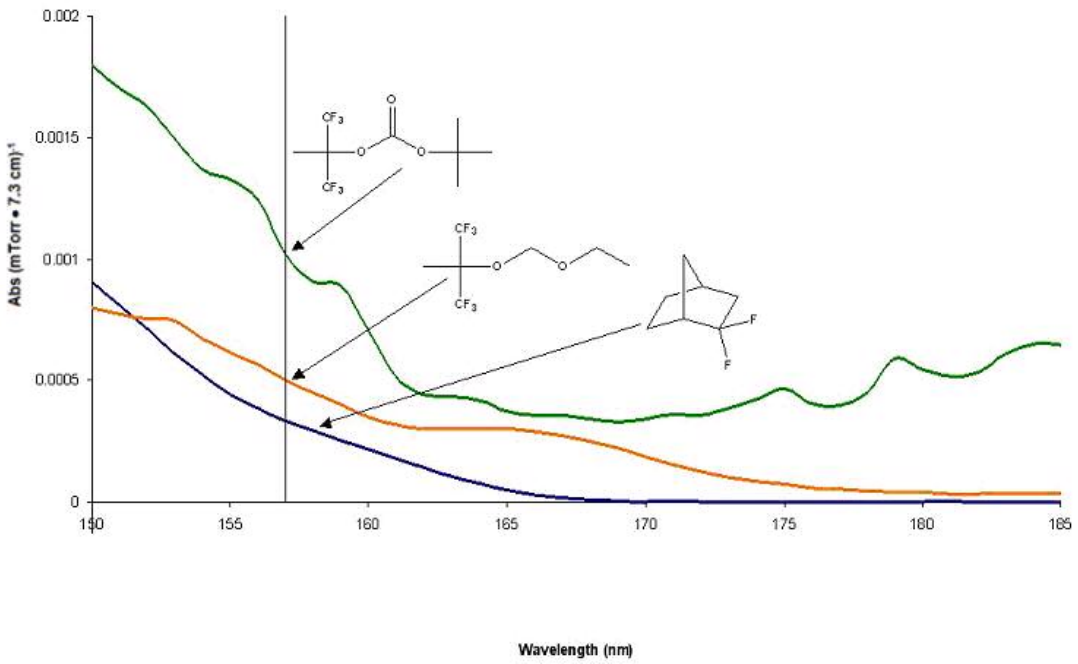

Figure 2.6: The absorbance impact of protecting groups at 157 nm.

Another interesting and highly transparent monomeric material at 157 nm is 2,2-difluoro-3-trifluoromethylnorbornen-3-ol (**Figure 2.7**). This heavily fluorinated norborneol has a transparency comparable to that of 2,2-difluoronorbornane and is soluble in standard 0.26 N TMAH developer. The corresponding norbornene does not readily undergo metal catalyzed addition polymerization but other means of incorporating this promising monomer into a polymer are being studied.

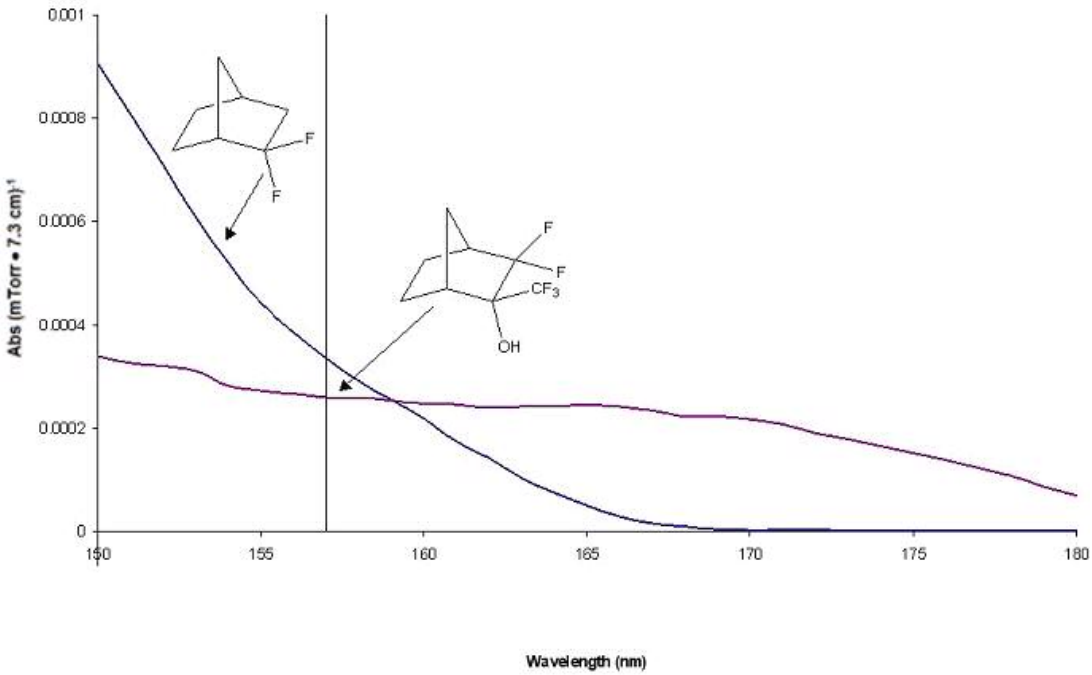

Figure 2.7: The highly fluorinated norbornane shows transparency higher than that of 2,2-difluoronorbornane.

In particular, our group has recently synthesized 7,7-diflouro-bicyclo[2.2.1]hept-5-ene-2-(1,1,1-trifluoro-2-trifluoromethylpropan-2-ol) and 2,2-diflouro-bicyclo[2.2.1]hept-5-ene-2-(1,1,1-trifluoro-2-trifluoromethylpropan-2-ol) (**Figure 2.8**). It was envisaged that a combination of fluorination at the 2 and 7 positions would lead to a more transparent molecule than NBHFA. Both compounds proved difficult to synthesize and attempts to polymerize either monomer via transition metal catalysis have been unsuccessful.

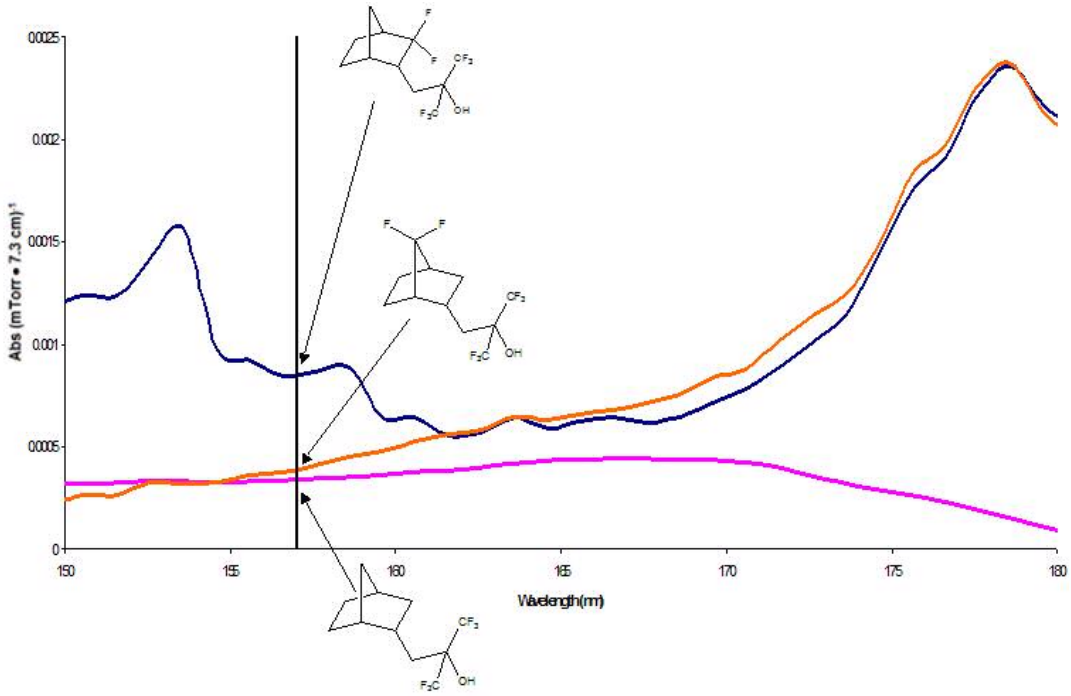

Figure 2.8: Difluoronorbornane hexafluoroisoproponal compounds and their spectra in the V-UV.

Work directed towards identifying 157 nm monomers led to the synthesis of a family of fluorinated and functionalized norbornanes that were found to be highly transparent. Several promising esters, norborneols and other fluoronorbornanes were identified in the screening (**Figure 2.9**). However, the materials that have the aforementioned geminal substitution pattern are poor substrates for addition polymerization (Hung 2001). As previously reported, the inability of geminally-substituted norbornenes to polymerize via transition metal catalysis limited the usefulness of several potential fluorinated norbornanes (Tran 2002).

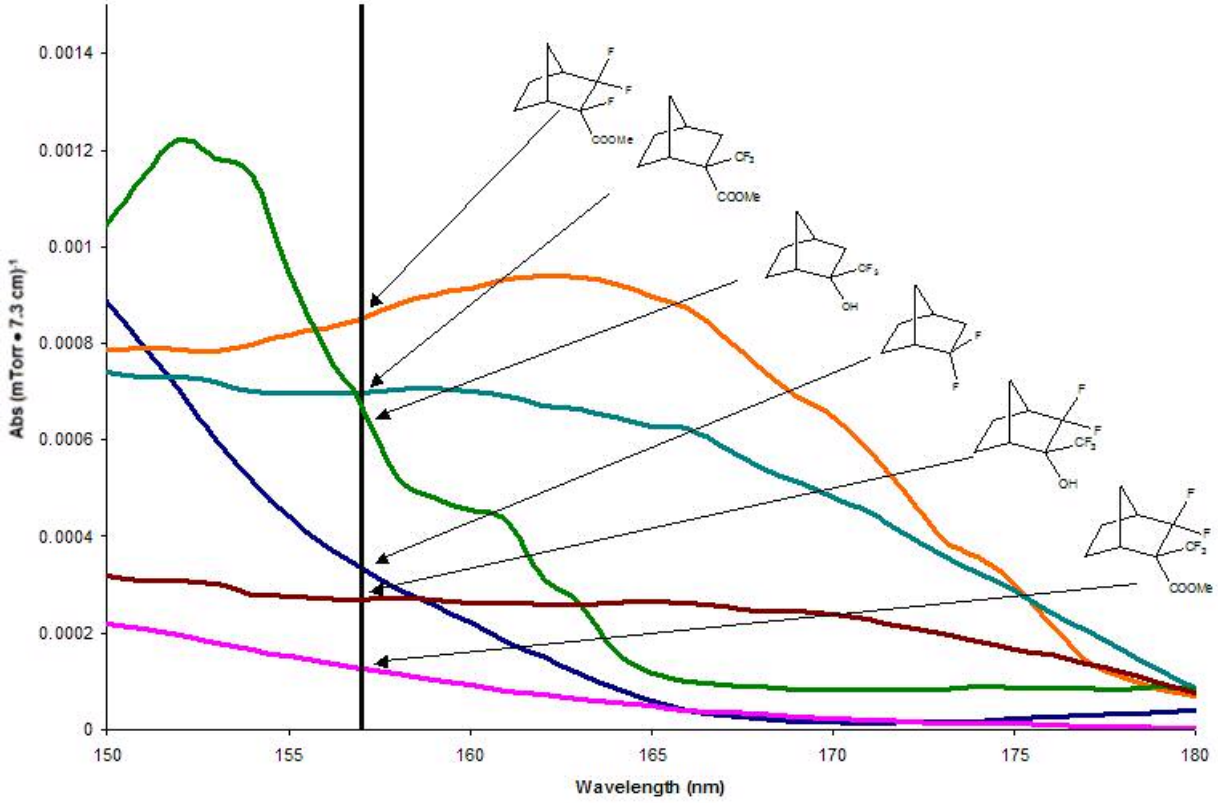

Figure 2.9: Various geminally substituted, fluoronorbornanes show high transparency at 157nm; unfortunately, geminal substitution prevented polymerizaztion via addition catalysts.

Tricyclononane and Oxetane Structures

Tricyclononanes (TCN) were synthesized in order to produce monomers that can be polymerized via nickel and palladium metal addition catalysts. The synthesis and imaging results from TCN polymers have been previously reported (Sanders 2003). The hydrogenated monomer spectra are reported here. The nonfluorinated, trifluorinated and pentafluorinated TCN methyl esters showed the same trend upon increased fluorine concentration as the analogous bicycloheptanes—higher transparencies at 157 nm upon geminal substitution (**Figure 2.10**).

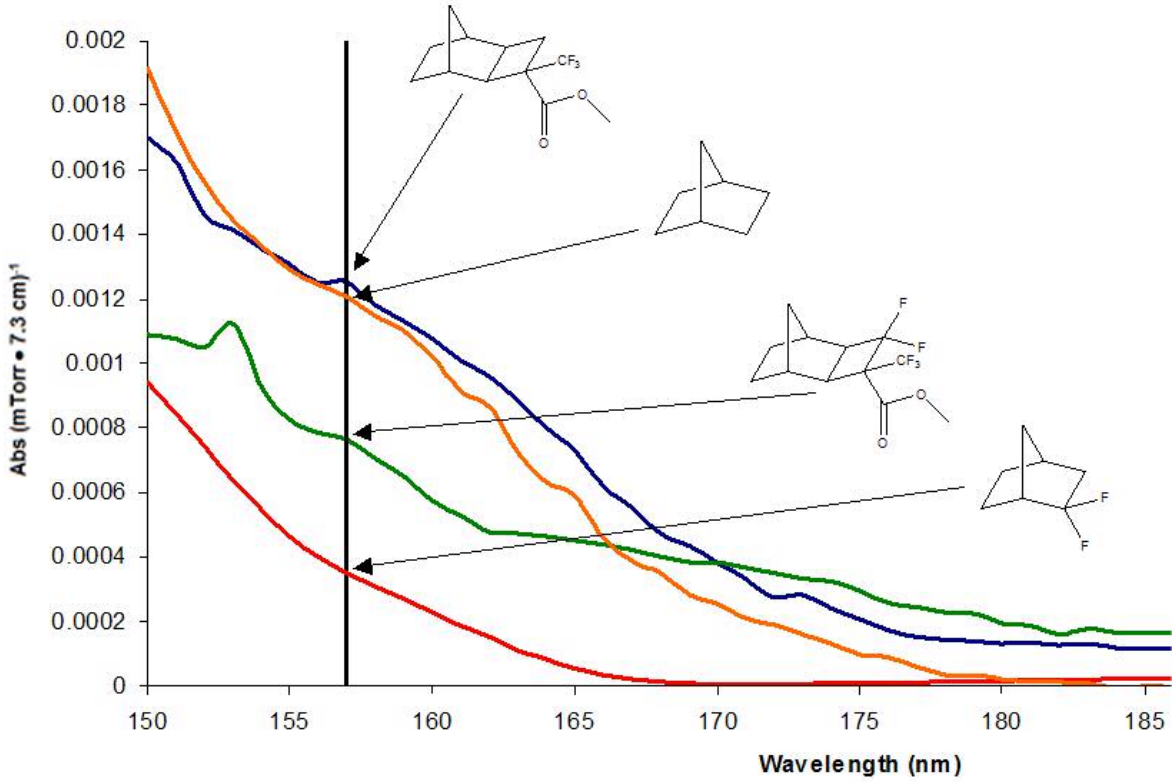

Figure 2.10: Tricyclononane-based monomers exhibit the effect of increased fluorination for higher transparency at 157 nm.

Another class of TCN-type compounds that was studied incorporates an oxetane ring. The oxetane-containing molecule has higher transparency than the TCN analogues (**Figure 2.11)**. This observation is leading to the development of new sets of copolymers based on this compound, for use as a possible 157 nm "mass persistent" photoresist (Pinnow 2002). Synthesis of copolymers of the oxetane was driven by the highly promising gas phase data. Homopolymerization of the oxetane has yielded polymer with, at best, absorbance of 2.3 μm^{-1} at 157 nm.

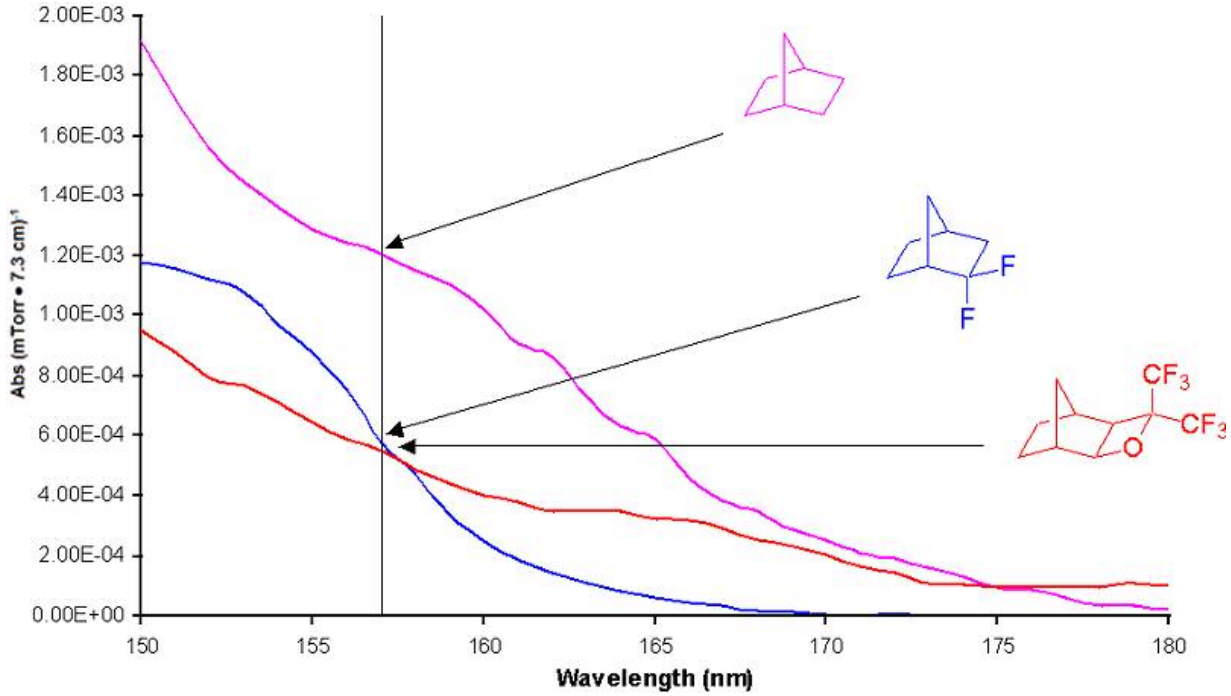

Figure 2.11: The oxetane structure exhibits a high transparency in addition to its ring-opening under acidic conditions, making this an ideal mass persistent 157 nm material.

Silicon-based Compounds

The preliminary V-UV thin film absorbance data from Kunz, *et al.* (1999) suggested that silicon-containing materials, in particular hydrogen silsesquioxane (HSQ), could be as transparent as fluorocarbon-based compounds. Our group has done a great deal of work in this area, and is now performing a systematic survey of silicon-based materials for V-UV photoresists (Tran 2002). An investigation of the effect carbon and fluorine content has on the absorbance, and other properties, of silicon-containing materials were carried out. These results were compared with those of the fluoronorbornanes (**Figure 2.12**).

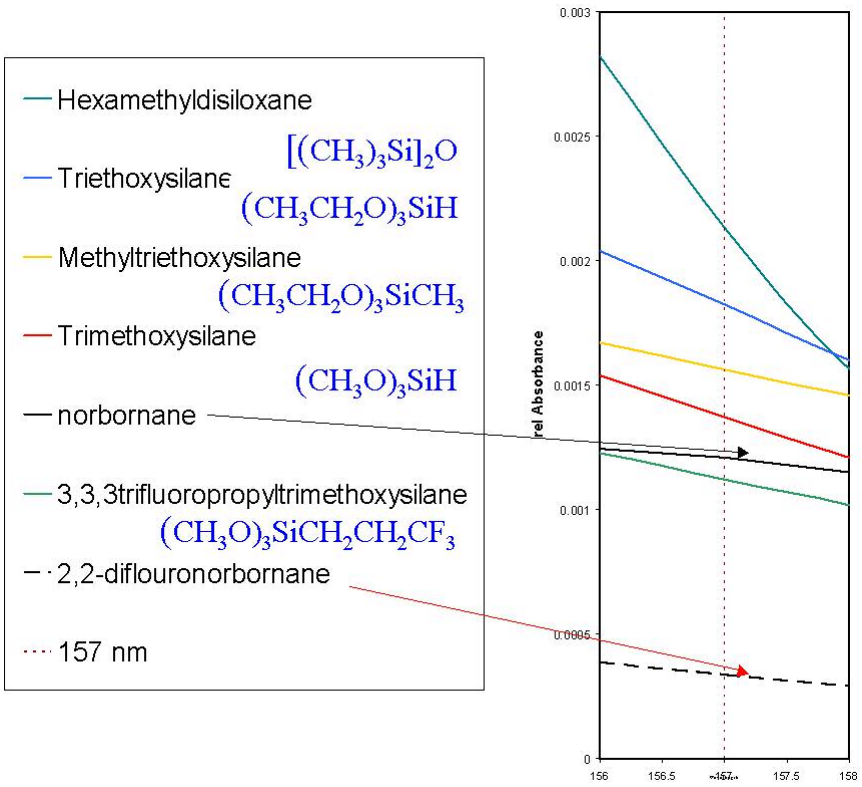

Figure 2.12: Preliminary survey of silicon-based materials for use at 157 nm; unfortunately, most of these compounds look to be too absorbing compared to norbornane-based compounds.

In the silicon-based materials evaluated, it has been found that adding carbon increases absorbance at 157 nm while fluorination decreases absorbance. In general, silicon-based molecules are not as transparent as fluorinated norbornanes. This argues against the use of modified siloxanes and silsesquioxanes as the basis of a 157 nm photoresist.

Sulfur and Phosphorus Compounds

The development of 2 and 3 component resists systems for 157 nm using dissolution inhibitors have been previously reported (Chambers 2003, Conley 2002). To explore which tethering groups are appropriate for use in dissolution inhibitors, several different sulfur- and phosphorus-based compounds were tested for V-UV transparency. **Figure 2.13** shows a variety of sulfur-containing compounds, which have high transparency at 157 nm. This result spurred the syntheses of various dissolution inhibitors that use sulfonates and sulfates as the central tethering group.

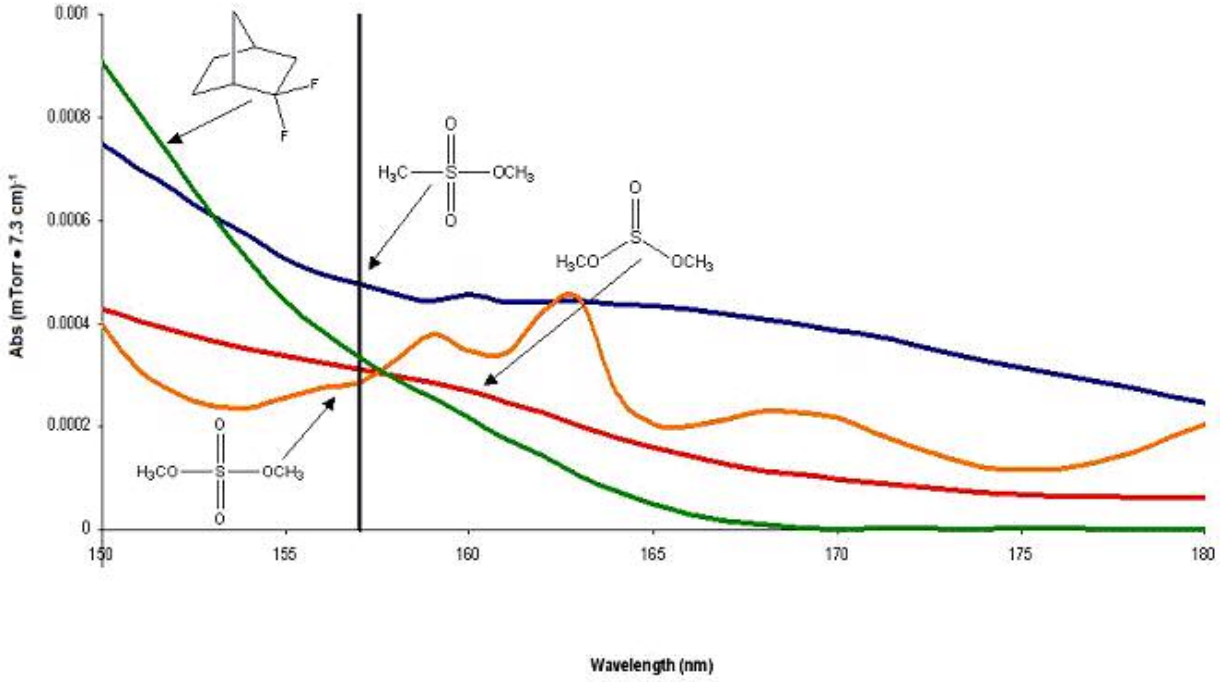

Figure 2.13: Sulfur-containing materials found to be highly transparent at 157 nm, which are currently being used in dissolution inhibitor design.

In a similar vein as the investigation of sulfur-based compounds, phosphorous compounds were analyzed for their transparency at V-UV wavelengths (**Figure 2.14**). These model compounds had very high transparencies at 157 nm. The only potential problem with this class of phosphorous compounds is poor hydrolytic stability. Adding a few drops of water to the diphosphorous compound, for example, results in rapid hydrolysis to the acid, likely eliminating these compounds as potential dissolution inhibitors.

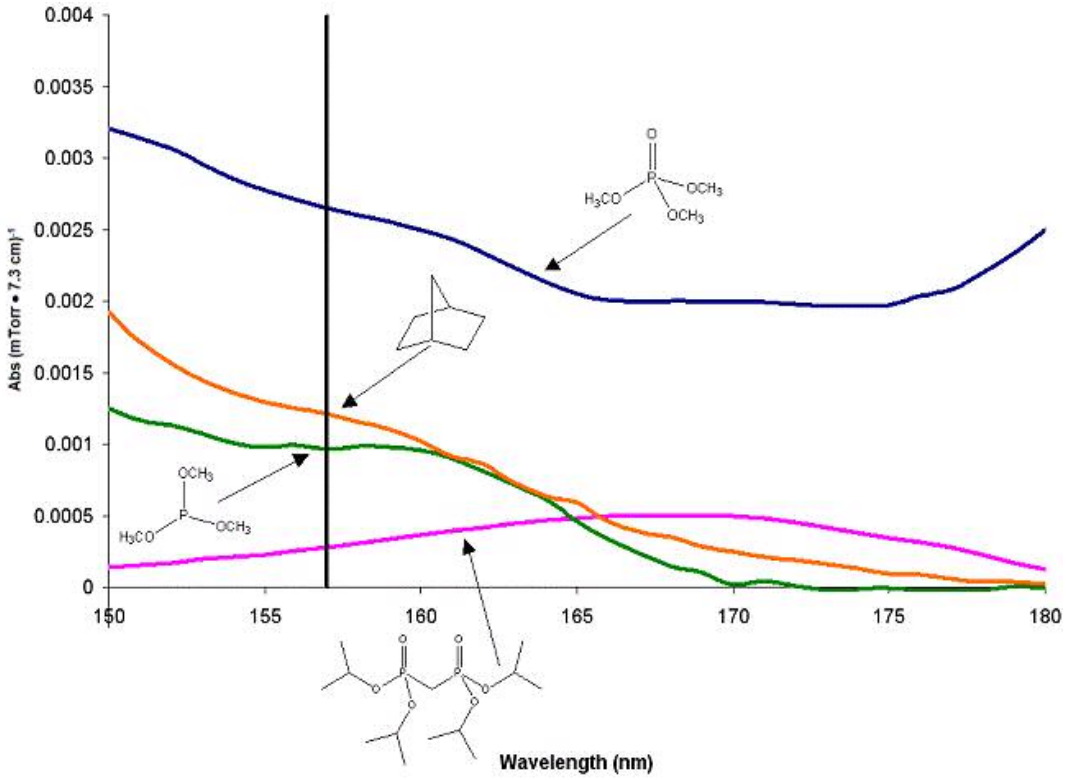

Figure 2.14: Phosphorus-based compounds reveal a surprising transparency at 157 nm.

Theoretical Calculations versus Experimental Data

Early 157 nm research involved the syntheses of novel fluorinated compounds, which also led to a collaboration with Pacific Northwest National Laboratories (PNNL) and now the University of Alabama. The relationship was instituted to utilize time dependent density functional theory (TD-DFT) to calculate theoretical spectra of compounds that would have taken an inordinate amount of effort to synthesize.

TD-DFT is applied as a computational methodology to solve certain molecular electronic properties of ground state compounds, such as transition states and oscillator strengths. More importantly, TD-DFT enjoys an order of magnitude faster computational time and less cost compared to conventional *ab initio* molecular orbital theory calculations. We sought, in collaboration, to obtain calculated photoabsorption spectra of model compounds in the vacuum ultraviolet.

Good correlation was found between the mono- and difluoronorbornane structures, and also norbornane itself, in the experimental gas phase spectra and PNNL's calculated spectra (Matsuzawa 2000). The trends of increasing transparency with added fluorination and difluorination at the 2 position of norbornane also evolved from the DFT calculations (**Figure 2.15**). This promising correlation led to the calculation of other fluoronorbornane spectra (Matsuzawa 2001a, Matsuzawa 2001b).

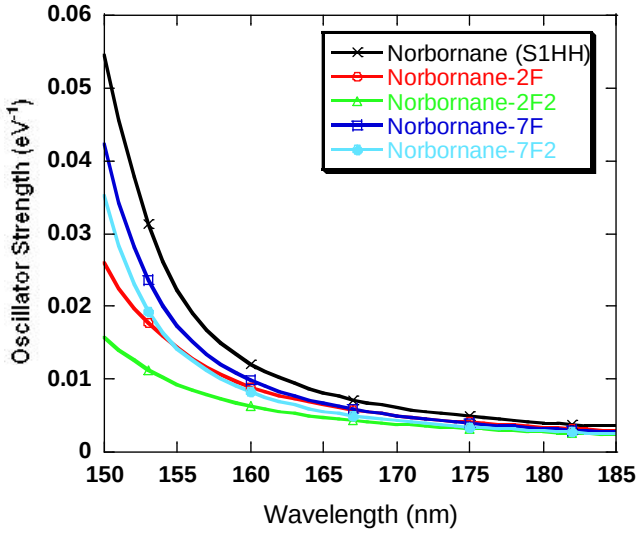

Compound	Nomenclature	DFT Assigned Name
	Norbornane	Norbornane (S1HH)
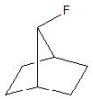	7-Fluoronorbornane	Norbornane-7F
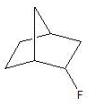	2-Fluoronorbornane	Norbornane-2F
	7,7-Difluoronorbornane	Norbornane-7F2
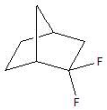	2,2-Difluoronorbornane	Norbornane-2F2

Figure 2.15: Calculated DFT spectra trends for fluoro- and difluoronorbornane compounds track well with those of experimental data.

The effect of higher levels of fluorination and functional groups on a norbornane system were examined with the 2,2-difluoro-3-trifluoromethylnorbornen-3-ol and was found to be highly transparent at 157 nm. The TD-DFT calculations tracked well with the experimental results (**Figure 2.16**).

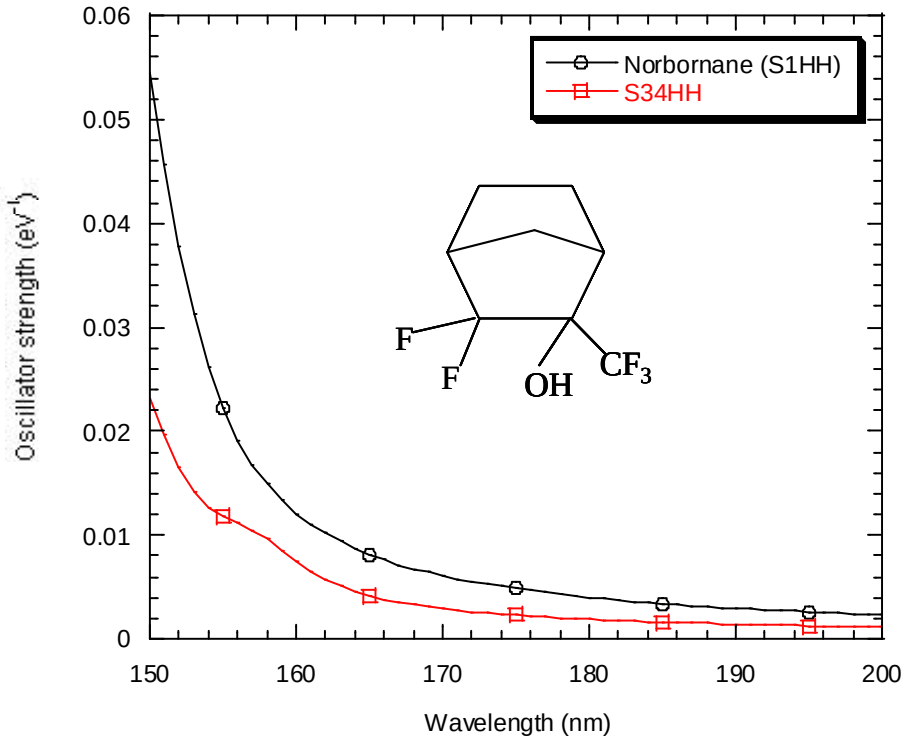

Figure 2.16: Calculated DFT spectra for 2,2-difluoro-3-trifluoromethylnorbornen-3-ol.

It was found that there was significant impact from carbonyl groups for V-UV absorbance, and this was confirmed via DFT calculations (**Figure 2.17**). The impact a carbonyl group or ether oxygen has on absorbance in the V-UV region was seen markedly in the calculated spectra. Having oxygen with either σ or π bonds introduces local maxima and minima to the spectra.

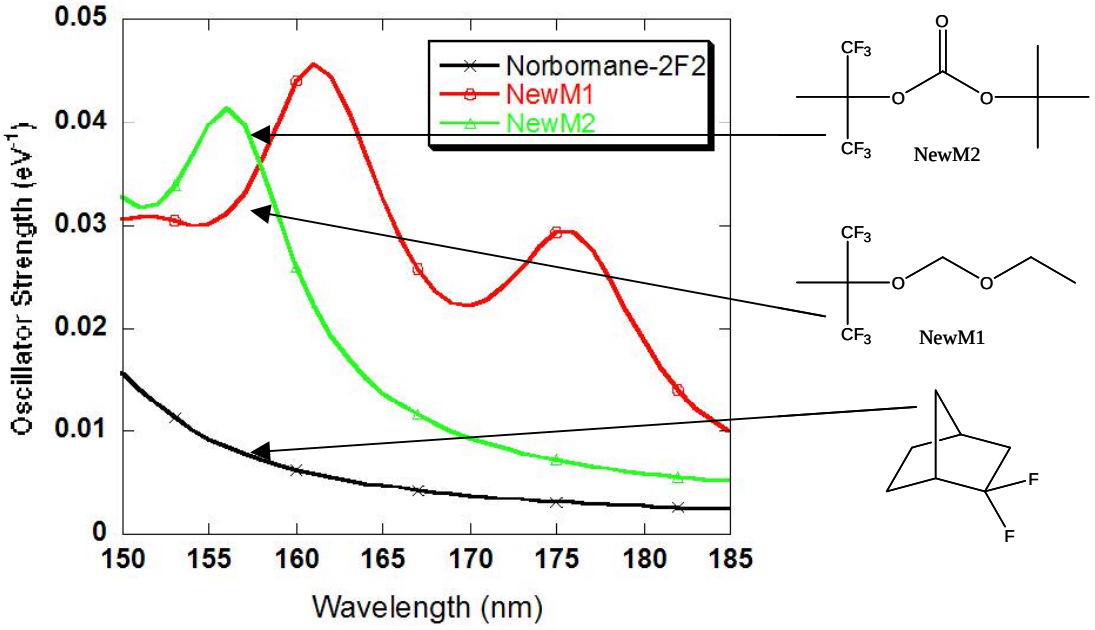

Figure 2.17: Calculated DFT spectra for *t*-BOC and acetal protected HMP again mirror that of the experimental V-UV absorbance data at 157 nm.

A prime example of how invaluable DFT calculations have been is seen in the calculated spectra of the tetrafluoronorbornenes and 1,4-difluorinated norbornenes. These compounds were synthetically more difficult to access and were not pursued in obtaining their experimental spectral data. The decision to forgo those syntheses was borne out by the DFT calculations from PNNL, which showed that tetrafluorination or 1,4-difluorination of the norbornane skeleton provided little or no significant increase in transparency at 157 nm. Overall, TD-DFT calculations accelerated and aided in the understanding, design and synthesis of materials for 157 nm resists (Ando 2002).

Gas Phase Data versus Polymer Thin Film Absorbance

The validation of the V-UV gas phase work came with the polymer synthesis of materials for 157 nm. The correlation between absorbance trends seen for monomers was likewise seen in the resulting polymer thin films at 157 nm. Variable angle scanning ellipsometry (VASE) on thin films of model polymers is currently the most accurate and representative measurement of photoresist material transparency at 157 nm (Johs 1994, French 2000). A collection of polymers was surveyed using VASE for absorbance trends similar to the ones seen in the V-UV tool.

The acrylate platform of materials was extensively studied early in the 157 nm resist program. Acrylate polymers are commonly used in 193 nm photoresists, and so fluorinated analogues were sought for 157 nm imaging. As can be seen here (**Figure 2.18**), poly(methyl methacrylate) (PMMA) is indeed more absorbing than poly(2-trifluoromethyl methacrylate). Fluorine has a significant impact on reducing absorbance at 157 nm not only with representative monomer species in the gas phase (Figure 2.3), but in the corresponding polymers as well.

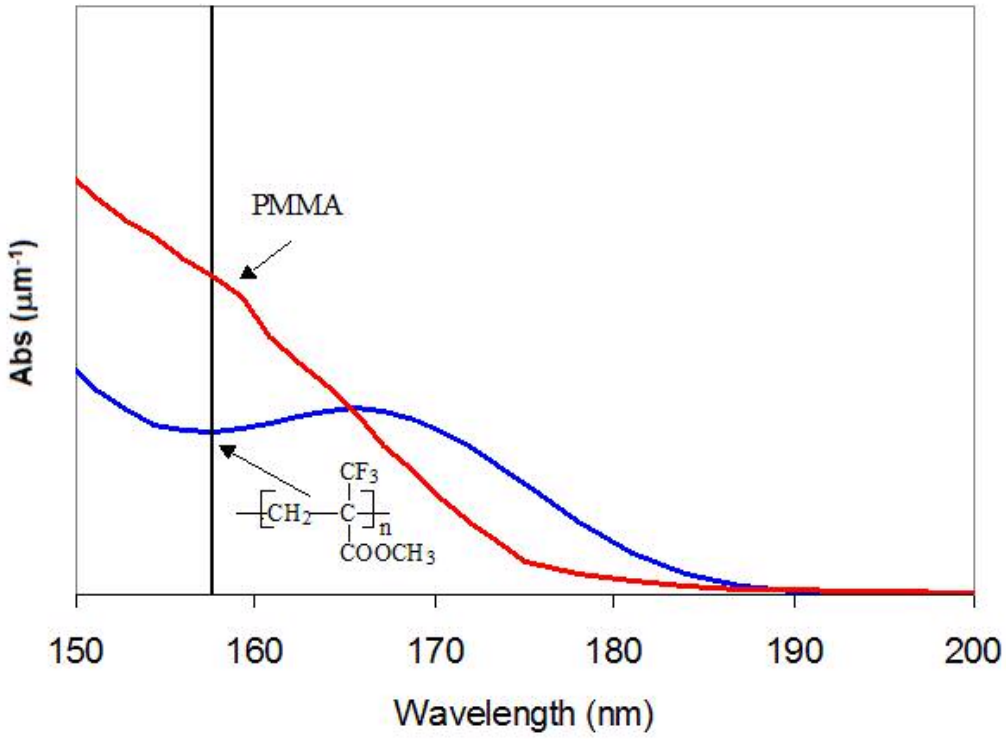

Figure 2.18: The absorbance at 157 nm of poly(methyl methacrylate) (PMMA) and poly(2-trifluoromethyl methacrylate) mirror that of their respective monomers.

Fluorinating the norbornane structure, as seen from the gas phase experiments with mono- and difluoronorbornane derivatives, can have a strong effect on the transparency at 157 nm. V-UV spectroscopy showed that norbornane was much more strongly absorbing than norbornane hexafluoroisopropanol (**Figure 2.5**). Incorporated into polymer, both polynorbornene and poly(3-(bicyclo[2.2.1]hept-5-en-2-yl)-1,1,1-trifluoro-2-(trifluoromethyl)propan-2-ol), also known as the compound poly(norbornene hexafluoroisopropanol) (PNBHFA) again show a marked difference in absorbance in the vacuum UV, tracking well with the gas phase data (**Figure 2.19**). The transparency of

the NBHFA homopolymer is well known (Somervell 2000, Ito 1998), and the correlation between its high transparency in the gas phase (monomer) and as a thin film polymer is one of the first, and most important examples of the value of the V-UV absorbance of hydrogenated monomers for our 157 nm resist research.

	Structure	A_{157} (μm^{-1})
Polynorbornene	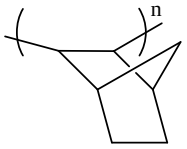	6.10
Polynorbornene hexafluoroisopropanol	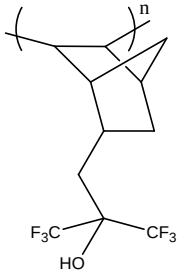	1.15 film thickness ≅ 150 nm

Figure 2.19: PNBHFA is far more transparent than polynorbornene, a trend that was seen in the gas phase absorbance of norbornane versus norbornane hexafluoroisopropanol (re: Figure 2.5).

The absorbance of the TCN series of monomers has a good correlation to the thin film absorbance of the corresponding homopolymers in the V-UV. The effect of increased fluorination in both monomers (going from 3 to 5 fluorines) (re : **Figure 2.10**) parallels that of the resulting polymers very well (**Figure 2.20**).

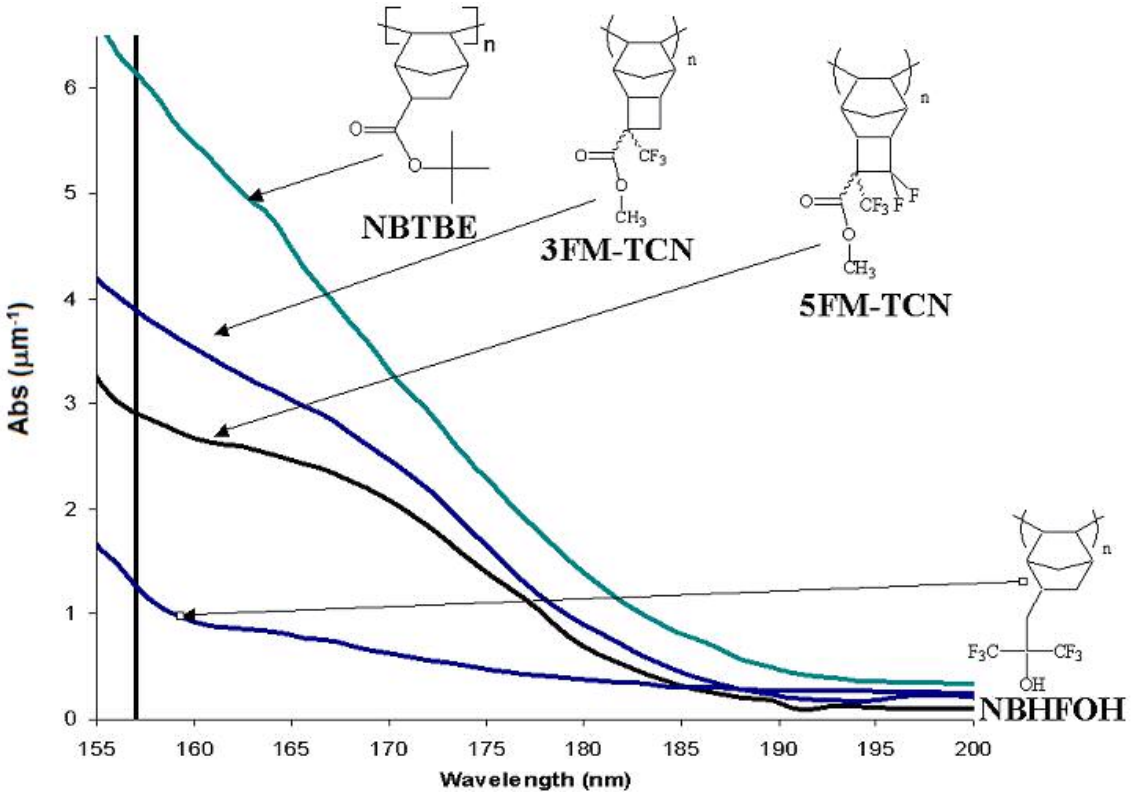

Figure 2.20: The absorbance of TCN homopolymers follows the same trends in transparency as the corresponding monomers.

It is possible to extrapolate what the absorbance of a homopolymer would be from the gas phase spectra of the hydrogenated monomer. Making simplified assumptions for film density (1 g/mL) and constant temperature makes such a calculation straightforward. Upon extrapolation of the gas phase absorbance of the TCN and NBHFA monomers, it was seen that the trend in absorbance tracks reasonably well with that of the actual homopolymer absorbance measurements (**Figure 2.21**), considering the relatively simplified method of extrapolating film absorbance from hydrogenated monomers.

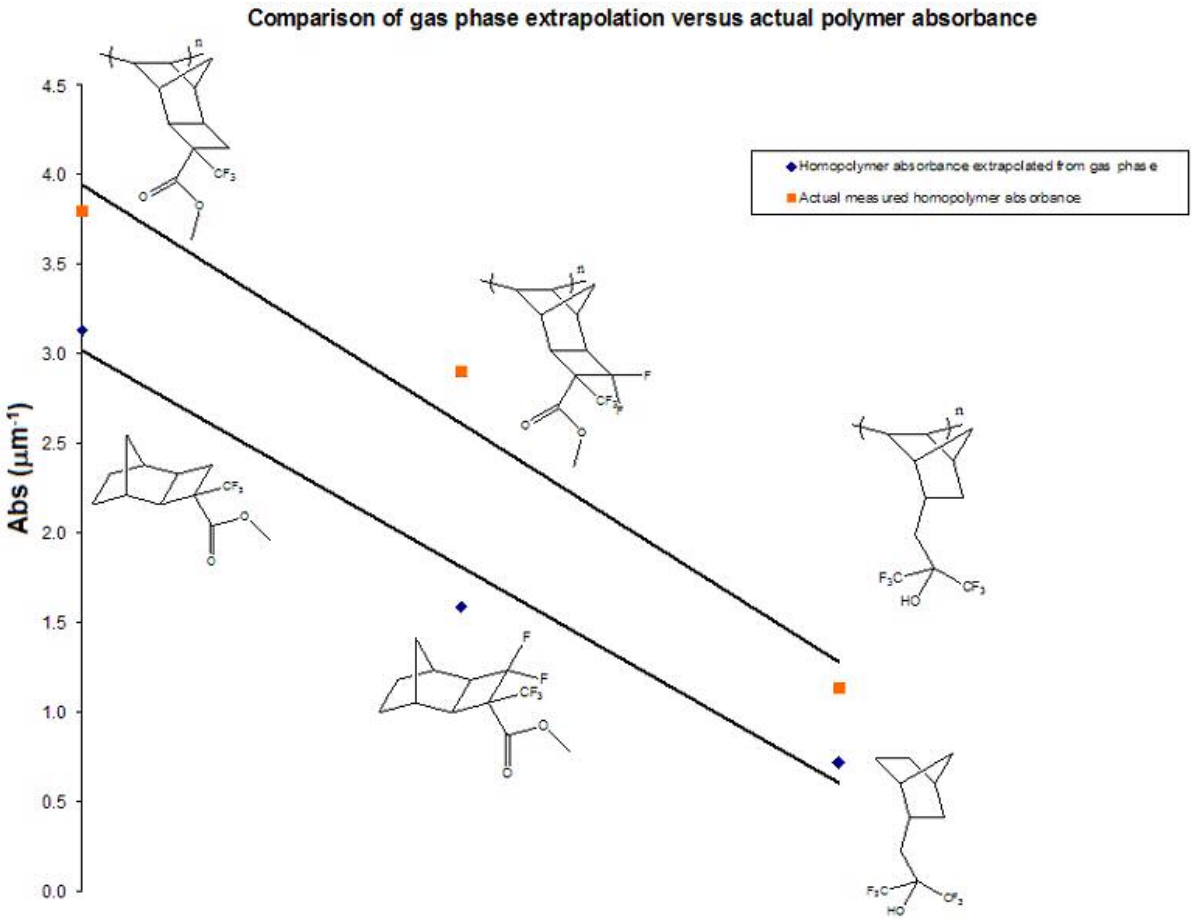

Figure 2.21: Correlation between gas phase measurements extrapolated into film absorbance versus that of actual polymer measurements.

The impact of carbonyl groups on the absorbance of fluorinated polymers is particularly important when considering the protecting group used in a resist. The acetal-protected NBHFA copolymer (**Figure 2.22**), was used for initial imaging studies at 157 nm.[38] One of the subsequent polymer platforms, which was also successfully imaged at 157 nm, was the partially *t*-BOC-protected homopolymer of NBHFA.

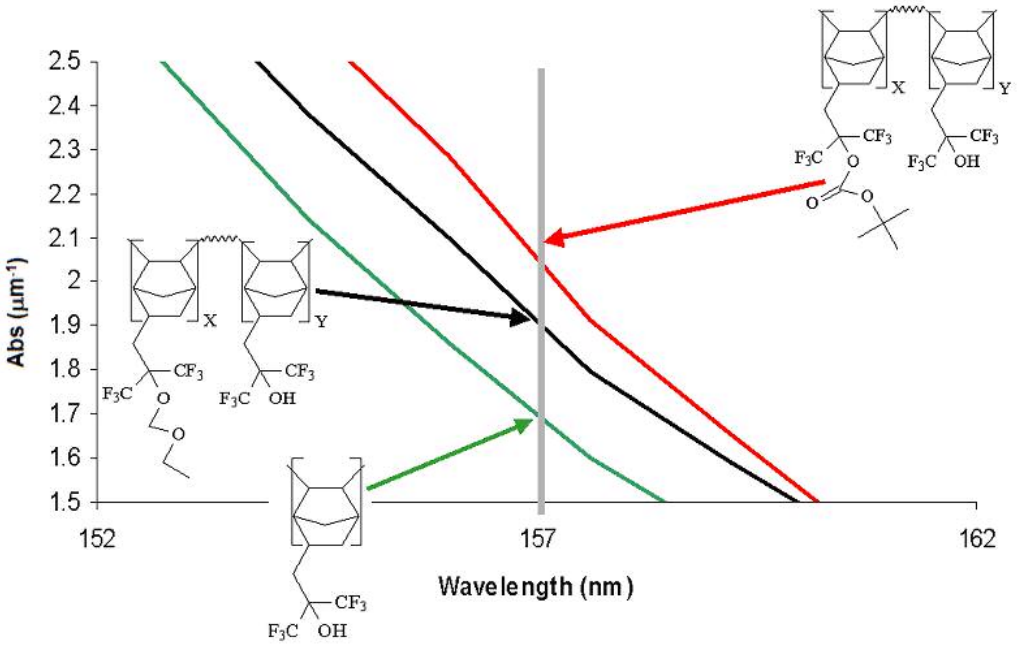

Figure 2.22: Acetal and *t*-BOC protected poly(NBHFA), reveal the same trends of transparency as observed in gas phase measurements of acetal and *t*-BOC protected HMP.

The V-UV absorbance of the hydrogenated monomers correlated extremely well with the thin film absorbance of the corresponding polymers obtained from VASE.

Vacuum UV Spectra Inspires Future Work for 157 nm

In light of the inherent difficulty of making addition polymers from geminally-substituted monomers, condensation polymerization has emerged as a possible route to transparent 157 nm polymers. The incredibly high transparency of the functionalized norbornane *cis*-diol (**Figure 2.23**) led to investigation of condensation polymers through such vicinal norbornane-diols, to be described later (Chapter 5).

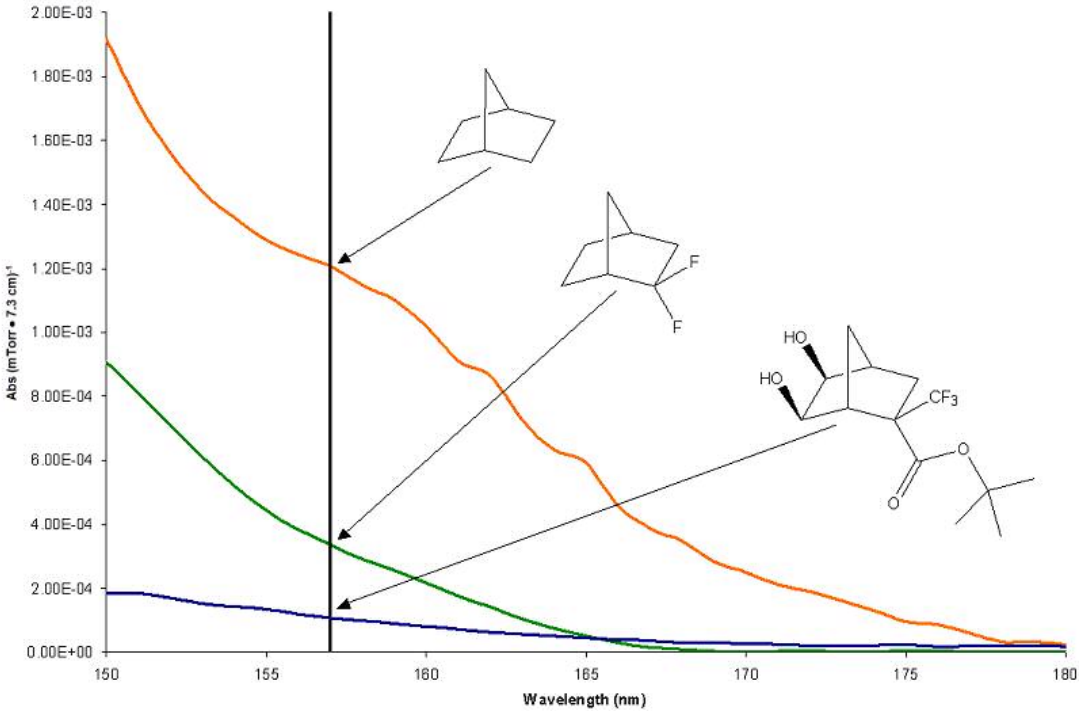

Figure 2.23: This highly fluorinated norbornane shows transparency higher than that of 2,2-difluoronorbornane.

Conclusions

The V-UV spectrophotometer has proved to be a valuable asset in the design of transparent resist materials for exposure at 157 nm. Our group has synthesized a number of unique compounds and has measured their gas phase absorbance. The gas phase absorbance at 157 nm was used to evaluate the potential utility of the model compounds for incorporation into a polymer. The relative absorbance of monomeric materials follows the same trend when looking at the measured spectra of the corresponding polymers, validating the invested work of measuring monomeric V-UV spectra.

Gas phase spectra data, in addition to TD-DFT calculations, enables 157 nm materials development to proceed at a faster rate since new compounds can be auditioned early in synthetic development. By screening hydrogenated molecules as models for the repeat units of polymers, one can save time and resources by first analyzing absorbance trends in the V-UV. This is borne out by the polymer sets that were measured at 157 nm that, when compared to the appropriate hydrogenated precursors, follow the same trend in absorbance as their monomer counterparts. This methodology for screening of new materials has become our *de facto* methodology for investigating new materials for use in 157 nm lithography.

Experimental

Vacuum Ultraviolet Spectroscopy

Gas phase V-UV measurements were made on an Acton *CAMS-507* spectrophotometer fitted with a custom-made gas cell attachment. The details of the cell design and implementation have been described previously (Brodsky 2000). Model compounds are purified, dried or distilled from Na_2SO_4 or $MgSO_4$, and degassed using three freeze-thaw-pump cycles under high vacuum. The samples were then sealed *in vacuo* within glass ampoules, which were then broken inside the evacuated spectrophotometer to obtain a gas phase absorbance measurement. Multiple sample readings were taken per sample, and all absorbance data were normalized for pressure. The absorbance was measured as a function of increasing pressure. The cell was then partially evacuated in steps and the measurements were made again. These hysteresis

tests were performed on all samples to ensure that measured compounds were not adsorbing onto the cell windows.

High voltage tables were generated prior to each use of the spectrophotometer. Spectra are reported only to 150 nm, as significant amounts of dark counts and noise occur between 120 and 140 nm. The full path length of the gas cell itself is 7.3 cm.

Absorbance data of polymer films was calculated from measurements made with a J.A. Woollam *VU-301 VUV-VASE* variable angle spectroscopic ellipsometer and/or measured with the Acton *CAMS-507* spectrophotometer. The films were cast on either silicon wafers (VASE) or calcium fluoride disks (Acton) from solutions in propylene glycol methyl ether acetate (PGMEA) or cyclohexanone and baked at 100-130°C for at least 5 min prior to analysis. The ellipsometric data were then collected as described previously. All absorbance data reported are in base 10.

Vacuum Ultraviolet Absorbance Measurement of 3-(bicyclo[2.2.1]hept-5-en-2-yl)-1,1,1-trifluoro-2-(trifluoromethyl)propan-2-ol (NBHFA)

Gas phase absorbance data collection is illustrated by the measurement of NBHFA: a glass ampoule was loaded with a purified and thoroughly characterized amount of NBHFA (*ca*. 0.1 mL) and thoroughly degassed with three freeze-pump-thaw cycles at 150 mTorr. The ampoule was placed in the sample holder and sealed to the system; the entire system was then evacuated to approximately 10-15 mTorr. A background scan was read and then transparency of the empty gas cell measured from 120-300 nm to ensure the lack of any contaminants in the system. The ampoule holder

was isolated and the ampoule broken *in vacuo*. The gas cell was then charged with 970 mTorr, and then closed off. Absorbance measurements began with the pressure at 920 mTorr, and when the sample reading was complete, the cell pressure was 780 mTorr. The resulting absorbance over 150 to 200 nm is shown below (**Figure 2.24**), for two readings of the same ampoule of sample, normalized to the total pressure in the gas cell at the beginning of the measurement.

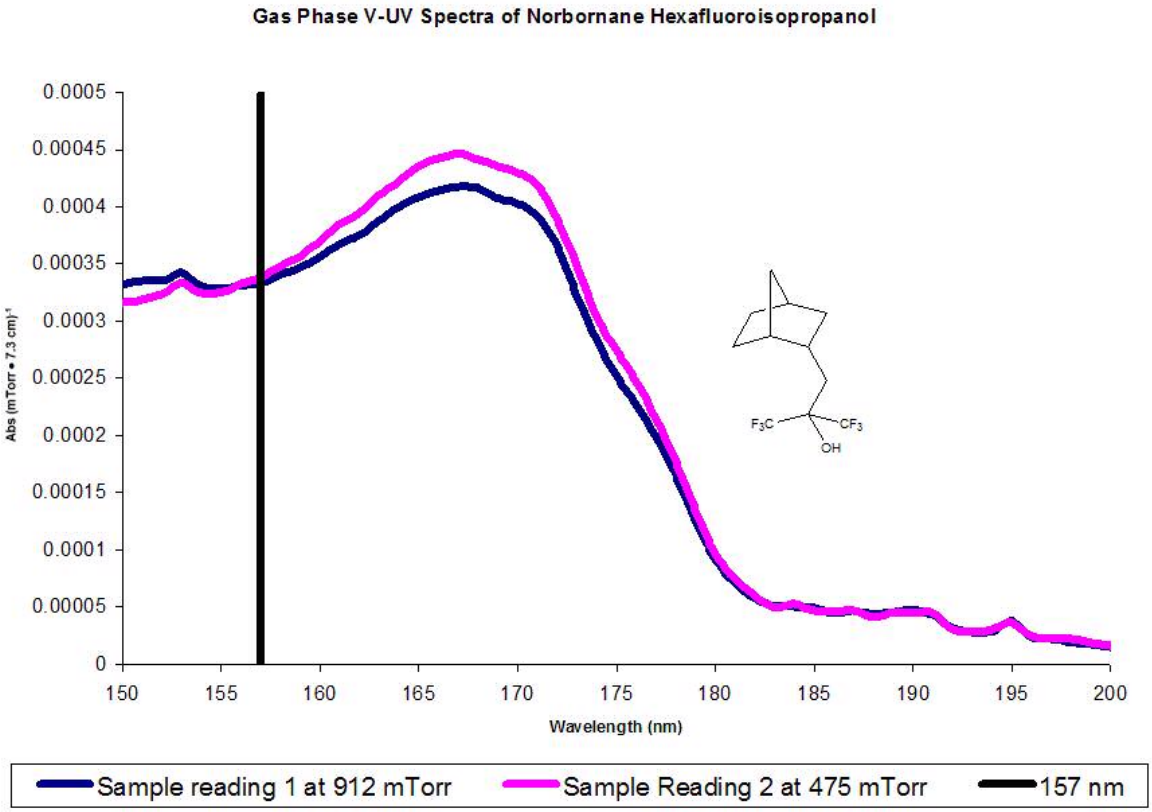

Figure 2.24: Optical density of gas phase NBHFA and the representative pressures at which the readings were taken.

Calculations

The spectral calculations were performed by using the program Gaussian98.[7] Geometries were optimized by using the density functional theory (DFT) (Hohenberg 1964, Kohn 1965, Parr 1989, Chong 1995) with the local spin density approximation (LSDA) functional (Vosko 1980) and DZVP2 basis set (Godbout 1992, DGauss) or at the gradient-corrected B3LYP level with Becke's three parameter exchange functional (Becke 1993) and the Lee-Yang-Parr (Lee 1988) correlation functional and the 6-31G* basis set. The calculations on the transition energy and oscillator strength were performed at the time-dependent density functional theory (TD-DFT) level (Bauernschmitt 1996, Casida 1998). The TD-DFT calculations were performed at the gradient-corrected B3LYP level with the cc-pVDZ (Dunning 1989) basis sets augmented by a set of Rydberg functions (3*s*3*p*3*d*) centered at the molecular center. The Gaussian exponents of this set of Rydberg functions are 0.005858 (3*s*), 0.003346 (4*s*), 0.002048 (5*s*), 0.009988 (3*p*), 0.005689 (4*p*), 0.003476 (5*p*), 0.014204 (3*d*), 0.008077 (4*d*), and 0.004927 (5*d*) (Kaufmann 1989). This set of Rydberg functions has been used in recent electronic excitation calculations with various methods leading to the results with high-accuracy (Wan 2000, Zhan 2002). For convenience, the cc-pVDZ basis set augmented by this set of Rydberg functions (3*s*3*p*3*d*) centered at the molecular center (mc) is denoted by cc-pVDZ+Ryd(mc). All calculations were performed on a 48-node IBM SP (Power2 SuperChip) or a 16-processor SGI Origin2000 computer. The B3LYP functional was chosen instead of a local functional because the former has been found to give a better correlation with experimental values as compared to the latter

(Casida 1998, Bauernschmitt 1997, Adamo 1999, Wiberg 1998, Handy 1999, Tozer 1998, Görling 1999). For example, it have previously found for a total of 25 transition energies of formaldehyde, benzene and ethylene that the linear correlation coefficient between the calculated and experimental transition energies are 0.790 and 0.984 at the SVWN/cc-pVTZ+Rydberg and B3LYP/cc-pVTZ+Rydberg levels, respectively (Matsuzawa 2001).

Chapter 3—Ring Opening Metathesis Polymerization for 157 nm Photoresists

Olefin Metathesis

Webster's dictionary defines chemical metathesis as, “The act, process, or result of exchange, substitution, or replacement of atoms and radicals; thus, by metathesis an acid gives up all or part of its hydrogen, takes on an equivalent amount of a metal or base, and forms a salt.” Salt metathesis is typically how one learns about metathesis in the realm of simple acid-base chemistry. In modern organic chemistry this term usually deals with double bond redistribution reactions (called *olefin metathesis*) in the presence of specific types of transition metal catalysts (**Figure 3.1**) (Calderon 1967). The reaction involves the cleavage of the double bond and subsequent alkylidene exchange between alkenes, it is an equilibrium reaction and so typically results in a distribution of various products (Truett 1960, Eleuterio 1957, Natta 1964).

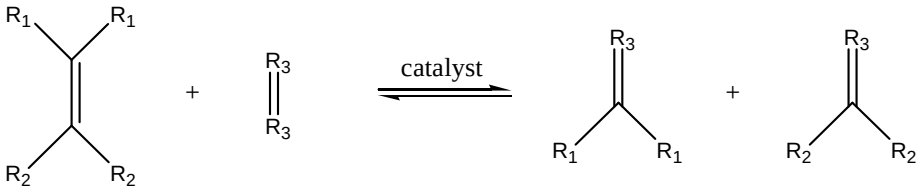

Figure 3.1: A conventional example of olefin metathesis with alklyidene exchange under equilibrium.

Modern Catalyst Systems

Current research in this area focuses on using transition metals such as tungsten (W), iridium (Ir), tantalum (Ta) and ruthenium (Ru), with a variety of ligands. The major players in the catalyst field today are the laboratories of Schrock and Grubbs (**Figure**

3.2). The more versatile and powerful metathesis catalysts are shown below, and modern metathesis catalysts such as these exhibit high reactivity, synthetic accessibility and, most importantly, tolerance to a wide range of functional groups (Ivin 1997, Fürstner 2000).

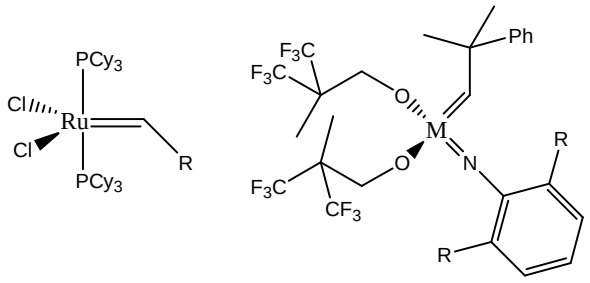

R = Ph, $CH=Ph_2$

Grubbs catalyst

M = Mo, W

R = $CH(CH_3)_2$

Schrock catalyst

Figure 3.2: The Grubbs and Schrock metathesis catalysts.

Metathesis Reaction Types

Metathesis reactions can mediate many different reaction types, such as polyolefin synthesis, closed and opened ring formations. The different types of reaction pathways that are possible through metathesis catalysts are shown below (**Figure 3.3**). Ring closing metathesis (RCM) and acyclic diene methathesis (ADMET) are driven thermodynamically by the expulsion of ethylene. This provides the strong entropic force for the creation of large ring systems by RCM. The other major synthetic conversion is of interest for photoresist synthesis: ring-opening methathesis polymerization, or ROMP. Here, the thermodynamic driving force is found in the release of ring strain, providing enough enthaplic driving force to produce polymers.

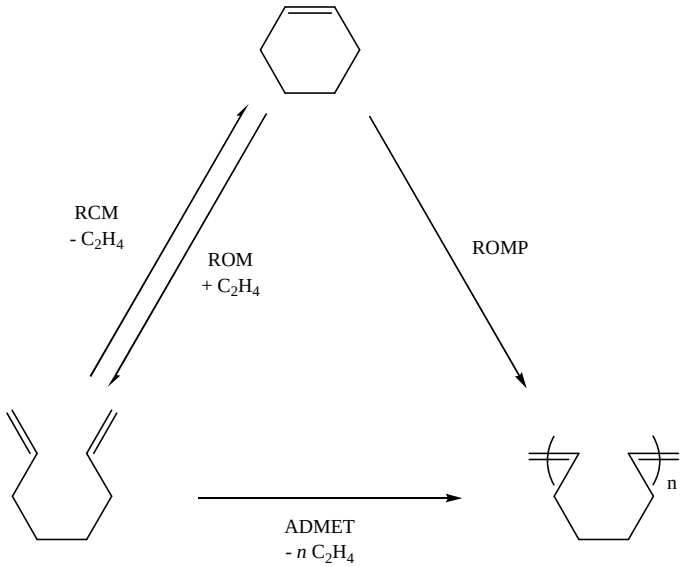

Figure 3.3: Metathesis reactions to yield polyolefins, dienes and cyclic olefins.

Ring Opening Methathesis Polymerization (ROMP)

The most interesting application of such metathesis catalysts here is the ring opening metathesis polymerization (ROMP) reaction, wherein highly strained, olefin-containing ring systems, such as norbornene, undergo metathesis resulting in a linear polymer, shown below (**Figure 3.4**). Such bicyclic systems such as norbornene compounds serve as excellent monomers for ROMP reactions; this bicyclic system has a large amount of strain due to the fused state of its rings. This makes the olefin highly reactive to metathesis.

The discovery of metal alkylidene complexes led to catalyst structures capable of olefin metathesis chemistry, but it also aided in the elucidation of the mechanism of the transformation itself. The accepted mechanism of the ring-opening reaction is the "Chauvin mechanism," involving the [2+2] cycloaddition or cycloreversion of olefins,

metal carbenes and metallocyclobutane intermediates. Such steps are in equilibrium, but in the case of ROMP, the relief of ring strain strongly drives the polymerization to completion (Fürstner 2000).

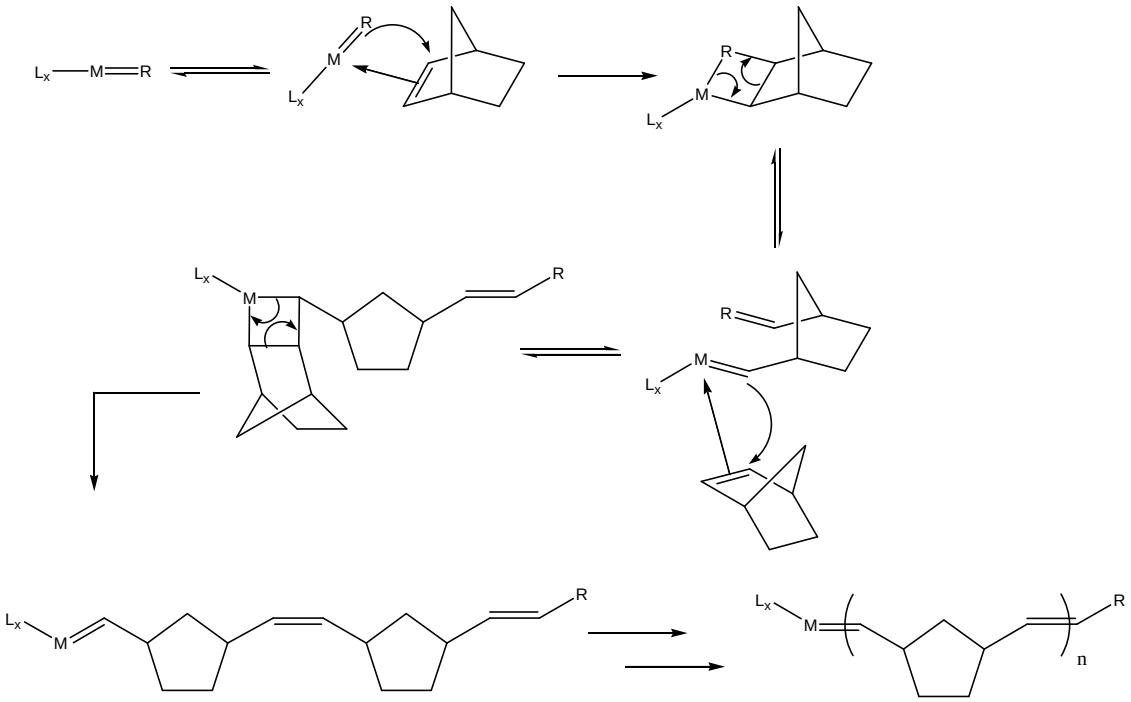

Figure 3.4: The stepwise mechanism for ring-opening metathesis polymerization of cyclic dienes.

Polymerization is terminated when a chain termination agent is introduced into the system, in the case of ROMP reactions, this typically be an ether, such as ethyl vinyl ether, or an aldehyde, such as benzaldehyde. The chain termination agent will bind to the catalyst complex, resulting a new Fischer carbene complex that is inactive towards further polymerization. However, even precipitation of an active polymer solution into a solvent such as methanol will drop the metal off the polymer chain end. A few precipitations will effectively remove all metal, resulting in “clean polymer.”

Molecular weight control of ROMP polymers is accomplished through using acyclic olefins that, once bound to the end of a polymer, will end further propagation. Symmetrical olefins do not work well for termination, but terminal olefins such as 1-hexene or allyl acetate work extremely well. These olefins can control the M_w of substituted polynorbornenes with predictable and reproducible results (Ivin 1997, Okoroanyanwu 1997).

The pertinent question in our investigation was whether it would be possible to create ROMP polymers of sufficient T_g and transparency for use at 157 nm. Since the final ROMP polymers from bicyclic alkene systems have unsaturations along the newly formed polymer backbone, these olefins will need to be reduced by some form of hydrogenation, due to the contribution of the olefin to absorbance at deep-UV wavelengths.

Hydrogenation of ROMP polymers is accomplished through a variety of reduction agents, from hydrogen gas with a metal catalyst to hydrazines. The best approach to polymer backbone hydrogenation has been shown to be the use of diimides formed *in situ* from *p*-toluenesulfonylhydrazide (TSH) in base (Hahn 1992). Unfortunately, hydrogenating a ROMP polymer backbone also results in polymer with a substantially lower T_g (**Figure 3.5**) (Six 2000). This led to the use of dinorbornene structures for ROMP polymers, so that the bulkier, extended ring system would give the higher T_g necessary for the lithography baking steps.

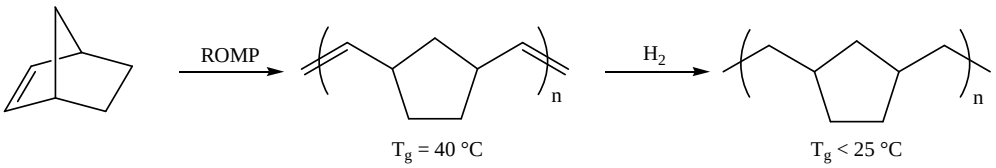

Figure 3.5: Polynorbornene displays low T_g especially after hydrogenation, making dinorbornenes more attractive as ROMP monomers (Six 2000).

ROMP for 193 nm Photoresists

ROMP has previously been used in our research group when searching for ideal 193 nm photoresist materials. The 193 nm ROMP project auditioned several types of functionalized norbornene and dinorbornene monomers for incorporation into different polymers (**Figure 3.6**) (Patterson 2000). The ROMP polymers were relatively easy to synthesize, using iridium-based methathesis catalysts. Purification and scale up were likewise successful. The resulting polymers then were measured for glass transition temperatures. In the studies of 193 nm polymers, it was found that carboxylic acid and ester incorporation provided a degree of hydrogen bonding sufficient to elevate the T_g to above 130 °C.

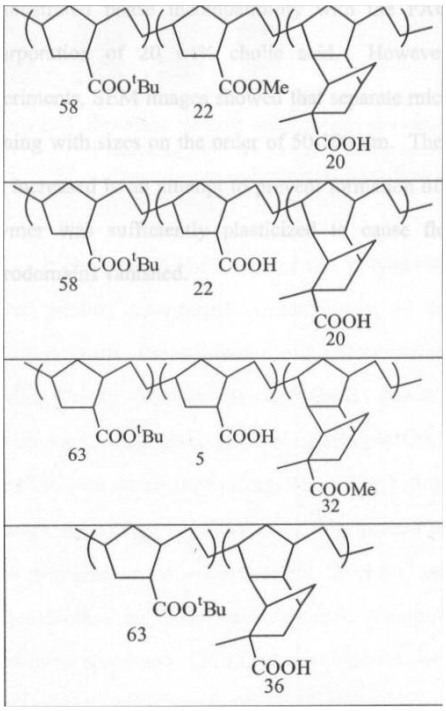

Figure 3.6: 193 nm ROMP copolymers (Patterson 2000).

The various copolymers made for 193 nm resists were evaluated for transparency and then imaged at 193 nm. Unfortunately, the ROMP polymers suffered from a variety of processing problems. These issues ranged from PAG phase incompatibility, swelling due to solvent uptake, slow dissolution rates and poor adhesion (Patterson 2000). Work then went on past ROMP, utilizing free radical and addition polymerizations instead, but the 193 nm research did teach how to direct 157 nm ROMP materials research.

157 nm ROMP Polymers

It was clear from the vacuum UV data that fluoropolymers of some type were necessary to gain high transparency at 157 nm. Addition polymer synthesis using traditional transition metal catalysts produced some fluoropolymers in acceptable yields,

e.g., PNBHFA. However, some of the more transparent monomeric materials were unable to undergo this polymerization pathway, in particular, the geminally substituted flouronorbornenes (**Figure 3.7**). It was hoped that fluorinated dinorbornenes could serve an analogous role to the functionalized dinorbornenes used at 193 nm and that ROMP would be able to incorporate these geminally disubstituted norbornenes into a polymer. Collaboration with Prof. Grubbs research group at CalTech, and a graduate chemist in his group, Daniel P. Sanders, were key to bringing 157 nm ROMP polymers to fruition.

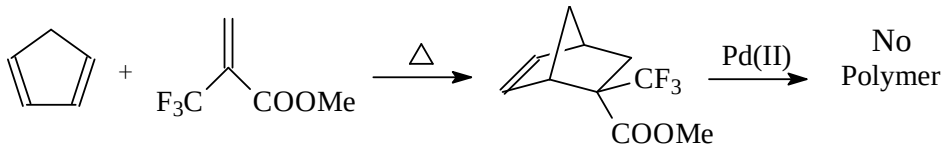

Figure 3.7: Geminally substituted norbornenes do not polymerize appreciably with nickel or palladium addition catalysts; ROMP was one method of circumventing this shortcoming.

Polymer synthesis at 157 nm was modeled on the types of polymers synthesized at 193 nm (**Figure 3.8**). Initial polymerization attempts were to be done on the dinorbornene hexafluoroisopropanol monomer (DNBHFA), which was available as a gift from the resist company JSR. Copolymers would be composed primarily of DNBHFA, adding in ester or acetal functionalized comonomers to create a working resist for 157 imaging.

193 nm System - Tsutomu Shimokawa, Kyle Patterson, *et al.*

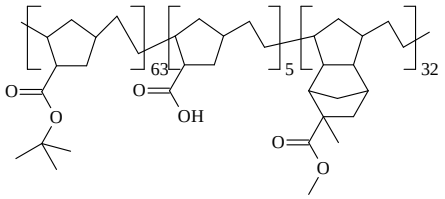

T_g: 132 °C
Higher T_g due to hydrogen bonding between acid and ester groups in polymer

157 nm Analogs

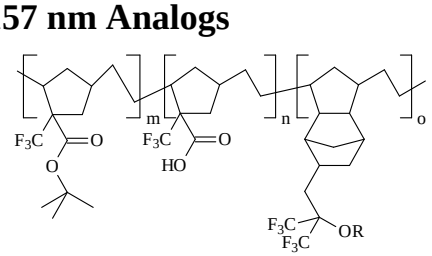

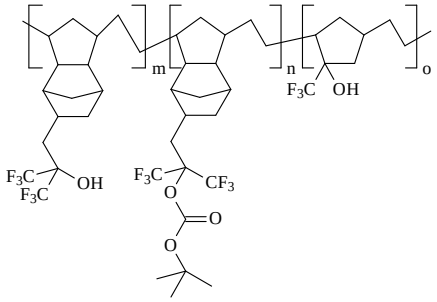

Figure 3.8: Deriving 157 nm ROMP polymer analogs from 193 nm ROMP polymers with high T_g.

It was found that the Grubb's second-generation catalyst, a far more active and effective catalyst than the first generation catalyst, was also tolerant of the acidic hexafluoroisopropanol group (**Figure 3.9**).

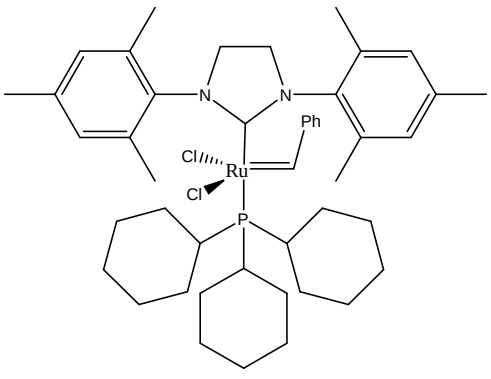

Figure 3.9: The Grubbs second-generation catalyst; the imidazole ligand increases the activity and effectiveness of the metathesis reaction.

The homopolymer of dinorbornene hexafluoroisopropanol (DNBHFA) was successfully synthesized (**Figure 3.10**). Allyl acetate was used as the chain termination agent to eventually control molecular weight to between M_w 5,000 and 10,000. Initial attempts yielded polymer with M_w in the 300,000 range, but optimization of the CTA loadings eventually led to low molecular weight polymer.

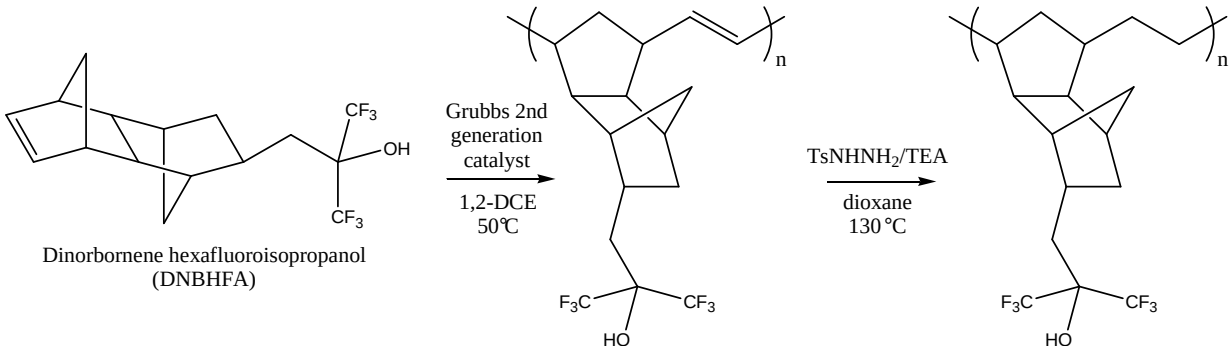

Figure 3.10: Synthesis of the homopolymer P(DNBHFA) using ROMP.

The ROMP homopolymer was the first material synthesized for use at 157 nm and found to have a T_g of approximately 85-90 °C as well as an absorbance of 3.3 μm^{-1} at 157 nm. One issue with DNBHFA in a ROMP polymer is that the dinorbornene ring system is very hydrophobic, while the hexafluoroisopropanol functional group is hydrophilic. This resulted in problematic precipitations into nonpolar and polar solvents, making isolation and purification via precipitation difficult.

One of the most difficult aspects of ROMP for 157 nm materials synthesis has been purifying the final polymer. Purification of hydrogenated ROMP copolymers based

on dinorbornene hexafluoroisopropanol (DNHFA) has always been a difficult process. Precipitation was extremely problematic, and using various tweaks (mixed solvent, cold solvents, etc.) proved wholly unsuccessful, with low yields of polymer resulting at best. The precipitation method most successful was precipitating the polymer from isopropyl alcohol into water, although this made the polymer difficult to workup and dry completely. Precipitation into a polar solvent (using water as the solvent and precipitating into isopropyl alcohol) worked well and yielded more polymer precipitate. The best results when using nonpolar solvents have been precipitation into cold hexane (~ 4 °C). However, polymer loss is high, as precipitating a solution of poly(DNBHFA) only yielded 16% of polymer from cold hexane.

A different technique was found to be far more successful in ROMP polymer purification and isolation: dialysis. This method of purification takes approximately 48 hours to complete to 95% or greater purity. The polymer solution is loaded into a dialysis bag, typically composed of regenerated cellulose, with a molecular weight cutoff pore size of 500-1000 M_w. Methanol is the typical solvent to immerse the dialysis enclosure into, useful not only for solubilizing the polymer, but washing out any residual ruthenium catalyst still bound to the polymer chain. The effects of dialysis purification are quite evident from the resulting GPC traces, before and after dialysis—all monomer is removed and only polymer remains.

Using this purification technique, a series of copolymers as shown below were purified, and their absorbance at 157 nm was measured using VASE (**Figure 3.11**).

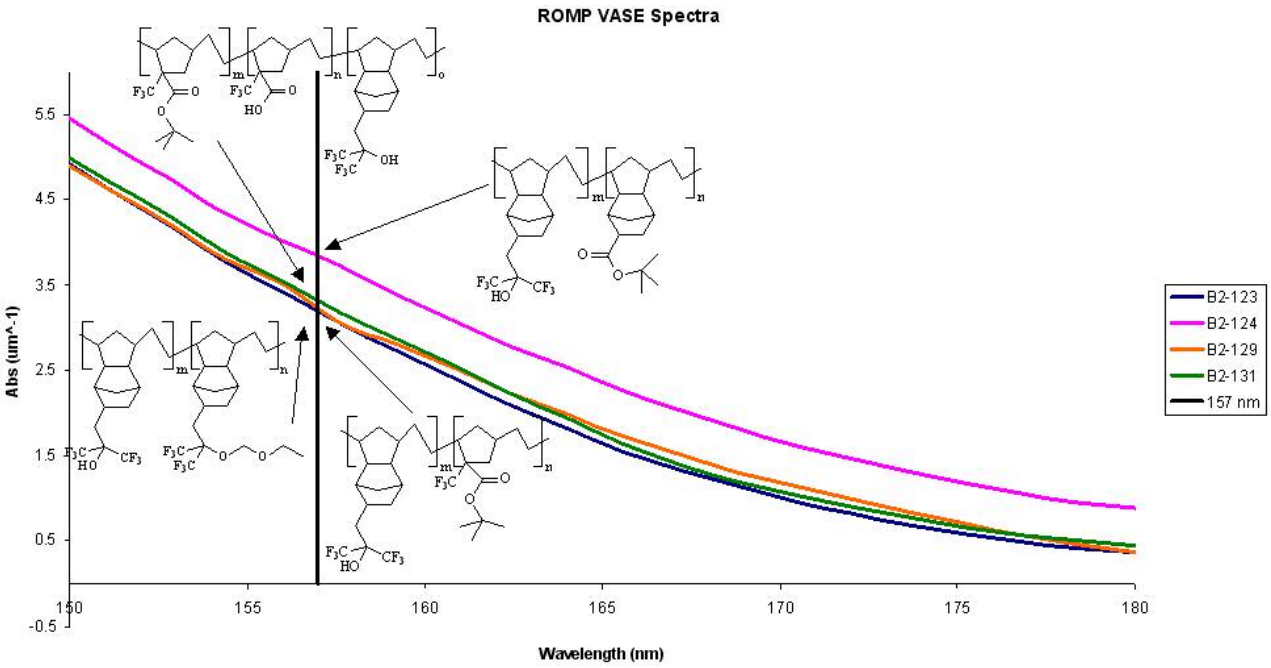

Figure 3.11: VASE spectra of the various ROMP copolymers show they are too strongly absorbing for use at 157 nm.

The purity of the polymers is better than in previous attempts and the absorbance of these polymers drops to approximately 3.1 μm^{-1} at 157 nm. These values remain too high for imaging applications at 157 nm, as current resist polymers have absorbance of between 1.0-1.5 μm^{-1}.

Impurities in Polymerizations via ROMP

Upon scale-up, it was discovered that crystals formed in situ while the polymer was in a variety of solvents during hydrogenation or purification. In solvents such as dioxane, dichloromethane and isopropyl alcohol, a significant amount of crystals precipitated post-hydrogenation. The first crystals observed are shown below in **Figure**

3.12; it appeared first as the hydrazine salt, then as the sulfone hydrazine-linked dimer of p-toluenesulfonhydrazide. These two crystal structures are the product of TSH undergoing an unusual substitution with 1,2-dichloroethane, the solvent used during the polymerization step.

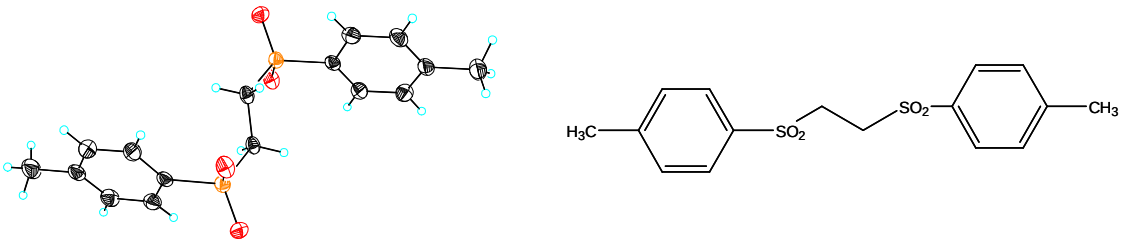

Figure 3.12: Crystal structure of an unexpected p-toluenesulfonhydrazide and 1,2-dichloroethane adduct, an impurity in ROMP polymers after hydrogenation.

Switching solvents for the polymerization step eliminated crystal formation. Instead of 1,2-dichloroethane, xylenes were used, and it was found that further side reactions did not occur during polymerization. However, subsequent ROMP polymers again showed a slow-growing crystal when the polymer was dissolved into a solvent such as isopropyl alcohol or acetone. The newly discovered crystals were again isolated, purified and resolved via X-ray analysis to the structure shown in **Figure 3.13**. This compound, 2-isoproplyidene-1-(p-toluenesulfono)hydrazide, is the product of acetone and TSH, as reported in the literature (Gleason 1998a and 1998b, Dabbagh 1981). It appears that this can occur, in this case, with isopropyl alcohol.

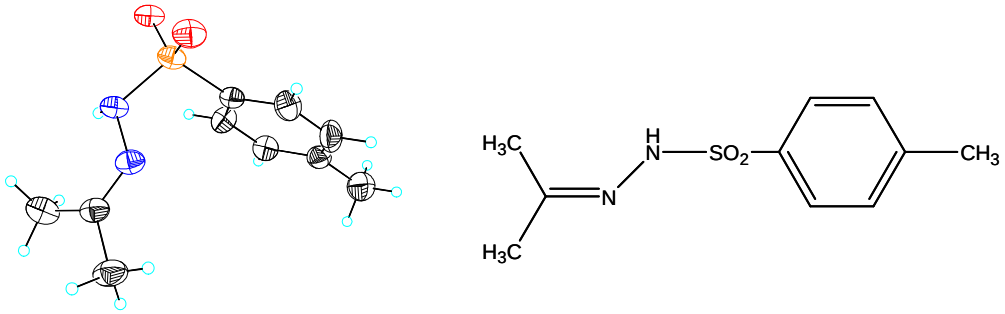

Figure 3.13: Crystal structure of acetone tosylhydrazone, found in hydrogenated ROMP polymers.

Unfortunately, these crystal impurities proved difficult to remove completely from polymer reactions, even upon immediately working up these polymer solutions. Attempts to extract away the crystalline impurities in an acetone-water mixture and then and extracting the polymer with dichloromethane was unsuccessful. Again the TSH crystals still had not been completely removed and crashed out of a polymer solution. Furthermore, each copolymer demonstrated vastly different solubilities, making the creation of a "standard" procedure for dissolution, precipitation and complete dialysis and purification of ROMP polymers slow and exacting at best.

Finally, even with repeated and varied attempts to further purify the homopolymer of DNBHFA, the working model ROMP polymer, its absorbance was found to range between 3.0-3.1 μm^{-1} at 157 nm, and its T_g unchanged at 85 °C. Changing chain transfer agents, precipitation solvents and dialysis solvents were unable to budge the absorbance of any of the ROMP synthesized polymers. Glass transition temperatures of several

copolymers were difficult to measure, likely due to the influence of impurities remaining with the various polymers synthesized (**Figure 3.14**).

In the end, it seemed apparent that ROMP copolymers using the monomer DNBHFA would not yield highly transparent polymers or high enough glass transition temperatures for 157 nm applications. ROMP polymers consistently displayed strong absorbance at 157 nm, and so alternate polymerization methods and materials were examined in lieu of ROMP.

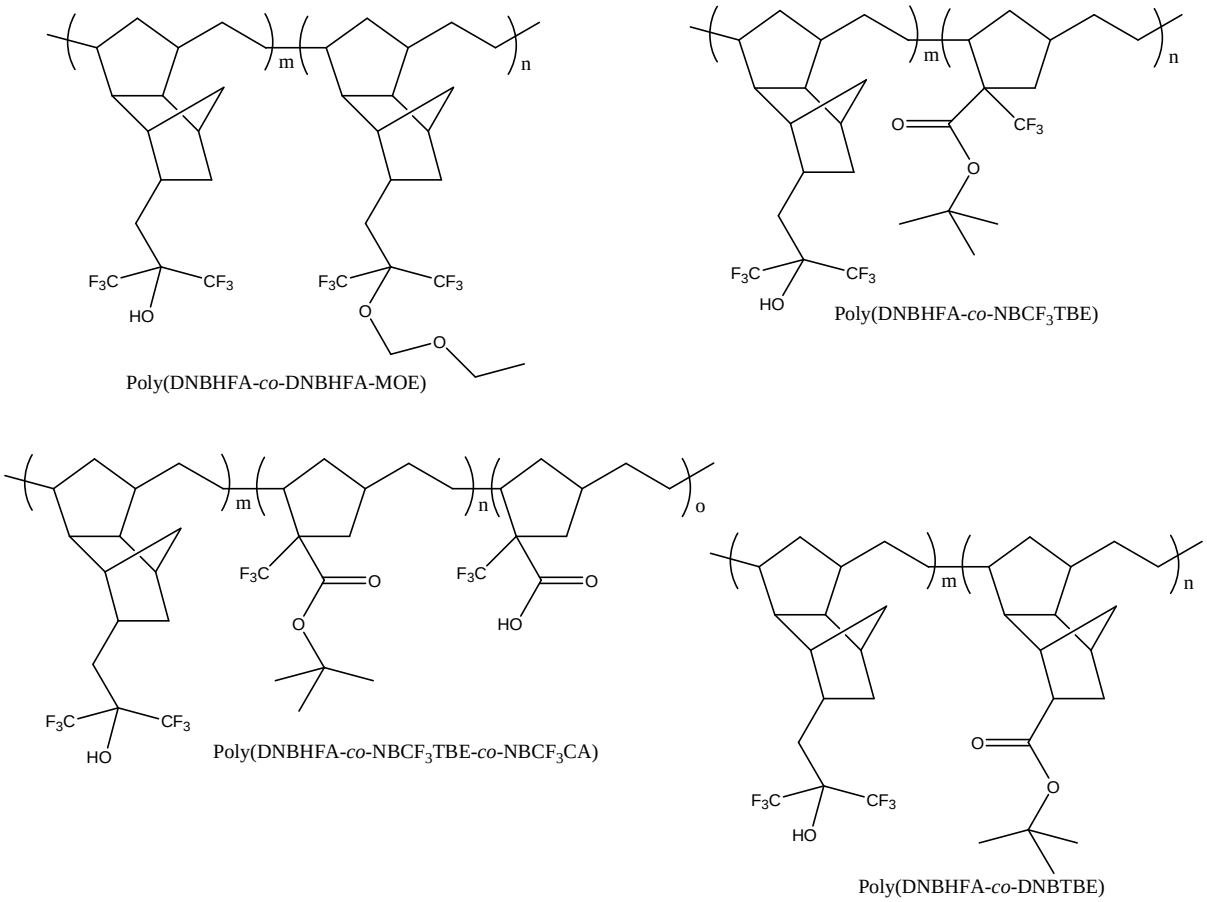

Figure 3.14: The primary set of ROMP copolymers synthesized studies, all found to be too highly absorbing at 157 nm.

Experimental

Materials Nitrogen was purified by passage through KOH, NaOH and Drierite $CaSO_4$. All solvents were dried by the standard methods. All manipulations and polymerizations with air-sensitive materials were performed in a helium-filled drybox or using standard Schlenk vacuum line techniques under argon. All starting materials were procured from Aldrich except (2-trifluoromethyl)acrylic acid (Honeywell Int., Inc.) and dinorbornene hexafluoroisopropanol (DNBHFA) (JSR), and were used as received unless noted otherwise.

Instruments and Equipment Nuclear magnetic resonance (NMR) spectra were obtained using either a Bruker AMX300 or a Varian *Unity Plus 300* spectrometer (^{1}H: 300 MHz, ^{13}C: 75 MHz, ^{19}F: 282 MHz). Shifts for NMR spectra are reported in ppm relative to TMS (for ^{19}F, $CFCl_3$) or to the chemical shift of the solvent. Infrared spectra were recorded on a Nicolet *Avatar 360* IR spectrometer. Melting points are uncorrected. Mass spectra were measured on a Finnigan *MAT TSQ-700* spectrometer. Molecular weights (M_w) and polydispersity indices (PDI) were measured from THF solutions using a Viscotek GPC equipped with a set of two 5 mm crosslinked polystyrene columns (linear mix and 100 Å) from American Polymer Standards and are reported relative to polystyrene standards. Polymers containing acidic functional groups were pretreated with either diazomethane or iodomethane/DBU before GPC measurement, unless noted otherwise. Differential scanning calorimetry (DSC) measurements and thermal gravimetric analysis (TGA) were performed on a Perkin Elmer *Series-7* thermal analysis system. Gas chromatographs were recorded on a Hewlett Packard *5890 Series II* with an *HP-5* (crosslinked 5% PH ME siloxane) capillary column and flame ionization detector (FID).

Synthesis of *tert*-butyl 2-(trifluoromethyl)acrylate In a cold finger (dry ice/acetone) trap was collected approximately 203 mL (120 g, 2.1 mol) of 2-methyl propylene. To a 1 L Parr bomb was added α-trifluoromethylacrylic acid (100 g, 0.71 mol), 7.7 mL H_2SO_4 and approximately 154 mL of diethyl ether. The bomb was cooled in a dry ice/isopropyl alcohol bath (0 °C) under a N_2 blanket. The collected 2-methyl propylene was added to the cold bomb, the bomb was sealed, allowed to warm to room temperature and stir overnight. After 24 h the bomb was vented and the clear, yellow solution was extracted into water (200 mL) and 5% wt. $NaHCO_3$ (200 mL). GC (RT, min): 1.9 (89%). ^{1}H NMR ($CDCl_3$, 300 MHz, ppm): δ 1.50 (s, 9H, t-Bu), 6.30-6.31 (m, 1H, C<u>H</u>=CH_2), 6.57-6.59 (m, 2H, CH=C<u>H</u>$_2$). ^{19}F NMR ($CDCl_3$, 282 MHz, ppm): δ -66.1. IR (NaCl, cm^{-1}): 2980, 2934, 1731 (C=O), 1405, 1365, 1348, 1268 (C-F), 1113, 849. HRMS-CI (*m/z*): $[M + H]^+$ calcd for $C_8H_{11}F_3O_2$, 195.063; found, 195.063.

Synthesis of 2-*tert*-butyl-2-trifluoromethyl-bicyclo[2.2.1]hept-5-ene-3-carboxylate To a 500 mL round bottom flask was added freshly cracked dicyclopentadiene (50 g, 0.75 mol) and α-trifluoromethyl-*tert*-butylacrylate (140 g, 0.71

mol assuming 100 % yield), and the solution was allowed to stir at room temperature. The solution turned from an off-yellow clear color to a lighter white-yellow color, and the solution also became slightly cloudy with some bubbling observed. The product was purified twice by vacuum distillation (b.p.78-80 °C @ 7-8 Torr) to yield the desired product (86.6 g, 46.5 %). GC (RT, min): 4.9, 5.0 (99%). ^{1}H NMR ($CDCl_3$, 300 MHz, ppm): δ 1.41-1.54 (9H, *endo*/*exo* t-Bu), 1.28-3.38 (m, 6H, aliphatic), 6.01-6.03 (m, 1H, CH=CH), 6.25-6.28 (m, 1H, CH=CH). ^{19}F NMR ($CDCl_3$, 282 MHz, ppm): δ -64.7, -67.2. IR (NaCl, cm^{-1}): 3071, 2979, 2887, 1731 (C=O), 1476, 1459, 1394, 1370, 1336, 1283 (C-F), 1225, 1155, 1120, 1100, 1072, 1047, 1038, 1015, 958, 931, 909, 857, 844, 822, 800, 787, 733, 717, 696, 666. HRMS-CI (*m/z*): $[M + H]^+$ calcd for $C_{13}H_{18}F_3O_2$, 263.126; found, 263.126.

Synthesis of 2-trifluoromethyl-bicyclo[2.2.1]hept-5-ene-3-carboxylic acid
Freshly cracked cyclopentadiene (24.8 g, 0.37 mol) and 2-trifluoromethyl acrylic acid (50.0 g, 0.36 mol) were added to a 250 mL round bottom flask. The solution was stirred under a N_2 blanket at room temperature overnight. The solution was initially clear and turned slightly cloudy with a slight exotherm observed. The resulting solution was extracted with two 200 mL portions of 5% $NaHCO_3$ and dried over $MgSO_4$. Rotary evaporation afforded an off-white solid (22.1 g, 29%). GC (RT, min): 6.122, 6.235 (98.1% purity). ^{1}H NMR ($CDCl_3$, 300 MHz, ppm): δ 1.55-1.63 (m, 4H, *endo/exo*), 2.20 (m, 4H), 2.90 (m, 1H), 3.05 (m, 1H), 6.10 (s, 1H, olefin), 6.75 (s, 1H, olefin), 12.0 (m, 1H, acid).

Synthesis of *tert*-Butyl 1,1,1-trifluoro-3-(tetracyclo[6.2.1.1^{3,6}.0^{2,7}]dodec-9-en-4-yl)-2-(trifluoromethyl)2-propyl carbonate (DNBHFABOC)

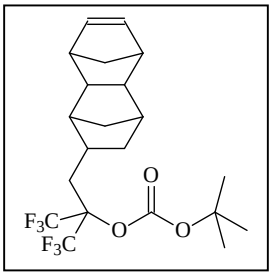

To a 100 mL three-neck round bottom flask under a N_2 blanket was added DNBHFA (5.0 g, 14.7 mmol), 4-dimethylaminopyridine (0.2 g, 1.5 mmol) and 50 mL of dry THF, with a rubber septum to seal the neck and needle used to vent CO_2 outgassing during the reaction. Di-*tert*-butyl-dicarbonate (3.8 g, 17.6 mmol) was added via a 3 mL syringe to the solution. Gas evolution (bubbling) was observed and the mixture was allowed to stir overnight at room temperature. Rotary evaporation of the THF solvent afforded a dark orange liquid. ^{1}H NMR ($CDCl_3$, 300 MHz, ppm): δ 1.20 (2H), 1.53-1.55 (9H), 1.60 (2H), 1.84 (2H), 1.87-1.89 (2H), 2.09-2.11 (2H), 2.20-2.22 (2H), 2.72-.75 (2H), 2.96-2.98 (2H), 5.95 (2H, olefinic).

Synthesis of 1,1,1-trifluoro-3-(tetracyclo[6.2.1.1^{3,6}.0^{2,7}]dodec-9-en-4-yl)-2-(trifluoromethyl)2-methoxyethoxy-propane

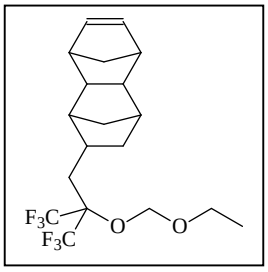

To a 100 mL three-neck round bottom flask under a N_2 blanket was added DNBHFA (3.0g, 8.8 mmol) and butyl lithium (2.5 M in THF, 20.2 mmol) at 0 °C to give a clear, orange solution. The solution was allowed to stir and warm to room temperature. The reaction mixture was then brought to 0 °C once again, and a solution of chloromethyl ethyl ether (2.0 g, 21.1 mmol) was added dropwise to the solution, to give a yellow solution with orange salt precipitating out of solution. The entire reaction mixture was allowed to warm to room temperature and stirred overnight under a N_2 blanket. Product was then taken up into $CHCl_3$ (100 mL), and washed with water (100 mL), $NaHCO_3$ (100 mL), brine (NaCl) (100 mL). The organic phase was dried over $MgSO_4$, isolated by gravity filtration and $CHCl_3$ rotary evaporated. The crude product solution was purified via column chromatography on basic alumina, eluting with a 9:1 mixture of hexane to ethyl acetate. After rotary evaporation of the eluent, purification gave 1.5 g product (45% yield). GC (RT, min): 11.3, 11.4, 11.5 (95%). ^{1}H NMR ($CDCl_3$, 300 MHz, ppm): δ 1.1 (3H), 1.3 (2H), 1.6 (2H), 1.7 (2H), 1.8 (1H), 2.1 (1H), 2.2 (2H), 2.3 (2H), 2.7 (1H), 2.8 (2H), 3.5 (2H), 4.9 (2H), 5.9 (2H, olefinic).

Preparation of ROMP Polymers

A typical ROMP procedure is illustrated by the preparation of poly(DNBHFA) starting with dinorbornene hexafluoroisopropanol:

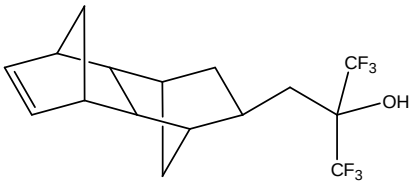

1,1,1-trifluoro-3-(tetracyclo[6.2.1.1^{3,6}.0^{2,7}]dodec-9-en-4-yl)-2-(trifluoromethyl)-2-propanol
Dinorbornene hexafluoroisopropanol (DNBHFA)

General ROMP Polymer Procedure To a 50 mL round bottom flask are added the cyclic olefin-containing monomer, DNBHFA (3.0 g, 8.8 mmol), Grubb's second-generation catalyst (0.002 g, 0.002 mmol), 1,2-dichloroethane (35 mL) and a stirbar. Allyl acetate (0.09 g, 0.88 mmol) chain transfer agent is injected via syringe to this 0.3 M solution to minimize exposure to air. N_2 gas is bubbled through the monomeric solution for 15 min to displace any atmospheric oxygen that may be present. In a separate 10 mL Erlenmeyer flask, N_2 gas is bubbled through approximately 5 mL of additional 1,2-dichloroethane for 15 min. After 15 min, the monomeric solution is heated to 55 °C. The Grubbs catalyst is weighed out and then dissolved in approximately 1.0-1.5 mL 1,2-dichloroethane. This catalyst solution is injected into the heated monomer solution and the entire mixture is stirred for 24 h. The resulting polymer solution is then rotary evaporated to remove solvent and the polymer is immediately hydrogenated according to the procedure below. The polymer was a light brown powder, 2.14 g (71% yield). Before hydrogenation—^{1}H NMR ($CDCl_3$, 300 MHz, ppm): δ 5.5 (m, 2H, CH=CH).

General ROMP Polymer Hydrogenation Procedure One equivalent of the unsaturated DNBHFA ROMP polymer (1.75 g, 5.1 mmol), was added to a round-bottom flask with 2.5 equivalents of p-toluene sulfonhydrazide (2.4 g, 12.8 mmol) and 2.5 equivalents of triethylamine (1.3 g, 12.8 mmol), as well as a sufficient amount of 1,4-dioxane (30 mL) to make a 1 M solution. The reaction flask is equipped with a water condenser under a nitrogen blanket, and the solution refluxed at 130 ºC overnight. Rotary evaporation affords the solid saturated polymer, which is then purified using the general dialysis procedure described below. After hydrogenation—^{1}H NMR ($CDCl_3$, 300 MHz, ppm): δ no peaks between 4.0-6.0 observed, i.e., near quantitative hydrogenation of polymer backbone was accomplished.

General Dialysis Purification Procedure Typical dialysis purification involves dissolving the impure polymer in a minimal amount of solvent (usu. methanol), using 0.6 g of polymer per 1 mL of solvent. This polymer solution is loaded into a dialysis bag of the appropriate molecular weight pore size, typically 1000 MW cutoff pore size. This tube of polymeric solution is placed into a 2 L beaker with stirbar, and 1.0 L methanol is added the dialysis bag stirred. After 12-18 h 1 L of solvent is exchanged for fresh methanol and allowed to stir for another 12-18 h. The dialysis bag is then removed and the contents poured into a 50 mL round bottom flask. All methanol is

then removed using rotary evaporation to yield the purified polymer solid (1.7 g, 97% yield from hydrogenation and dialysis). ^{1}H NMR ($CDCl_3$, 300 MHz, ppm): δ 0.5-0.6 (m, 2H), 0.7-0.8 (m, 2H), 1.0-1.1 (m, 2H), 1.2-1.4 (m, 4H), 1.5-1.6 (m, 4H), 1.7-2.1 (m, 2H), 2.2-2.3 (m, 1H), 2.8-2.9 (s, 1H, -OH). GPC (polystyrene standard, THF): M_w 328800; M_n 160000; PDI = 2.055. DSC: T_g = 85 °C. A_{157} = 3.5 μm^{-1}. Additional purification and optimization yields A_{157} = 3.1 μm^{-1}.

ROMP Copolymers

Poly(1,1,1-trifluoro-3-(tetracyclo[6.2.1.1^{3,6}.0^{2,7}]dodec-9-en-4-yl)-2-(trifluoromethyl)2-propanol)-*co*-[(3-*tert*-butyl-3-tetracyclo[6.2.1.1^{3,6}.0^{2,7}]dodec-9-en-yl) carbonate]) Poly(DNBHFA-*co*-DNBTBE)

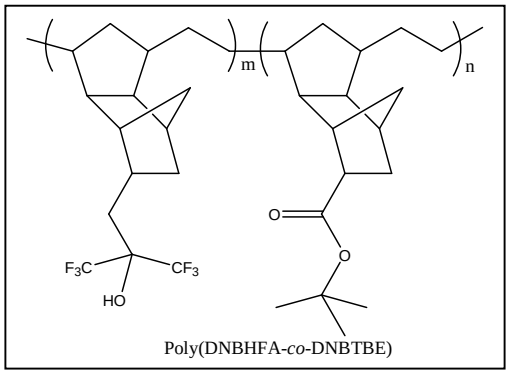

Poly(DNBHFA-*co*-DNBTBE)

To a 100 mL round bottom flask was added DNBHFA (1.5 g, 4.4 mmol), DNBTBE (0.13 g, 0.5 mmol), allyl acetate (0.33 g, 3.3 mmol), 27 mL of 1,2-dichloroethane and a stirbar to afford a 0.3 M solution in 1,2-dichloroethane. Grubb's catalyst (0.002 g, 0.003 mmol) was added according to the above procedure. Precipitation of the polymer into hexanes, methanol and water was attempted on a small scale (1 drop of polymer solution, 5 mL solvent), but yielded little polymer or had the polymer sticking to the vessel walls. The 1,2-dichloroethane solvent was removed by 4 freeze-pump-thaw cycles in liquid N_2 at 400 mTorr to yield a light brown solid (1.49 g, 91% crude yield) and immediately hydrogenated according to the above procedure.

Hydrogenation of poly(DNBHFA-*co*-DNBTBE) To a 100 mL round bottom flask was added poly(DNBHFA-*co*-DNBTBE) (1.49 g, 4.6 mmol), *p*-toluenesulfonhydrazide (2.15 g, 12 mmol), triethylamine (1.17 g, 12 mmol) and dioxane (30 mL) to give a 1.0 M solution in dioxane. The reaction mixture was stirred at 130 °C under reflux (b.p., dioxane 100-102 °C) overnight. The dioxane solvent was rotary evaporated at approximately 35 °C to afford a light brown, viscous solution. Dialysis was performed with methanol per the above procedure to yield 1.2 g of a white powder (80% yield). GPC (polystyrene standard, THF): M_w 6900; M_n 3200; PDI = 2.156. A_{157} = 3.8 μm^{-1}.

Synthesis of poly(1,1,1-trifluoro-3-(tetracyclo[6.2.1.1^{3,6}.0^{2,7}]dodec-9-en-4-yl)-2-(trifluoromethyl)-2-propanol)-*co*-(*t*-butyl 2-trifluoromethyl-norbornene carboxylate) co-(2-trifluoromethyl-norbornene-2-carboxylic acid) Poly(DNBHFA-co-NBCF3TBE-co-NBCF3CA)

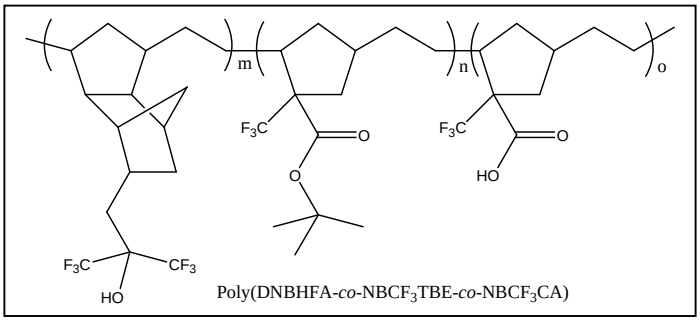

Poly(DNBHFA-*co*-NBCF$_3$TBE-*co*-NBCF$_3$CA)

DNBHFA (5.0g, 14.7 mmol), 2-trifluoromethyl-norbornene carboxylic acid (0.23 g, 1.1 mmol), *t*-butyl 2-trifluoromethyl-norbornene carboxylate (1.8 g, 6.8 mmol), *cis*-1,4-diacetoxy-2-butene (1.2 g, 6.8 mmol), Grubbs second-generation catalyst (0.005 g, 6.0 mmol) and 1,2-dichloroethane (100 mL) were combined in a 250 mL round bottom flask and the general ROMP procedure used to produce a solid polymer (7.0 g, 97%) and immediately hydrogenated according to the above procedure.

Hydrogenation of poly(DNBHFA-co-NBCF3TBE-co-NBCF3CA) To a 100 mL round bottom flask was added the polymer (7.0 g, 23 mmol), *p*-toluenesulfonhydrazide (TSH) (10.6 g, 57 mmol), triethylamine (5.7 g, 57 mmol) and dioxane (35 mL) for an approximately 1.0 M solution. The reaction mixture was stirred at 130 °C reflux overnight. The resulting white solution was rotary evaporated and to afford an off-white solid. The polymer was purified using the above dialysis procedure in methanol to yield a white, crystalline polymer (0.7 g, 10% yield). GPC (polystyrene standard, THF): M_w 9120; M_n 4950; PDI = 1.842. A_{157} = 3.05 μm^{-1}.

Synthesis of Poly(1,1,1-trifluoro-3-(tetracyclo[6.2.1.1^{3,6}.0^{2,7}]dodec-9-en-4-yl)-2-(trifluoromethyl)2-propanol)-*co*-(2-*tert*-butyl-2-trifluoromethyl-bicyclo[2.2.1]hept-5-ene-3-carboxylate) Poly(DNBHFA-*co*-NBCF$_3$TBE)

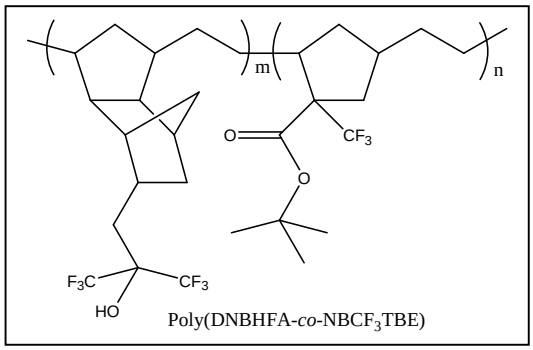

Poly(DNBHFA-*co*-NBCF$_3$TBE)

To a 100 mL round bottom flask was added DNBHFA (1.5 g, 4.4 mmol), NBTBE-CF3 (0.3 g, 1.1 mmol), allyl acetate (0.33 g, 3.3 mmol), 30 mL of 1,2-dichloroethane and a stirbar to afford a 0.3 M solution in 1,2-dichloroethane. Grubb's catalyst (0.002 g, 0.003 mmol) was added according to the above procedure used to produce a solid polymer (1.8 g, 98% yield) that was immediately hydrogenated according to the above procedure.

Hydrogenation of poly(DNBHFA-*co*-NBCF$_3$TBE) To a 100 mL round bottom flask was added poly(DNBHFA-*co*- NBCF$_3$TBE) (1.5 g, 4.6 mmol), *p*-toluenesulfonhydrazide (2.2 g, 12 mmol), triethylamine (1.2 g, 12 mmol) and dioxane (30 mL) to give a 1.0 M solution. The reaction mixture was stirred at 130 °C under reflux overnight. The dioxane solvent was rotary evaporated at 35 °C to afford a light brown, viscous solution. Dialysis was performed with methanol per the above procedure to yield a white polymer (1.2 g, 80% yield). GPC (polystyrene standard, THF): M_w 44700; M_n 17700; PDI = 2.525. $A_{157} = 3.18\ \mu m^{-1}$.

Synthesis of poly(1,1,1-trifluoro-3-(tetracyclo[6.2.1.1^{3,6}.0^{2,7}]dodec-9-en-4-yl)-2-(trifluoromethyl)2-propanol)-*co*-(1,1,1-trifluoro-3-(tetracyclo[6.2.1.1^{3,6}.0^{2,7}]dodec-9-en-4-yl)-2-(trifluoromethyl)2-methoxyethoxy-propane) Poly(DNBHFA-co-DNBHFA-MOE)

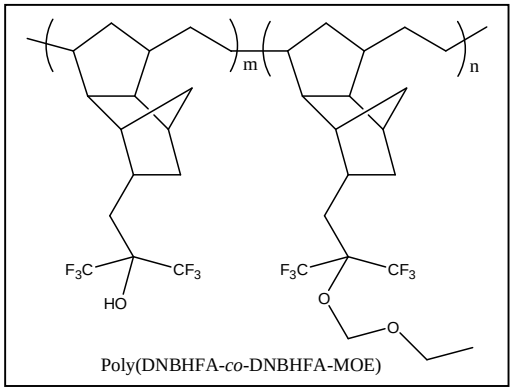

Poly(DNBHFA-*co*-DNBHFA-MOE)

To a 100 mL round bottom flask was added DNBHFA (1.5 g, 4.4 mmol), DNBHFA-MOE (0.54 g, 1.1 mmol), allyl acetate (0.16 g, 1.6 mmol), 25 mL of 1,2-dichloroethane and a stirbar to afford a 0.3 M solution in 1,2-dichloroethane. Grubb's catalyst (0.001 g, 0.001 mmol) was added according to the above procedure to produce an off-white polymer (1.0 g, 67% yield) and immediately hydrogenated according to the above procedure.

Hydrogenation of Poly(DNBHFA-co-DNBHFA-MOE) To a 100 mL round bottom flask was added poly(DNBHFA-*co*-DNBHFA-MOE) (1.5 g, 4.2 mmol), *p*-toluenesulfonhydrazide (2.0 g, 10.5 mmol), triethylamine (1.1 g, 10.5 mmol) and dioxane (25 mL) to give a 1.0 M solution in dioxane. The reaction mixture was stirred at 130 °C under reflux overnight. The dioxane solvent was rotary evaporated at 35 °C to afford a light brown, viscous solution. Dialysis was performed with methanol on 0.8 g of hydrogenated polymer, per the above procedure to yield a light yellow crystalline solid (0.2 g, 23% yield). GPC (polystyrene standard, THF): M_w 26600; M_n 9800; PDI = 2.714. $A_{157} = 3.05\ \mu m^{-1}$.

Chapter 4—Tricyclononene and Difluoronorbornene Systems for Addition Polymerizations using Palladium Catalysts

Addition Polymerization

Polynorbornenes have many attractive properties for research purposes: high transparency in the optical and UV wavelength ranges, high glass transition temperatures and a high refractive index (Hennis 2001, Haselwander 1996). Most polynorbornenes exhibit high solubility in a range of organic solvents, and can easily be spin-coated to provide homogeneous, amorphous thin films on silicon substrates. Many types of these polynorbornene systems have been used as photoresist materials already: they find significant use as 193 nm resists in research and industry (Okoroanyanwu 1997). Polynorbornenes are readily formed when using transition metal addition catalysts, typically palladium or nickel-based initiators. Our research group has used nickel catalysts previously (Yamada 2000), but palladium catalysts were preferred due to better molecular weight control during polymerizations. Molecular weight control was accomplished by varying the catalyst loading for each particular polymerization (Hung 2001).

There are a variety of available palladium-based catalysts. From simple catalysts such as palladium chloride ($PdCl_2$) to the various (η^3-allyl)palladium(II) type catalysts, there are many available for different addition polymerizations. Palladium catalysts are particularly popular due to their tolerance of a wide range of functional groups, especially photoresist functional groups such as carboxylic acids, alcohols and ethers. There is no

opening of the olefin-containing ring, just simple addition across the olefin as polymerization proceeds (**Figure 4.1**). Activity of the catalyst can drastically change depending on the *endo/exo* ratio of functional groups pendant to th e norbornene monomers. Polar functional groups (*e.g.,* carbonyl-containing groups) can readily coordinate to the metal center, reducing catalyst activity. Pure *exo*-norbornene monomers typically give higher yielding polymerizations (Hennis 2001).

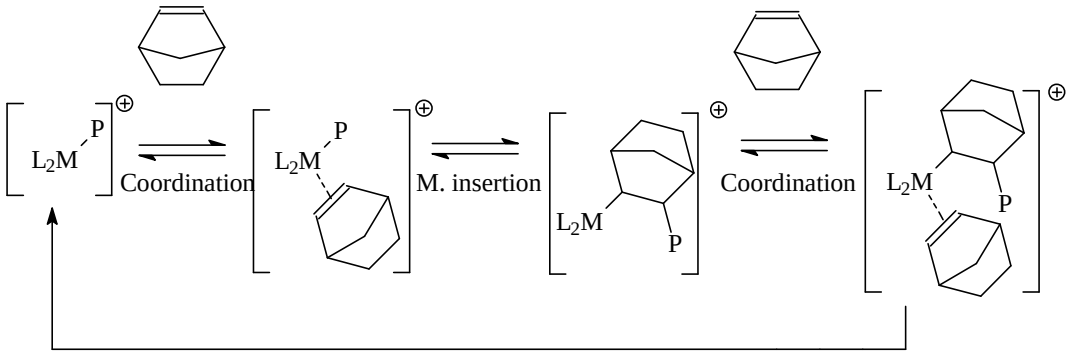

Figure 4.1: The mechanism for the addition polymerization of norbornenes (Hung 2001).

Polymerization is initiated by approach of the active metal-alkyl complex as the catalyst approaches the norbornene from the least hindered, *exo* face on the olefin side of the bicyclic system. The norbornene inserts migratory into the metal-alkyl bond, and this cycle continues until termination occurs. This is brought about by classical β-hydride elimination. Elimination yields the active metal-hydride complex, with the terminus of the polymer a double bond. Fortunately, the same *cis-exo* complex formed during polymerization of a norbornene effectively blocks access to the β-hydride of the ring system. This leads to high molecular weight polymer, unless controlled with chain

transfer agents or varying the amount of catalyst loading for the reaction (Cossee 1964, Hughes 1973).

The palladium catalyst of choice for 157 nm materials was first reported to give greater than 70% conversion for mostly *endo* norbornene monomers (80/20 *endo/exo*) (Mathew 1996). This is one of the previously mentioned (η^3-allyl)palladium(II) type catalysts, which forms an *in situ* active complex with weak coordination anions such as hexafluoroantimonate or tetrafluoroborate. The steric bulk and weakly anionic nature of these two groups leads to the higher activity of the catalyst complex.

Unfortunately, this catalyst complex, while still functional group tolerant like most palladium initiators, generates strong acid during the polymerization process. This acid is strong enough to cleave *t*-butyl ester and *t*-BOC groups on the growing polymer chain (Sanders 2003). Since water is required for acetal cleavage, any acetal protecting groups are safe from such cleavage. It is suspected that reduction of the palladium metal to Pd(0) generates an acidic proton, which forms the strong acid $HSbF_6$ or HBF_4 from the counteranion. Either of these acids is strong enough to promote such deprotection in the polymer.

In order to avoid having to polymerize norbornenes with unprotected acidic functional groups, polymer-bound proton sponges were used during the polymerization to quench the acid as it is generated during polymerization. This was successful and produced polymer of controlled molecular weight with protecting groups intact (Tran 2002).

Palladium Catalyst Preparation

[(η^3-Allyl)palladium(II)][SbF6] was prepared *in situ* using a modified literature procedure (Mathew 1996, Hung 2001) (**Figure 4.2**). One equivalent of ally palladium chloride dimer was mixed with two equivalents of silver hexafluoroantimonate in a dry box; dichloromethane was added via cannula transfer and the mixture stirred for 15 min. The resulting precipitate (silver chloride salts) were removed with an inline 0.45 mm syringe filter as the resultant yellow [(h3-Ally)palladium(II)][SbF6] catalyst solution was generated and cannula transferred to a monomer solution. Polymerization typically takes 72 h for high conversion of polymer.

Figure 4.2: In situ preparation of [(h3-Ally)palladium(II)][SbF6] (Yamada 2000, Hung 2001).

Addition Polymerization Issues with 157 nm Monomers

The inability to polymerize norbornene compounds such as 2-(trifluoromethyl)bicyclo[2.2.1]hept-5-ene-2-carboxylic acid methyl ester led the search into alternate polymerization techniques (ROMP), already described in Chapter 3, and free radical copolymerizations, which resulted in strongly absorbing polymeric material at 157 nm. This search also led to modifying norbornene-type systems to facilitate polymerization using addition metal catalysts.

The inability of metal addition catalysts to polymerize these geminally disubstituted norbornenes is thought to stem from a few key factors: steric hindrance

from the *endo* functional group influences the opposite olefinic hydrogen, this hinders the catalyst's approach from the *exo* face of the norbornene. Any substituents on the norbornene that have polar functionality can chelate to any catalyst that might be near the *endo* face of the norbornene, effectively neutralizing the activity of the catalyst. Finally, simple induction from any fluorine substituents will decrease the electron density of the olefin, rendering the norbornene less reactive to polymerization (**Figure 4.3**).

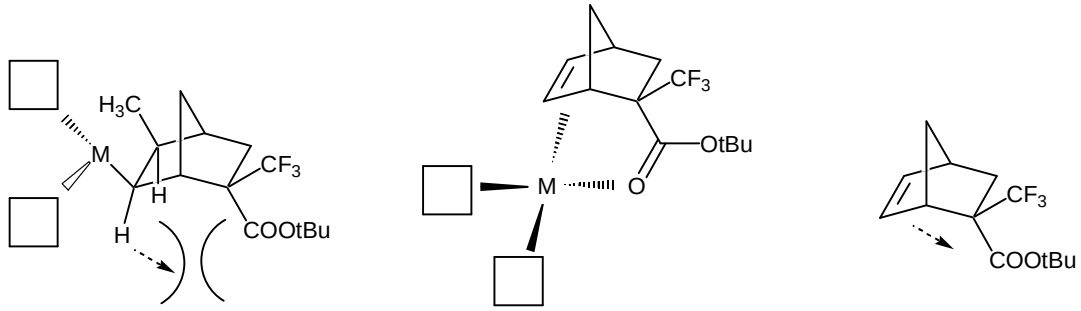

Steric influence of geminal substituents can crowd the incoming catalyst

Chelation of the catalyst with polar functionalities on the norbornene

Induction from fluorine substituents effectively deactivates the catalyst

Figure 4.3: Possible rationales for inactivity of geminally disubstituted norbornenes with addition catalysts: sterics, chelation and electronics.

It is possible to physically move the functional groups themselves further away from the olefin. As described earlier, ROMP was one such example of moving the functional groups away from the olefin by using dinorbornene cyclic systems. However, it is also possible to move the functional groups further from the olefin using a different ring system, known as tricyclononanes (TCN). Attempts to polymerize and image TCN

copolymer systems with norbornene hexafluoroisopropanol (NBHFA) were then examined.

It was also hoped that simple fluorine incorporation, instead of a trifluoromethyl group, would lead to a more transparent material that could still be polymerized via conventional transition metal addition catalysts. This led to difluoronorbornene hexafluoroisopropanol systems, with fluorine incorporation at the 2 and 7 positions of the norbornene system, examination of the V-UV spectra and subsequent polymerization attempts.

Tricyclononene Systems for 157 nm

Recent reports by Grubbs *et al* showed that instead of using similarly functionalized norbornenes in metal-catalyzed addition polymerizations with ethylene, one could instead use an analogous tricyclo[4.2.1.$0^{2,5}$]non-7-ene (TCN) monomer (Connor 2002). Over 30 mol% of a TCN monomer containing a polar functional group was incorporated into polymer using traditional addition catalysts. The increased amount of TCN inclusion into polymer is due to the increased distance of the geminal substituents from the olefin, as well as added ring strain due to the added cyclobutane ring. Further, that cyclobutane ring is 100% *exo* relative to the norbornene skeleton, all of which culminates and allows for metal-catalyzed polymerization of the tricyclononene.

These tricyclononene adducts are formed by the thermal [$2\sigma + 2\sigma + 2\pi$] cycloaddition of quadricyclane (tetracyclo[3.2.0.$0^{2,7}$.$0^{4,6}$]heptane) with a variety of dieneophiles, such as alkenes and alkynes (Smith 1966, Prinzbach 1967 and 1968, Rieber 1969, Tabushi 1972, Noroyi 1975). There are other methods to form TCN type materials.

Metal can catalyze certain [2π + 2π] cycloadditions can also occur to produce a mixture of tricyclononenes in which the cyclobutane ring appears be in either the *exo* or the *endo* configuration (Schrauzer 1964). This results in a mixture of *exo* and *endo* isomers, however, and this TCN structure is unable to be polymerized using either nickel or palladium initiators (McBee 1956). Therefore, the quadricyclane pathway described here remains as the most accessible and reasonable method to produce monomers able to polymerize via addition catalysts.

There is a variety of electron-deficient olefins that can be used in the cycloaddition reaction with quadricyclane. This obviously favors investigation of TCN structures for use in 157 nm photoresist polymers. It also permits the use of TCN monomers in much the same way as norbornenes are used for 193 nm resist synthesis. The synthesis, characterization, absorbance and lithographic properties of TCN monomers and polymers will be presented here (**Figure 4.4**).

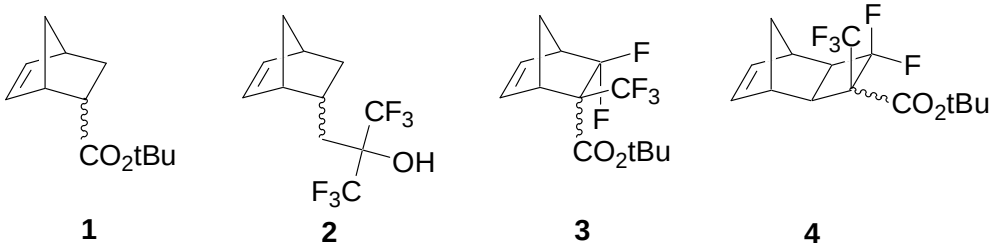

Figure 4.4: Norbornene-type monomers for lithography applications.

Synthesis of TCN Monomers

A series of tricyclononene compounds were synthesized from quadricyclane and the appropriate olefin as shown in **Scheme 4.1**. The method for numbering the carbons

of the TCN system is shown below (**Figure 4.5**). The functional groups located at C(3) of the cyclobutane ring is *syn* or *anti* to the C(1)-C(2) bond. As the cyclobutane ring is constantly referred to as *exo*, this serves to clear up some confusion.

The TCN compounds were made with disubstituted olefins, usually with a trifluoromethyl group or fluorines to aid in transparency at 157 nm. Esters with an easily removable *t*-butyl protecting group to function as a solubility switch. However, methyl esters of fluorinated acrylates were readily available from commercial sources and so these were used to synthesize TCN adducts for model V-UV studies after hydrogenation. The *t*-butyl ester can readily be accessed through base hydrolysis of the methyl ester, followed by esterification with isobutylene.

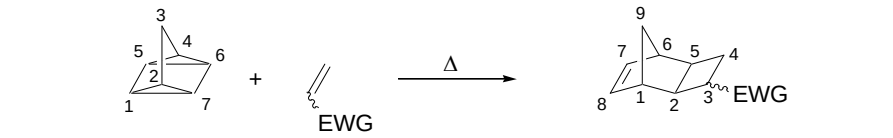

Tetracyclo[3.2.0.0^{2,7}.0^{4,6}]heptane
(Quadricyclane)

3-EWG-tricyclo[4.2.1.0^{2,5}]non-7-ene

Figure 4.5: Cyclizations of quadricyclane with electron deficient olefins (EWG = electron withdrawing group).

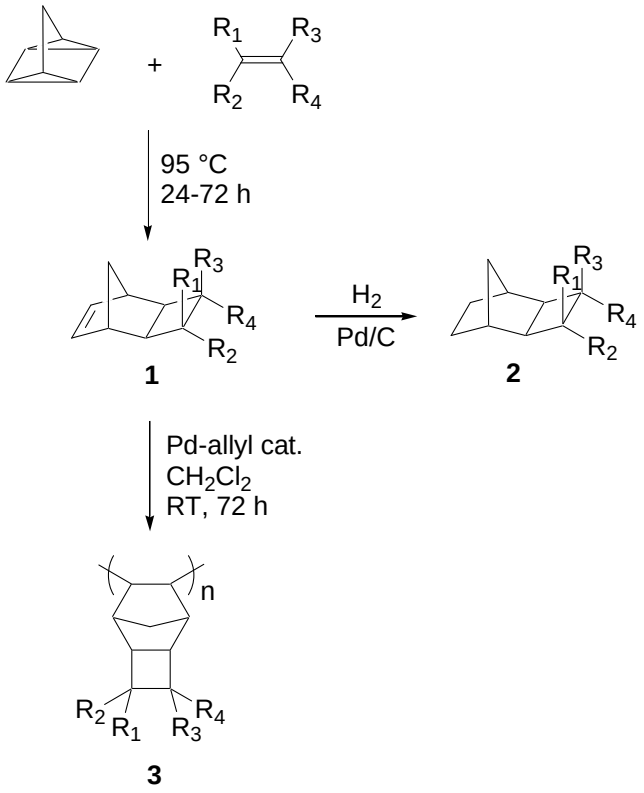

Scheme 4.1: Synthesis of TCN monomers, model compounds, and polymers.

The only side products of the cyclization reaction are norbornadiene (which quadricyclane isomerizes to over time) and a small amount of acrylate homopolymer.

Quadricyclane and methyl 2-(trifluoromethyl)acrylate were reacted to form the TCN adduct with a final, purified yield of 85-90% product. Fluorinated acrylates are less prone to radical polymerization, and no polymeric side products were detected. However, the reaction of methyl 3,3-difluoro-2-(trifluoromethyl)acrylate and quadricyclane, resulted in a much lower yield (~30%) of the TCN adduct. Fortunately, the reaction yield was increased to 78% after several days of reaction time. This is not without precedent; cycloadditions with furan only reach higher yields after extended

reaction time (Leroy 1990). More work is necessary to rationalize the slow cyclization of quadricyclane with this heavily fluorinated acrylate.

V-UV Spectroscopy of TCN Adducts

The biggest concern in the synthesis of these fluorinated TCN monomers was whether or not the added cyclobutane ring would strongly impact the transparency of the monomer. To this end, both the trifluoro- (3F) and pentafluoro-(5F)TCN methyl ester adducts were hydrogenated, purified by distillation, dried and degassed for V-UV analysis. The gas phase results were extremely encouraging. Both TCN adducts demonstrate very high transparency at 157 nm, even more transparent than norbornane (**Figure 4.6**). When compared to 2,2-difluoronorbornane, the TCN adducts are more strongly absorbing, but the initial hydrogenated monomers demonstrated a high transparency that validated using them in copolymers with norbornane hexafluoroisopropanol (NBHFA).

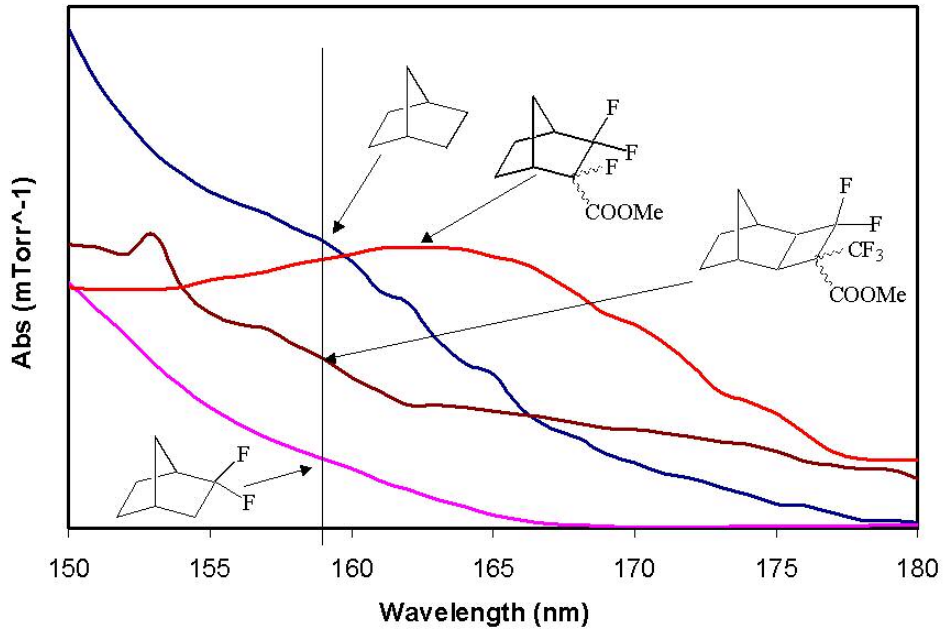

Figure 4.6: Vacuum UV spectra of a model tricyclononane structure.

In order to see if TCN monomer transparency led to transparent polymers for use at 157 nm, homopolymers of both the 3F and 5F TCN methyl esters were synthesized. VASE was used again to analyze the absorbance spectra of the resulting addition polymers.

TCN Homopolymers and Copolymers

Norbornene polymers are typically made using transition metal catalyst initiators, usually with nickel or palladium centers, for polymerization (Goodall 1995 and 1998, Safir 1995, Sen 1988, Rhodes 2001, Lin 1985, Gastinger 1980). As described earlier, the 3F and 5F TCN methyl ester monomers were polymerized for VASE transparency measurements and later imaging experiments. The TCN monomers were polymerized using a catalyst first reported by Risse, a cationic palladium allyl hexafluoroantimonate

catalyst, (η^3-allyl)Pd(II)(SbF_6) (Mathew 1996). The polymerization of the fluorinated TCN monomers was done at room temperature and typically ran for 72 hours; ^{1}H NMR was used to monitor complete disappearance of monomer.

The polymerization of TCN materials is slower than the analogous norbornene compounds when using palladium catalysts (Mathew 1996, Breuning 1992). However, conversion is acceptable, and the resulting polymers have high glass transition temperatures and a complete lack of any olefin peaks in the ^{1}H NMR. Molecular weight and polydispersities are relatively moderate (PDI 1.7-2.7), typical of polymerizations with palladium catalysts (Hennis 2001, Lipian 2000, Heinz 1998). Since the TCN homopolymers were found to have such similar properties to their norbornene analogues, the next step was VASE analysis for transparency in the polymer state.

VASE Analysis of TCN Homopolymers

Removal of the palladium from the polymer chains by treatment with hydrogen followed by filtration and multiple precipitations produced polymer sufficiently clean for VASE analysis (**Figure 4.7**). The homopolymer of *tert*-butyl bicyclo[2.2.1]hept-5-ene-2-carboxylate, norbornene *t*-butyl ester (NTBE), a common monomer for 193 nm resists, has an absorbance coefficient at 157 nm of 6.02 μm^{-1}, compared to the homopolymer of NBHFA, which is around 1.14 μm^{-1}. In any copolymer of these two monomers, even small amounts of the highly absorbing ester-containing monomer will raise the overall absorbance of the polymer considerably. In comparison, the homopolymer of methyl 3-(trifluoromethyl)tricyclo[4.2.1.$0^{2,5}$]non-7-ene-3-carboxylate possesses an absorbance coefficient of 3.79 μm^{-1}at 157 nm. The addition of the trifluoromethyl group alpha to the

ester increases the transparency of the material by approximately 2 orders of magnitude. The further incorporation of fluorine in the homopolymer of 4,4-difluoro-3-(trifluoromethyl)tricyclo-[4.2.1.$0^{2,5}$]non-7-ene-3-carboxylate serves to increase the transparency of the homopolymer by another order of magnitude (A_{157} = 2.86 μm^{-1} at 157 nm).

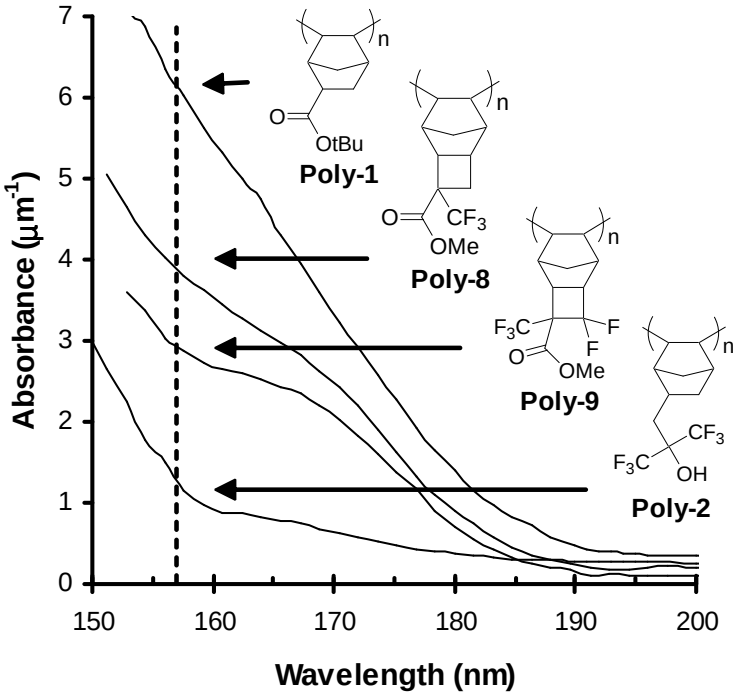

Figure 4.7: VASE spectra of TCN homopolymers.

There is an interesting discrepancy in absorbance between 3F-TCN methyl ester homopolymers made using differing initiators: *t*-butyl peroxide (radical), palladium (addition) catalyst and the Grubbs second-generation ruthenium catalyst (ROMP) (**Figure 4.8**). As seen by VASE, the ROMP polymer has the highest absorbance,

followed by the free radical polymer, while the addition polymer has the lowest absorbance of all.

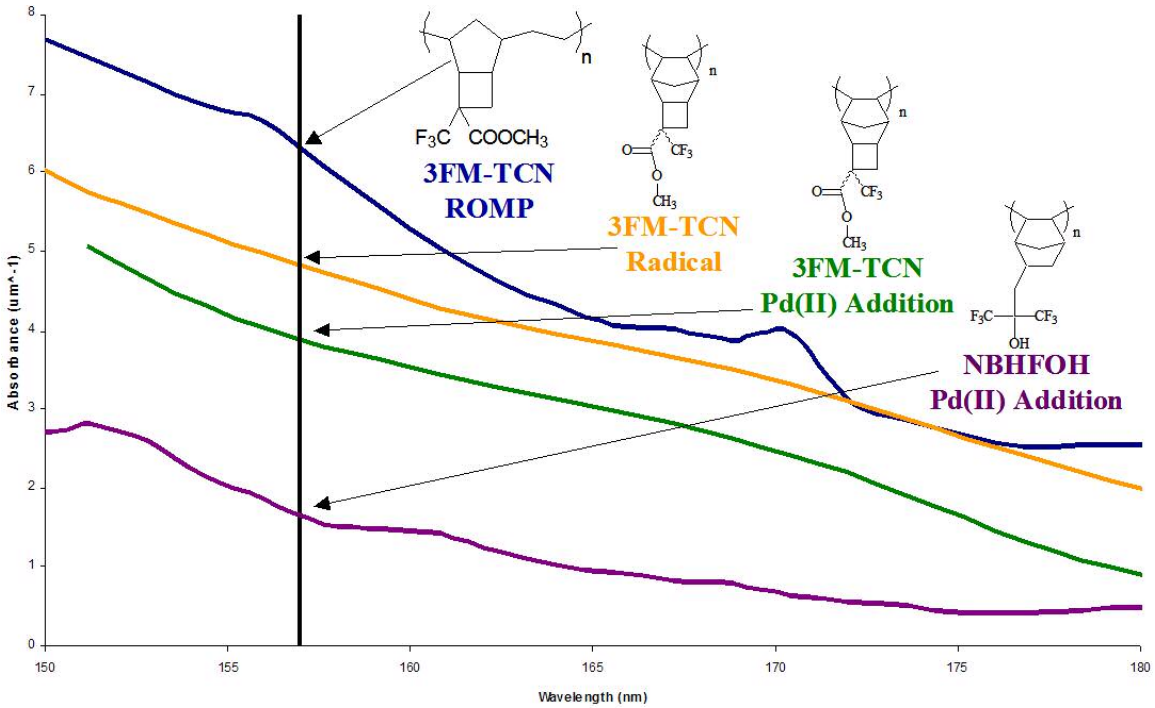

Figure 4.8: VASE spectra of 3F-TCN homopolymers prepared with different initiators; the addition polymer is the most transparent making it an attractive polymerization route.

157 nm Imaging Experiments using TCN Copolymers

Copolymers from monomers NBHFA and methyl 3-(trifluoromethyl)tricyclo[4.2.1.$0^{2,5}$]non-7-ene-3-carboxylate (3F TCN) were made for initial imaging studies. Copolymer ratios were determined by thermalgravimetric analysis, and the final monomer ratios of the polymer is close to that of the initial feed ratio. This demonstrated that the ratio of monomer components in the copolymer could be controlled when using the palladium addition catalyst. The VASE spectroscopy

results for the TCN copolymers absorbance are shown in **Figure 4.9**. Preliminary imaging experiments using these copolymers indicated high performance printing could be obtained with such TCN systems (**Figure 4.10**). The first imaging experiments at 157 nm produced 90 and 80 nm features. Copolymers incorporating the more transparent methyl 4,4-difluoro-3-(trifluoromethyl)tricyclo-[4.2.1.$0^{2,5}$]non-7-ene-3-carboxylate (5F TCN) monomer should also improve imaging performance at 157 nm.

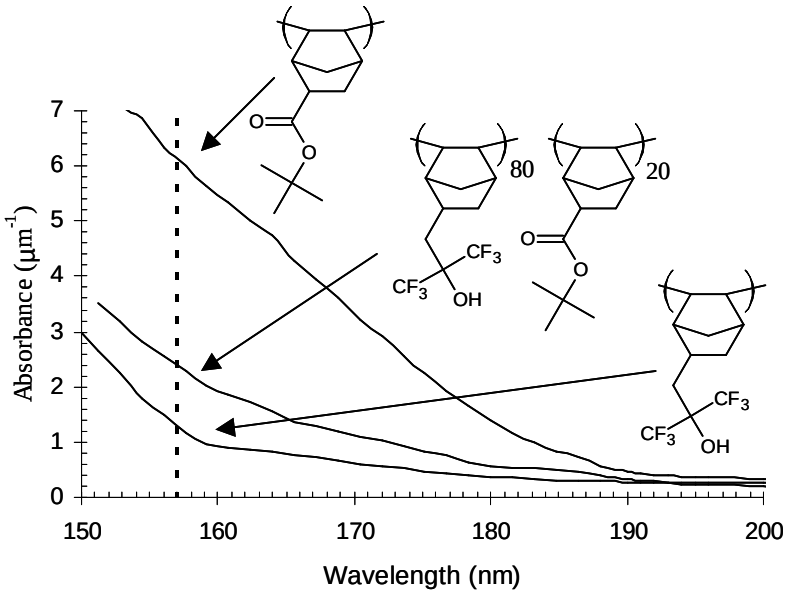

Figure 4.9: VASE spectra of TCN copolymers.

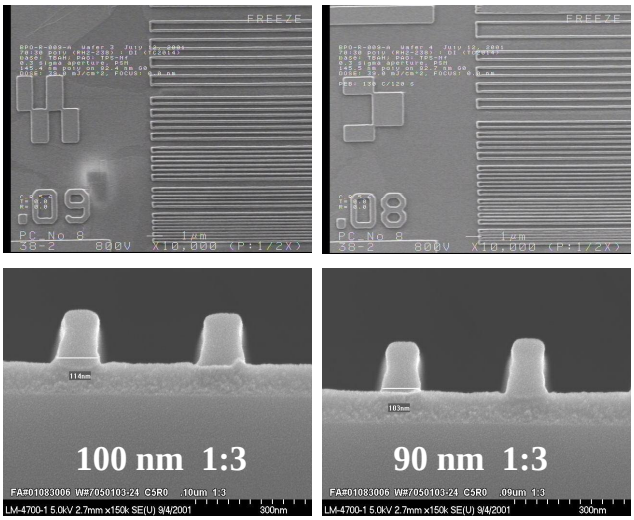

Figure 4.10: Scanning electron micrographs of images in resist formulated from NBHFA/TCNCF$_3$TBE copolymer.

Tricyclononene Conclusions

The use of partially fluorinated tricyclo[4.2.1.0^{2,5}]non-7-ene monomers containing ester functionalities enabled the use of metal-catalyzed addition polymerizations, resulting in copolymers with well-controlled copolymer ratios, low molecular weights (with high molar loading of initiator), and low monomeric and polymeric absorbance at 157 nm. A variety of non- and partially-fluorinated methacrylic acid esters undergo cyclization with quadricyclane to give moderate to excellent yields of the resultant TCN compound. In particular, monomer synthesis proceeded in high yields of the methyl 3-(trifluoromethyl)tricyclo-[4.2.1.0^{2,5}]non-7-ene-3-carboxylate and, with additional reaction time, methyl 4,4-difluoro-3-(trifluoromethyl)tricyclo-[4.2.1.0^{2,5}]non-7-ene-3-carboxylate, which was hydrolyzed in base and then esterified to yield the *t*-butyl ester functionalized TCNs. The 100% *exo*-configuration of the fused cyclobutane ring increases ring strain, which in turn may help increase the reactivity of the olefin towards polymerization. The

TCN structure also places the crowded geminal substituents one carbon removed from the double bond, minimizing any steric and/or electronic effects that may hinder polymerization.

This monomer pathway provided a good compromise for norbornene-like 193 nm structures that maintain low absorbance at 157 nm. Polymerization is initiated readily using palladium or nickel catalysts, whereas the analogous norbornene monomers yield no polymer with the same initiators. The impact of selective fluorination shows the low absorbance of model TCN monomers, while VASE measurements on the resultant homopolymers reveal the high transparency that fluorination imparts. Copolymers of NBHFA and the methyl 3-(trifluoromethyl)tricyclo-[4.2.1.$0^{2,5}$]non-7-ene-3-carboxylate resulted in an imageable, low absorbance resin which was successfully printed at 157 nm to produce 90 and 80 nm features sizes in a 145 nm thick film.

Bicyclic [2.2.1] and [2.2.2] Compounds

The synthesis of materials containing the hexafluoroisopropyl alcohol (HF*i*P) group with applications towards the microelectronics industry has been an ongoing investigation within academia and industry these past few years. Incorporation of the HF*i*P group has been shown to decrease the absorbance of compounds at 157 nm, and is acidic enough (pKa • 11) to behave as a solubility switch during lithographic development stages (Patterson 2000, Chiba 2000, Brodsky 2000).

The synthesis of 3-(1,1,1-trifluoro-2-(trifluoromethyl)-2-propanol)-bicyclo[2.2.1]hept-5-ene (NBHFA) is known (Hung 2001), and was one of the early compounds studied for use at 157 nm (**Figure 4.11**). Although NBHFA looked

promising for microlithography applications, reported absorbance values for the monomer in the gas phase and polymer VASE spectra (Tran 2002) are too strong to be useful for 157 nm lithography.

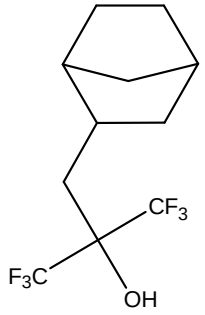

1

Figure 4.11: The NBHFA monomer and polymer, although promising at first, revealed too strong an absorbance at 157 nm.

The incorporation of fluorine into molecules has shown to decrease those same molecules absorbance at 157 nm (Kunz 1999), and based on these findings the incorporation of fluorine into the bicyclic structure of NBHFA (**1**) was viewed as a viable method for improving the transparency of NBHFA, while retaining the beneficial functionality of the HF*i*P group. The synthetic approach used in the difluorination of **1** focused on geminal substitution at the 2 and 7 positions.

To gain an understanding of the potential use of new HF*i*P containing monomers two new NBHFA analogues were synthesized in order to study the affect that increased fluorine content had on absorbance at 157 nm, as well as compare their vacuum ultraviolet absorbance spectrum to TD-DFT calculated spectra. Whereas the vacuum ultraviolet absorbance measurements and TD-DFT calculations are currently ongoing, the synthesis is completed, and reported herein. In addition to [2.2.1] systems, a [2.2.2] system containing the HF*i*P group was also investigated.

Bicyclic[2.2.1] Systems

The difluorination at the 7 position of NBHFA (**Figure 4.12**) was accomplished through the cycloaddition of 1,2,3,4-tetrachloro-5,5-dimethoxy cyclopentadiene and 1,1,1-trifluoro-2-(trifluoromethyl)pent-4-en-2-ol in a Parr reactor heated to 155 ºC. The Diels-Alder adduct (**2a**) underwent dechlorination with Na metal and *t*-butyl alcohol to give **2b**.

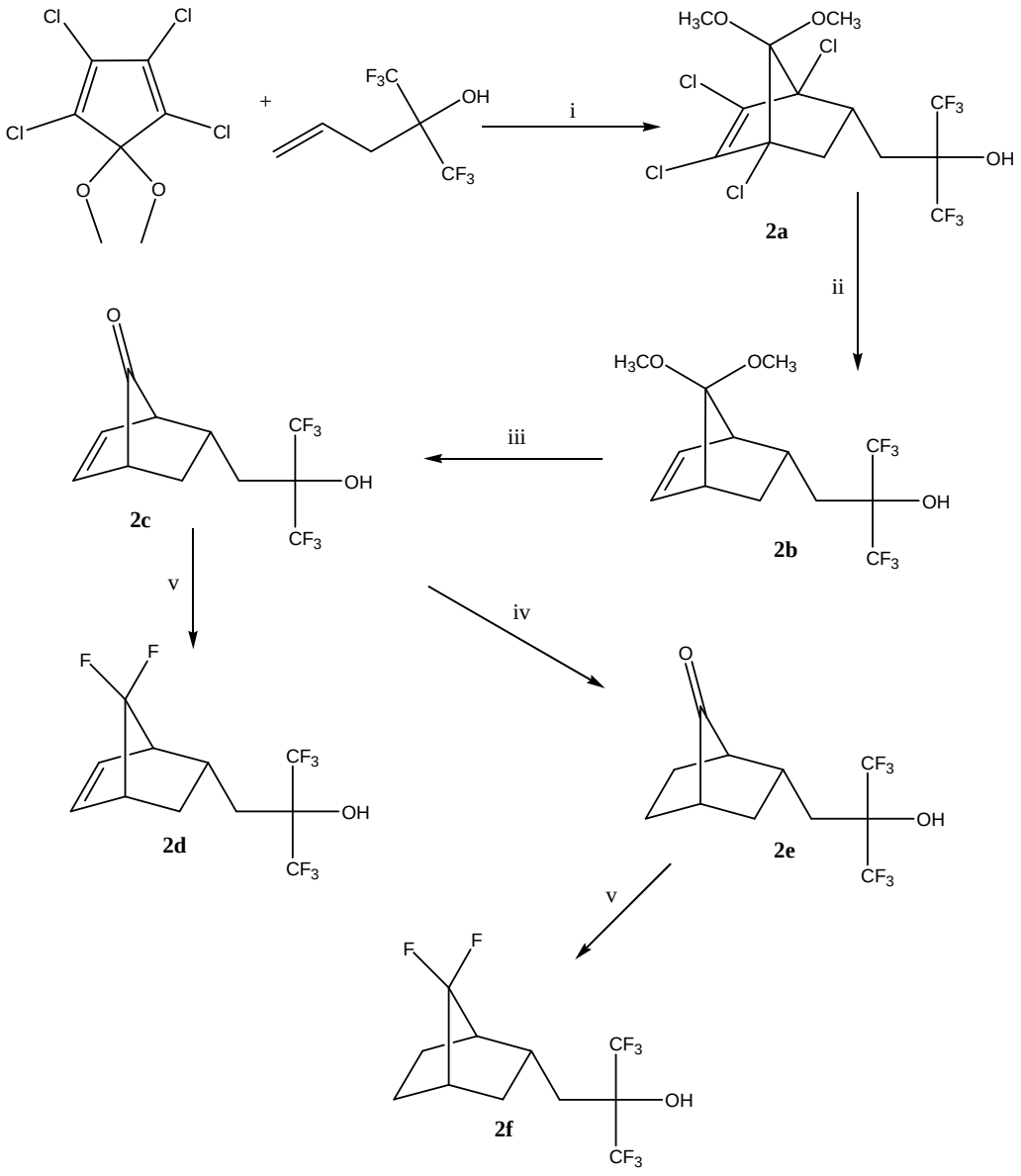

Figure 4.12: (i) 155 ºC for 24hrs, (ii) Na/*t*-butanol, (iii) HCl/dioxane reflux (iv) Pd/C, H_2 (v) DAST.

The ketal (**2b**) was hydrolyzed to the ketone (**2c**) of which crystals suitable for X-ray analysis was obtained (**Figure 4.13**).

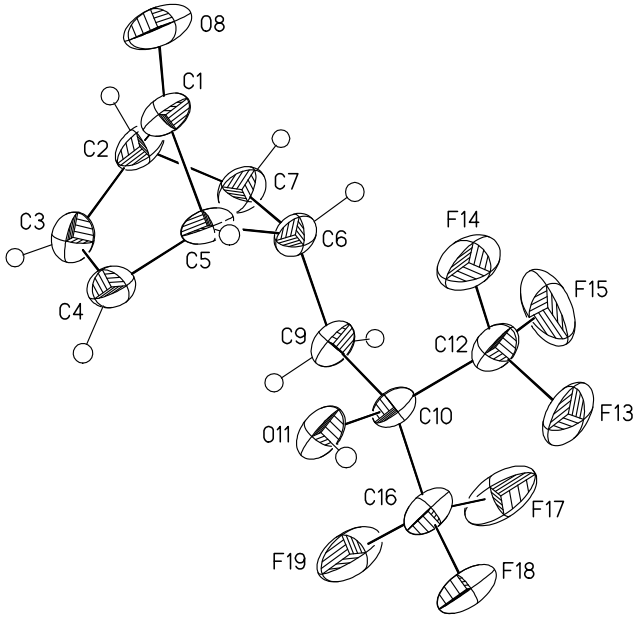

Figure 4.13: View of ketone 2c showing the atom-labeling scheme. Displacement ellipsoids are scaled to the 50% probability level.

DAST was used to convert **2c** to the unsaturated 7,7-difluoro product **2d**. The reduction of the olefin in **2d** was not successful using Pd/C. In all reactions ran, only the starting material was recovered. Therefore, the synthesis of **2f** required the reduction of the olefin prior to fluorination with DAST. The ketone **2c** was reduced via Pd/C to give **2e**, which then underwent fluorination with DAST to give the 7,7-difluoro product (**2f**).

The inability of **2d** to undergo Pd catalyzed reduction was underscored when attempts at polymerization were initiated. The use of Pd or Ni catalysts in attempts at the addition homopolymerization of **2d** resulted in recovery of starting material only (**Figure 4.14**). Free radical polymerizations were studied using AIBN as the initiator, and again, only starting material was recovered. This is in contrast with **1**, which readily undergoes polymerization via these methods (Tran 2002).

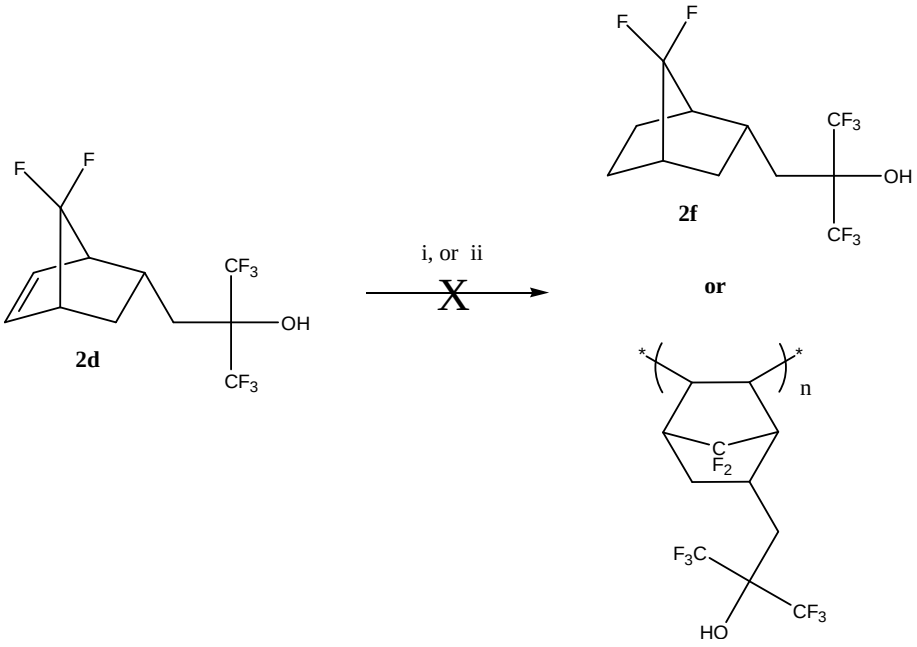

Figure 4.14: (i) Pd/C, H_2 (ii) Pd, Ni or AIBN catalyzed polymerizations. In both reactions only starting material was recovered.

The 2,2-difluoro analogue of NBHFA was synthesized through the substitution of the brominated alcohol onto norcamphor. The brominated alcohol was synthesized through a known literature procedure and was combined with the enolate of norcamphor to give **3a** (**Figure 4.15**) (Grushin 2002).

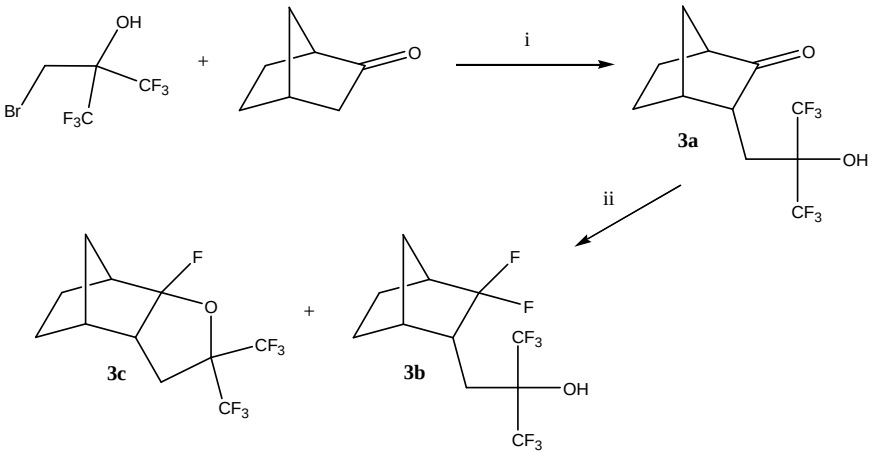

Figure 4.15: (i) LDA, -78ºC (ii) DAST.

The resulting yellow oil was a mixture of the *endo*/*exo* isomers in an approximate 95:5 ratio respectively. Recrystallization from water/acetonitrile isolated the *endo* product and gave crystals suitable for x-ray analysis (**Figure 4.16**).

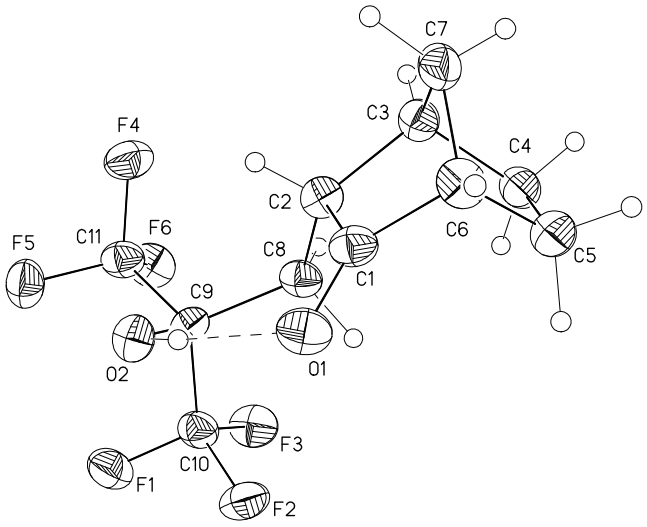

Figure 4.16: View of 3a showing the atom labeling scheme. Displacement ellipsoids are scaled to the 50% probability level. The dashed line is indicative of an intramolecular H-bonding interaction. The geometry of this interaction is: O2-H2O···O1, O···O 2.696(6)Å, H···O 1.97(4)Å, O-H···O 176(6)°.

The substitution adduct (**3a**) was converted to the 2,2-difluoro product (**3b**)using DAST as the fluorinating agent.

During the workup, an unexpected side product was discovered and upon isolation and characterization was found to be the cyclic ether **3c**. Reproduction of the DAST fluorination while constantly monitoring product formation by GC/MS revealed that **3b** and **3c** formed in a 1:1 ratio throughout the fluorination. Modification of the reaction temperature did not induce selectivity in the formation of either **3b** or **3c**.

Bicyclic[2.2.2] Systems

One method of incorporating the HF*i*P group into a [2.2.1]bicyclic compounds is the use of hexafluoroacetone and the enolate of norcamphor to give the resulting HF*i*P

group bound directly to the ring system (no methylene unit between ring and HF*i*P) (Bensel 2003).

Using this method and applying it to a bicyclic[2.2.2] system, 3,6-Bis-(2,2,2-trifluoro-1-hydroxy-1-trifluoromethyl-ethyl)-bicyclo[2.2.2]oct-7-ene-2,5-dione (**4c**) was synthesized (**Figure 4.17**).

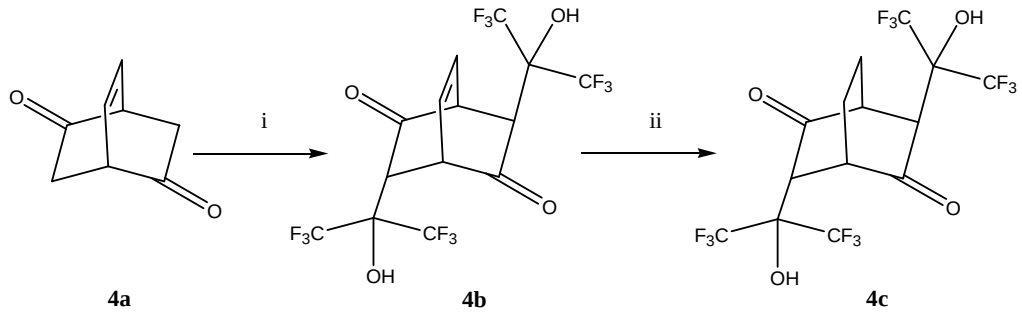

Figure 4.17: (i) LDA, -78ºC, hexafluoroacetone (ii) Pd/C, H_2.

The starting dione (**4a**) was treated with lithium diisopropyl amine (LDA) to generate the bis-enolate which, upon addition of hexafluoroacetone, underwent double addition to give **4b** (Lightner 1988). Isolation of **4b** and recrystallization from the slow evaporation of **4b** in dichloromethane gave crystals suitable for X-ray analysis (**Figure 4.18**). Reduction of **4b** with Pd/C gave the saturated product **4c** quantitatively.

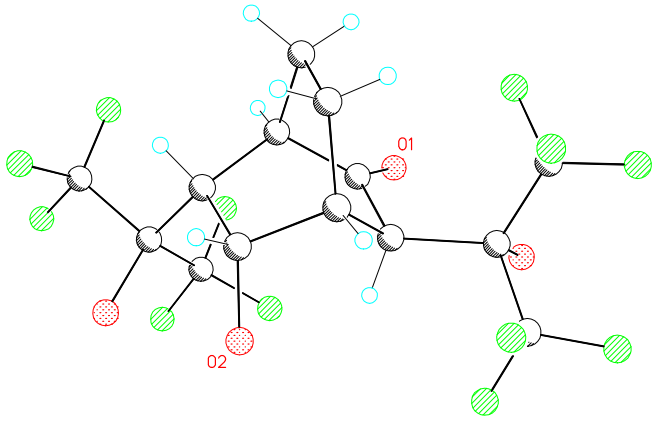

Figure 4.18: View of mono-reduced 4b showing the atom labeling scheme. Displacement ellipsoids are scaled to the 50% probability level. . O1 is a carbonyl O (C=O bond length 1.23Å) while O2 is a hydroxy O (C-O bond length 1.41Å).

Although the *mono* substituted analogue of **4b** was a minor side product in the first experiment, in subsequent experiments where an excess of hexafluoroacetone was used, the *bis*-substituted adduct was formed exclusively. No attempts were made to form the *mono* adduct of **4b** exclusively.

The conversion of the carbonyl groups in **4c** to the corresponding *gem*-difluoro analogue via fluorination with DAST resulted in complete loss of starting material with only unidentifiable products recovered. The inability to fluorinate the carbonyl group with DAST suggested a prohibitive affect due to the interaction between the carbonyl group and the *alpha* HF*i*P group. Protection of the HF*i*P -OH group with either *t*-BOC or acetal groups were unsuccessful, as only starting material was recovered from these reactions. The inability to either protect the HF*i*P –OH group, or convert the carbonyl group to the analogous *gem*-difluoro compound, has led to the current study of the reduction of the carbonyl groups to the corresponding methylene, or secondary alcohols.

These reductions have so far proven to be problematic, with only the partially reduced products being recovered, complete reduction to the *bis*-diol or *bis*-methylenes has not yet been accomplished.

During the isolation of **4b,** a side product was isolated and identified to be the *bis*-HF*i*P enamino alcohol **4d** (**Figure 4.19**). Recrystallization of **4d** gave crystals suitable for x-ray analysis.

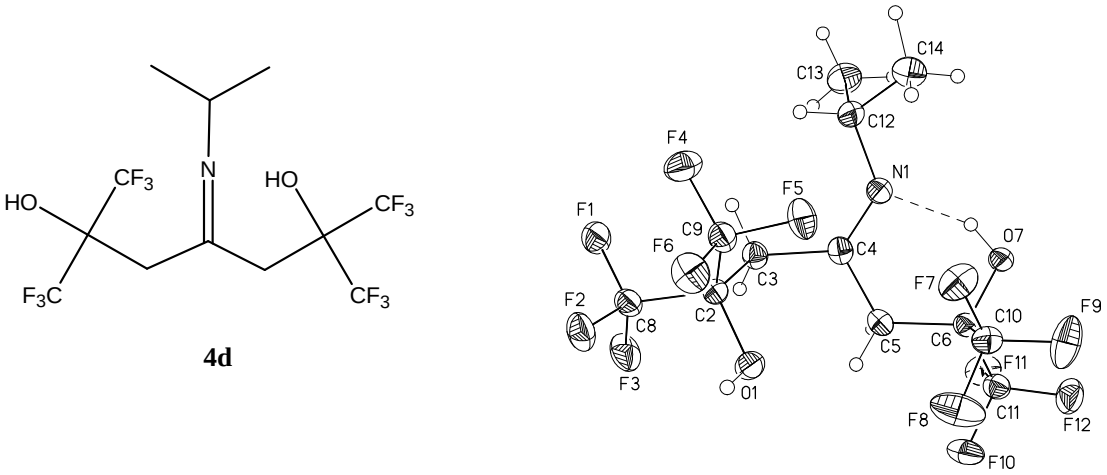

4d

Figure 4.19: (4d): The bis-HF*i*P enamino alcohol product of the reaction between diisopropyl amine, n-butyl lithium and hexafluoroacetone. On the right: View of 4d showing the atom labeling scheme. Displacement ellipsoids are scaled to the 50% probability level. Hydrogen atoms are drawn to an arbitrary size. The dashed line is indicative of an intramolecular H-bond. The geometry of this interaction is: O7-H7…N1, O…N 2.563(2)Å, H…N 1.78(3)Å, O-H…N 152(3)°.

To understand whether or not this was a byproduct of the reaction with hexafluoroacetone and the enolate of the [2.2.2] dione, or if hexafluoroacetone reacts directly with LDA to form the enamino alcohol **4d**, a study of the reaction between LDA and hexafluoroacetone was initiated. Diisopropyl amine was treated with *n*-butyl lithium

to generate the lithium salt, to which hexafluoroacetone was added in excess (**Figure 4.20**).

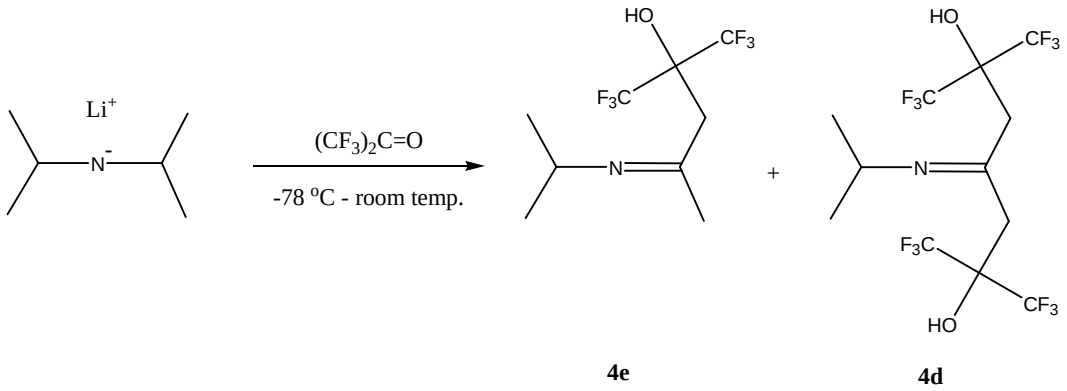

4e **4d**

Figure 4.20: The addition of hexafluoroacetone to LDA resulted in the formation of the mono and di HFA imine.

Both **4d** and **4e** were formed during this reaction in a 9:1 ratio respectively. Recrystallization of products from hexane/ethyl acetate (3:1) afforded the isolation of **4d**. The suggested formation of the enamino alcohol (**4d**) is the result of the imine tautomer interaction with a strong electrophile such as hexafluoroacetone (Barten 2002). Although the formation of enamino alcohols is not unknown with lithiated compounds (Schlosser 1995), the use of LDA and hexafluoroacetone has not previously been reported.

Bicyclic Conclusions

The synthesis of two HF*i*P containing compounds with the bicyclic[2.2.1] ring system have been reported. In addition to the reported [2.2.1] compounds, a [2.2.2] compound containing HF*i*P was synthesized and reported. The unexpected side products formed during these syntheses have been characterized and reported as well. Unfortunately, these compounds are unsuitable for polymer formation and hence

photoresist use, but were quite interesting studies into fluorinated compounds for use at 157 nm.

Experimental

Materials All manipulations and polymerizations were carried out in a He-filled drybox, glovebag or using standard Schlenk techniques. Nitrogen was purified by passage through KOH, NaOH and Drierite $CaSO_4$. Dichloromethane was rigorously degassed in 3 L reservoirs. All starting materials were procured from Aldrich except methyl 2-(trifluoromethyl)-3,3,3-trifluoropropenoate (SynQuest) was used as received unless noted otherwise. All liquid reagents used for vacuum UV measurements were distilled from appropriate drying agents, thoroughly degassed by freeze, pump, thaw cycles and sealed in glass ampoules under vacuum.

Instruments and Equipment Nuclear magnetic resonance (NMR) spectra were obtained using either a Bruker AMX300 or a Varian *Unity Plus 300* spectrometer (^{1}H: 300 MHz, ^{13}C: 75 MHz, ^{19}F: 282 MHz). Shifts for NMR spectra are reported in ppm relative to TMS (for ^{19}F, $CFCl_3$) or to the chemical shift of the solvent. Infrared spectra were recorded on a Nicolet *Avatar 360* IR spectrometer. Melting points are uncorrected. Mass spectra were measured on a Finnigan *MAT TSQ-700* spectrometer. Molecular weights (M_w) and polydispersity indices (PDI) were measured from THF solutions using a Viscotek GPC equipped with a set of two 5 mm crosslinked polystyrene columns (linear mix and 100 Å) from American Polymer Standards and are reported relative to polystyrene standards. Polymers containing acidic functional groups were pretreated with either diazomethane or iodomethane/DBU before GPC measurement, unless noted otherwise. Differential scanning calorimetry (DSC) measurements and thermal gravimetric analysis (TGA) were performed on a Perkin Elmer *Series-7* thermal analysis system. Gas chromatographs were recorded on a Hewlett Packard *5890 Series II* with an *HP-5* (crosslinked 5% PH ME siloxane) capillary column and flame ionization detector (FID).

Vacuum UV Spectroscopy Gas phase V-UV measurements were made on an Acton *CAMS-507* spectrophotometer fitted with a custom-made gas cell attachment. The details of the cell design and implementation have been described previously.[23] VUV spectra of polymer films were calculated from measurements made with a J. A. Woollam *VU301* variable angle spectroscopic ellipsometer (VASE) and/or measured with the Acton *CAMS-507* spectrophotometer. The films were cast on either silicon wafers (VASE) or calcium fluoride disks (Acton) from solutions in propylene glycol methyl ether acetate (PGMEA), 2-heptanone or cyclohexanone and baked at 100-130°C for at least 2 min prior to analysis. All absorbance data reported are in base 10.

General Synthesis Procedure for Tricyclononene Compounds One equivalent of tetracyclo[3.2.0.0^{2,7}.0^{4,6}]heptane (quadricyclane) and 1-3 equivalents of acrylate were placed in a thick walled Schlenk tube. The components were degassed and the flask sealed under an atmosphere of argon. For reactions in which radical polymerization of the olefin occurs readily, small amounts of suitable radical inhibitors, such as hydroquinone, were added. The reaction mixture was heated to 96 °C for 24-72 hours. The tricyclononene product was separated from the residual quadricyclane starting material and norbornadiene and polymeric by-products by Kugelröhr vacuum distillation to yield colorless liquids (or solids).

Palladium(II) Addition Polymerization. Initially, polymers made from Risse's allyl palladium catalyst, (η^3-allyl)Pd(II)(SbF_6) (Breunig 1992, Mathew 1996), also had very high molecular weights. Employing less active catalysts to achieve lower molecular weights was considered. This would lower the yield of the polymer obtained, but due to the limited quantities of the monomers available, this route was postponed. The addition of 1-hexene did not significantly reduce the molecular weight of the Pd(II) catalyzed polymers either.

In addition, unlike the Ni(II) system previously employed in resist synthesis, this catalyst cleaved any *t*-butyl esters present on the norbornene monomers. Apparently, some acid is formed during polymerization. The only anion available is $^-SbF_6$, and the formation of $HSbF_6$, a very strong acid, is disastrous. This presented a large problem because the end use demands incorporation of some norbornene monomers with acid-labile functionalities. This problem was solved through the introduction of sterically hindered, polymer-bound pyridines as "proton sponges" to neutralize any acid that is produced. These hindered amines do not effectively bind to the active catalyst, so the rate of polymerization was not significantly affected. In addition, the proton sponge beads can be easily filtered away from the reaction media, providing a convenient way to eliminate any residual highly absorbing, basic pyridine species which could interfere with resist performance.

In contrast to the Ni(II) polymerizations discussed above, lower molecular weight polymers were successfully obtained by increasing the loading of palladium catalyst. Vinyl addition polymers with molecular weights below 9,000 were obtained by using ≥ 5 mol% catalyst. Using large amounts of catalyst is expensive and not ideal for photoresist applications because of the cost related to removal of metal contamination. Most of the catalyst was removed from the final polymers by precipitation and filtration. This has provided polymers that are acceptable for initial lithographic testing purposes, although reduction of residual metallic impurities to less than 20 ppb levels will be necessary for commercial resist applications.

In summary, using hindered, polymer-bound amines and higher catalyst loadings allow the synthesis of useful polymers by the palladium addition polymerization route. All the polymers discussed in this chapter were made with the allyl palladium catalyst using this described procedure.

Tricyclononene Compounds

Quadricyclane Toxicity. Quadricyclane is a colorless, flammable liquid with a boiling point of 180 °C with *extremely* high toxicity. Although quadricyclane is available commercially, no acute toxicity information is readily available in the literature. The Air Force screened various propellant candidates and in the process accrued some toxicity data, finding it to be a highly dangerous material to work with in chemistry. "Quadricyclane produced 100% mortality in male Fischer 344 rats within 24 h following gavage at 3.5 g/kg. Gavage treatment with a quadricyclane/kerosene mixture (70% quadricyclane, 30% kerosene), similar to the proposed rocket fuel mixture, produced toxic effects at a dose level below the EPA limit test. No treatment-related deaths occurred in rabbits following a 24-h dermal exposure to the EPA limit dose of 2 g test material/kg body weight." This information was taken from Kinkead, *et al* (Kinkead 1993). Quadricyclane should always be handled in a hood, never without proper personal protective equipment nor adequate ventilation. This material should be treated as extremely toxic substance, any and all safety precautions are not recommended, they are required.

***t*-Butyl 3-(methyl)tricyclo[4.2.1.0^{2,5}]non-7-ene-3-carboxylate**. Quadricyclane (15 mL, 14.7 g, 0.16 mol) and 3 equiv. *t*-butyl methacrylate (78 mL, 68.2 g, 0.48 mol) were reacted according to the general procedure mentioned above to produce, after Kugelröhr vacuum distillation, 3.0 g (0.013 mol) of colorless liquid. Yield: 8%. Isomer composition: 55 % *syn*, 45 % *anti*. ^{1}H NMR ($CDCl_3$, 300 MHz, ppm): δ 5.98 (m, 4H, H-7+8, *syn*+*anti*), 3.12 (ddd, *J* = 7.8, 9.6, 11.1 Hz, 1H, H-2, *syn*), 2.95 (br s, 1H, H-1, *syn*), 2.74 (br s, 1H, H-1, *anti*), 2.65 (br s, 2H, H-6, *syn*+*anti*), 2.1-1.6 (6H, *syn*+*anti*), 1.56-1.48 (m, 1H), 1.46 (s, 9H, C(CH_3)$_3$, *syn*), 1.45 (s, 9H, C(CH_3)$_3$, *anti*), 1.40 (d, 3H, -CH_3, *syn*), 1.36-1.18 (4H, *syn*+*anti*), 1.16 (d, 3H, -CH_3, *anti*). ^{13}C NMR ($CDCl_3$, 75 MHz, ppm): δ 178.25 (*C*OOtBu, *anti*), 176.43 (*C*OOtBu, *syn*), 136.37 (olefin C, *anti*), 136.23 (olefin C, *syn*), 135.71 (olefin C, *anti*), 135.48 (olefin C, *syn*), 79.94 (*C*(CH_3)$_3$, *syn*), 79.79 (*C*(CH_3)$_3$, *anti*), 48.91 (CH, C-2, *syn*), 44.63 (CH, C-6, *syn*), 44.30 (CH, C-2, *anti*), 43.53 (CH, C-6, *anti*), 42.99 (CH, C-1, *syn*), 41.88 (CH_2, C-9, *anti*), 41.52 (CH, C-1, *anti*), 41.35 (quat. C, C-3, *syn*), 41.07 (quat. C, C-3, *anti*), 40.65 (CH_2, C-9, *syn*), 33.09 (CH, C-5, *anti*), 31.36 (CH_2, C-4, *anti*), 31.08 (CH_2, C-4, *syn*), 30.48 (CH, C-5, *syn*), 28.37 (CH_3, *syn*), 28.32 (C(*C*H_3)$_3$, *syn*), 28.17 (C(*C*H_3)$_3$, *anti*), 16.91 (CH_3, *anti*). IR (KBr, cm^{-1}): 3057 (alkene), 2972, 1720 (C=O), 1470, 1456, 1391, 1367, 1313, 1281, 1256, 1227, 1131, 849, 757, 703. HRMS-EI (*m/z*): [M + H]$^+$ calcd for $C_{15}H_{23}O_2$, 235.1698; found, 235.1698.

Methyl 3-(trifluoromethyl)tricyclo[4.2.1.0^{2,5}]non-7-ene-3-carboxylate. Quadricyclane (1.5 equiv., 4.25 g, 0.046 mol) and methyl (2-trifluoromethyl)acrylate[6a] (1 equiv., 4.55 g, 0.30 mol) were reacted according to the general procedure mentioned above to produce, after Kugelröhr vacuum distillation, 6.78 g (0.028 mol) of colorless liquid. Yield: 94%. Isomer composition: 32 % *syn*, 68 % *anti*. ^{1}H NMR ($CDCl_3$, 300 MHz, ppm): 6.1-5.9 (m, 4H, H-7+H-8, *syn*+*anti*), 3.80 (s, 3H, COOCH_3, *syn*), 3.78 (s,

3H, COOCH_3, *anti*), 3.06 (br s, 1H, H-1, *syn*), 2.99 (br s, 1H, H-1, *anti*), 2.82 (br s, 1H, H-6, *syn*), 2.74 (br s, 1H, H-6, *anti*), 2.683 (ddd, *J* = 3.0, 7.5, 13.2 Hz, 1H, H-2, *anti*), 2.5-1.9 (7 H), 1.48-1.24 (4 H). ^{13}C NMR ($CDCl_3$, 75 MHz, ppm): δ 171.16 (d, *J* = 2.9 Hz, *C*OOMe, *syn*), 168.85 (d, *J* = 2.4 Hz, *C*OOMe, *anti*), 136.74 (olefin C, *anti*), 136.62 (olefin C, *syn*), 135.24 (olefin C, *syn*), 135.06 (olefin C, *anti*), 126.32 (q, *J* = 280 Hz, CF_3, *anti*), 125.16 (q, *J* = 281 Hz, CF_3, *syn*), 53.30 (COO*C*H3, *syn*), 52.81 (COO*C*H_3, *anti*), 49.56 (q, *J* = 28.6 Hz, quat. C, C-3, *syn*), 49.40 (q, *J* = 26.5 Hz, quat. C, C-3, *anti*), 44.50 (CH, C-6, *anti*) 44.18 (CH, C-6, *syn*), 44.15(CH, C-2, *syn*), 41.95 (m, *J* = 2.0 Hz, CH, C-2 *anti*), 42.86 (CH, C-1, *syn*), 42.50 (CH, C-1, *anti*), 41.14 (m, CH_2, C-9, *anti*), 40.71 (CH_2, C-9, *syn*), 32.98 (CH, C-5, *syn*), 32.83 (CH, C-5, *anti*), 26.07 (d, *J* = 2.4 Hz, CH_2, C-4, *anti*), 25.93 (d, *J* = 1.9 Hz, CH_2, C-4, *syn*). ^{19}F NMR ($CDCl_3$, 282 MHz, ppm) (referenced to external C_6F_6 standard at -166.717 ppm): δ –66.25 (s, 3F, -CF_3, *syn*), δ –75.13 (s, 3F, -CF_3, *anti*). IR (KBr, cm^{-1}): 3060 (alkene), 2970, 2892, 1742 (C=O), 1473, 1436, 1333, 1322, 1275, 1225, 1163, 1132, 1087, 712, 671. HRMS-EI (*m/z*): $[M]^+$ calcd for $C_{12}H_{14}F_3O_2$, 246.0868; found, 246.0868.

Triethylaminoboron trifluoride.[24] To a cooled (dry ice/acetonitrile) 250 mL round-bottom flask equipped with a stir bar and addition funnel was added boron trifluoride diethyl etherate (30 g, 211 mmol). Triethylamine (60 mL) was added dropwise to the flask via an addition funnel. The formation of white precipitate was immediately observed. After the addition of triethylamine, the reaction was allowed to warm to room temperature, and excess triethylamine was removed *in vacuo*. The white residue was purified by vacuum fractional distillation (85°C / 3 mm Hg) to give a white solid (32.0 g, 91%), which melted at approximately 25°C. The compound was kept in the refrigerator and used in the next step without further purification.

Methyl 3,3-difluoro-2-(trifluoromethyl)acrylate. A slight modification of the literature procedure was used.[25] To a 100 mL round-bottom flask equipped with a magnetic stir bar and reflux condenser were added triethylaminoboron trifluoride (32.0 g, 189 mmol) and methyl 2-(trifluoromethyl)-3,3,3-trifluoropropionate (30.5 g, 145 mmol). The reaction mixture was refluxed for 3 h and then cooled to room temperature. The residue was purified by vacuum transfer (bulb to bulb distillation) to give a clear oil (19.8 g, 71%). ^{1}H NMR ($CDCl_3$, 300 MHz, ppm): δ 3.84 (s, 3H, methyl). ^{19}F NMR (CD_3OD, 282 MHz, ppm): δ -58.5 (m, 1F), -59.1 (m, 3F), -59.5 (m, 1F). IR (NaCl, cm^{-1}): 2960, 1767 (C=O), 1710, 1439, 1372, 1152, 1081, 1040, 1024. HRMS-CI (*m/z*): $[M + H]^+$ calcd for $C_5H_3F_5O_2$, 191.0131; found, 191.014.

Methyl 4,4-difluoro-3-(trifluoromethyl)tricyclo-[4.2.1.0^{2,5}]non-7-ene-3-carboxylate. To a 300 mL Parr pressure reactor equipped with a magnetic stir bar were added quadricyclane (1.5 g, 16.3 mmol) and methyl 3,3-difluoro-2-(trifluoromethyl)acrylate (3.9 g, 20.4 mmol). The pressure vessel was sealed, and the reaction mixture was stirred at 100°C for 72 h. After cooling to room temperature, the residue was purified by fractional vacuum distillation (39-40°C / 0.30 mm Hg) to yield a clear oil (1.0 g, 22%). Isomer composition: 49% *syn*, 51% *anti*. ^{1}H NMR ($CDCl_3$, 300

MHz, ppm): δ 6.27 (dd, *J* = 2.7, 5.7 Hz, olefin H, 1H, *anti*), 6.05-6.15 (m, olefin H, 3H, 2 *syn*+1 *anti*), 3.87 (s, COOC*H*$_3$, 3H, *anti*), 3.86 (s, COOC*H*$_3$, 3H, *syn*), 3.53 (br s, 1H, H-1, *syn*), 3.22 (m, 2H, H-1, H-6, *anti*), 3.13 (br s, 1H, H-6, *syn*), 2.84-2.75 (m, 1H, H-5, *anti*), 2.75-2.6 (m, 1H, H-5, *syn*), 2.39-2.31 (m, 1H, H-2, *syn*), 2.10 (d, *J* = 10.2 Hz, 1H, H-2, *anti*), 1.50-1.30 (m, 4H, H-9 *syn*, H-9 *anti*, *syn*+*anti*). ^{13}C NMR (C_6D_6, 75 MHz, ppm): 165.11 (COOMe, *syn*), 162.91 (COOMe, *anti*), 139.62 (olefin, *anti*), 137.82 (olefin, *syn*), 136.93 (olefin, *syn*), 136.77 (olefin, *anti*), 123.97, (q, J = 283 Hz, CF_3, *anti*), 123.68 (q, J = 280 Hz, CF_3, *syn*), 118.02, (t, *J* = 296 Hz, C-5, *anti*), 116.72 (t, *J* = 292 Hz, C-5, *syn*), 53.32 (COO*C*H$_3$, *anti*), 52.64 (COO*C*H$_3$, *syn*), 50.70 (dd, *J* = 19.2, 26 Hz, CH, C-5, *anti*), 50.36 (t, *J* =23 Hz, CH, C-5, *syn*), 43.71 (CH, C-1, *anti*), 43.26 (CH, C-1, *syn*), 43.11 (dd, *J* = 4.4, 8.2 Hz, CH_2,C-9, *anti*) 42.82 (d, *J* = 6.6 Hz, CH_2, C-9, *syn*), 42.08 (CH, C-6, *anti*), 41.29 (t, *J* = 2.3 Hz, CH, C-6, *syn*), 37.21(dd, J = 4.9, 12 Hz, CH, C-2, *anti*), 36.90 (m, CH, C-2, *syn*). ^{19}F NMR (Acetone, 282 MHz, ppm): δ –61.67 (d, *J* = 6.7 Hz. 3F, CF_3, *anti*), -68.36 (d, *J* = 2.0 Hz, 3F, CF_3, *syn*), -85.70 (ddd, *J* = 6.8, 11.0, 211 Hz, 1F, F-4 *anti*, *anti*), -97.15 (dddt, *J* = 4.2, 15.8, 31.9, 217 Hz, 1F, F-4 *anti*, *syn*), -106.87 (d, *J* = 217 Hz, 1F, F-4 *syn*, *syn*), -113.94 (d, *J* = 211 Hz, 1F, F-4 *syn*, *anti*). IR (NaCl, cm^{-1}): 3058 (alkene), 2991, 2909, 1752 (C=O), 1429, 1317, 1219, 1045, 897, 794, 697. HRMS-CI (*m/z*): $[M + H]^+$ calcd for $C_{12}H_{12}F_5O_2$, 283.0757; found, 283.0755.

4,4-Difluoro-3-(trifluoromethyl)tricyclo-[4.2.1.0^{2,5}]non-7-ene-3-carboxylic acid. Hydrolysis of methyl 4,4-difluoro-3-(trifluoromethyl)tricyclo-[4.2.1.0^{2,5}]non-7-ene-3-carboxylate with KOH and water under standard conditions produced the carboxylic acid. One of the isomers selectively crystallized from solution and was determined to be the *syn* isomer by x-ray crystallography. *Syn* isomer: ^{1}H NMR ($CDCl_3$, 300 MHz, ppm): δ 9.6-8.4 (br s, 1H, COOH), 6.16 (m, 2H, H-7+H-8), 3.50 (br s, 1H, H-1), 3.16 (br s, 1H, H-6), 2.69 (m, *J* = 4.2 Hz, 1H, H-5), 2.35 (m, 1H, H-2), 1.45 (s, 2H, H-9 *syn*, H-9 *anti*). ^{13}C NMR ($CDCl_3$, 125 MHz, ppm)(Varian 500MHz NMR): δ 167.63 (COOH), 137.94 (olefin C), 137.082 (olefin C), 122.93 (q, *J* = 282 Hz, CF_3), 116.08 (t, *J* =290 Hz, C-4), 59.5 (quat. C, C-3), 50.25 (t, *J* =23 Hz, CH, C-5), 43.04 (CH, C-1), 42.80 (d, *J* = 6.4 Hz, CH_2, C-9), 41.25 (t, *J* = 1.8 Hz, CH, C-6), 36.77 (m, CH, C-2). ^{19}F NMR ($CDCl_3$, 282 MHz, ppm): δ -68.94 (dd, *J* = 1.4, 10.2 Hz, 3F, CF_3), -97.81 (dddt, *J* = 2.4, 10.2, 19.2, 130 Hz, 1F, F-4 *anti*), -107.95 (d, *J* = 130 Hz, 1F, F-4 *syn*). HRMS-CI (*m/z*): $[M + H]^+$ calcd for $C_{11}H_{10}F_5O_2$, 269.0601; found, 269.0589.

General Hydrogenation Procedure. Norbornene or tricyclononene monomer (5.86 mmol) was dissolved in 16 mL ethyl acetate or pentane in a 250 mL Parr bomb (Parr Instrument Company, MAWP 3000psi at 350 °C). 10 % Pd/C (10%, 0.015g) was added to the bomb, which was pressurized to 50 psi with H_2. The reaction mixture was stirred overnight at room temperature, the catalyst was removed with a 0.45 μm PTFE syringe filter, and the solvent was removed by rotary evaporation to yield a clear oil.

General Polymerization Procedure. To a 20ml vial equipped with a stir bar were added allyl palladium chloride dimer (13.0 mg, 0.032 mmol) and silver

hexafluoroantimonate (28 g, 0.064 mmol) in a dry box. Dichloromethane (5 mL) was added and the mixture was stirred at room temperature for 20 min. The mixture was filtered through a 0.45 μm PTFE syringe filter into a 25 mL round-bottom flask containing a solution of tricyclononene monomer (3.25 mmol, [M]/[C]=50:1) in dichloromethane (10 mL). For resist evaluation, higher catalyst loadings ([M]/[C] = 10) were used to ensure only low molecular weight polymer (< 10,000 g/mol) was formed. For monomers with *t*-butyl ester functionalities, the resulting solution was stirred for 10 min at room temperature and then transferred to a 25 mL round-bottom flask containing polymer-bound 2,6-di-*t*-butyl-pyridine (1 mg/mg catalyst). The reaction mixture was stirred at room temperature for 96 h, then filtered through a 0.45 μm PTFE syringe filter to remove the polymer-bound base, concentrated *in vacuo*, and precipitated into hexanes (100 mL). The crude polymer was dissolved in ethyl acetate (50 mL), and stirred vigorously under a hydrogen atmosphere overnight. The solution was allowed to sit, unstirred, for another hour, at which time a black solid (Pd) aggregated and precipitated. The black solid was removed by filtration through celite. The filtrate was treated with activated carbon and stirred for 3 h. The activated carbon was removed by filtration through celite, and the resulting filtrate was washed with saturated $NaHCO_3$, water, and brine, dried with $MgSO_4$, filtered, concentrated *in vacuo* at 50°C, and precipitated into hexanes. Filtration provided the product as a white powder.

Poly(3-(bicyclo[2.2.1]hept-5-en-2-yl)-1,1,1-trifluoro-2-(trifluoromethyl)propan-2-ol). 3-(Bicyclo[2.2.1]hept-5-en-2-yl)-1,1,1-trifluoro-2-(trifluoromethyl)propan-2-ol (NBHFA)[6a] was polymerized by the general procedure mentioned previously ([M]/[C] = 10:1) to produce a 55% yield of white powdery polymer. ^{1}H NMR (DMSO-d_6, 300 MHz, ppm): δ 7.6 (br s, OH), 2.80-0.50 (br m, aliphatic). ^{19}F NMR (CD_3OD, 282 MHz, ppm): δ -75.0 to -77.0. IR (KBr, cm^{-1}): 3600, 3471, 2954, 2881, 1453, 1214, 1145, 1025, 714. GPC: M_n = 3,860; PDI= 2.11. A_{157} = 1.15 μm^{-1}.

Poly(methyl 3-(trifluoromethyl)tricyclo[4.2.1.0^{2,5}]non-7-ene-3-carboxylate). Methyl 3-(trifluoromethyl)tricyclo[4.2.1.0^{2,5}]non-7-ene-3-carboxylate was polymerized by the general procedure mentioned previously ([M]/[C] = 50:1) to produce a 79% yield of white polymeric powder. ^{1}H NMR (CD_2Cl_2, 300 MHz, ppm): δ 4.20-3.30 (br s, COOC*H*$_3$), 0.50-3.20 (br m, aliphatic). A_{157} = 3.79 μm^{-1}. SEC (GPC): M_n = 66,300, PDI = 2.11

Poly(methyl 4,4-difluoro-3-(trifluoromethyl)tricyclo-[4.2.1.0^{2,5}]non-7-ene-3-carboxylate) Methyl 4,4-difluoro-3-(trifluoromethyl)tricyclo-[4.2.1.0^{2,5}]non-7-ene-3-carboxylate was polymerized by the general procedure mentioned previously ([M]/[C] = 10:1) to produce a 50% yield of white polymeric powder. A_{157} = 2.86 μm^{-1}. SEC (GPC): M_w = 7,200, PDI = 2.58.

Poly(NBHFA-*co*-TCNCF$_3$TBE). NBHFA and methyl 3-(trifluoromethyl)tricyclo[4.2.1.0^{2,5}]non-7-ene-3-carboxylate was polymerized by the general procedure mentioned previously to produce a 20-30% yields of white polymeric powder. ^{1}H NMR (DMSO-d$_6$, 300 MHz, ppm): δ 1.40 (bs, t-Bu), 0.40-3.60 (bm, aliphatic), 7.67 (bs, OH). FT-IR (KBr, cm^{-1}): 3600, 3467, 2955, 2878, 1716 (C=O), 1613, 1460, 1371, 1219, 1137, 1014, 988, 707, 661. GPC: Mw = 13800; PDI = 2.19 (not treated with diazomethane). Composition as determined by TGA: NBHFA/TCNCF$_3$TBE = 74/26. A_{157} = 1.97 μm^{-1}. ^{1}H NMR (DMSO-d$_6$, 300 MHz, ppm): δ 1.41 (bs, t-Bu), 0.40-3.20 (bm, aliphatic), 7.67 (bs, OH). FT-IR (KBr, cm^{-1}): 3595, 3452, 2955, 2878, 1710 (C=O), 1613, 1454, 1372, 1214, 1142, 1024. GPC: Mw = 5200; PDI = 2.78 (not treated with diazomethane). Composition as determined by TGA: NBHFA/TCNCF$_3$TBE = 83/17. A_{157} = 1.67 μm^{-1}.

ROMP of Methyl 3-(trifluoromethyl)tricyclo[4.2.1.0^{2,5}]non-7-ene-3-carboxylate One equivalent (1.8 g, 7.3 mmol) of methyl 3-(trifluoromethyl)tricyclo[4.2.1.0^{2,5}]non-7-ene-3-carboxylate monomer and 1,2-dichloroethane (26.8 ml) were combined in a 100 ml 3-neck round-bottom flask to give a 0.3 M solution and purged with nitrogen for 15 minutes. Allyl acetate (0.1 equivalents, 0.073 g, 0.73 mmol) was syringed into the flask through the rubber septum, and then the reaction flask was heated to 55 ºC. During this time, a separate 5 ml of 1,2-dichloroethane solvent was purged with nitrogen for 15 minutes, and then 2 ml were used to dissolve the second-generation ruthenium-based Grubbs catalyst (0.0016 g, 0.0018 mmol). The dissolved catalyst was syringed into the reaction flask after it had been heating for 15 min. Rubber septum was replaced with an air condenser under a nitrogen blanket and the reaction stirred overnight at 55 °C. The resulting polymer was hydrogenated and purified according to the above procedures (hydrazine reduction and dialysis in methanol) to yield 0.76 g of the final polymer.

Free-Radical Polymerization of Methyl 3-(trifluoromethyl)tricyclo[4.2.1.0^{2,5}] non-7-ene-3-carboxylate One equivalent of monomer (1.8 g, 7.31 mmol) was added to a 100 ml round-bottom flask with 0.8 equivalents t-butyl peroxide (0.86 g, 5.85 mmol). Four freeze/pump/thaw cycles were performed on the reaction mixture using liquid nitrogen and a vacuum. The vacuum was then replaced with a nitrogen blanket, and the reaction mixture was heated to 135 ºC for 24 hours behind a blast shield. The polymer was purified by precipitation into hexanes: one equivalent of the polymer (1.8 g, 7.31 mmol) was dissolved in 2 ml of dichloromethane and then added drop wise to 12 ml hexanes while rigorously stirring. The mixture turned into a thick yellow solution with fine precipitate. The solution was vacuum filtered with fine filter paper to yield 0.33 g of polymer.

Bicyclic [2.2.1] and [2.2.2] Compounds

(2a) 1,4,5,6-tetrachloro-7,7-dimethoxy-3-(5-bicyclo [2.2.1] hepten-2-yl)-1,1,1-trifluoro-2-(trifluoromethyl)-2-propanol 1,2,3,4-tetrachloro-5,5-dimethoxy

cyclopentadiene (26.5 g, 101 mmol) and 1,1,1-trifluoro-2-trifluoromethyl-pent-4-en-2-ol (31.5 g, 152 mmol), in 50 mL of ether, were placed in a Parr reactor (10 mg of hydroquinone was added as a radical scavenger) and heated to 155 ºC. After 48 hrs the reaction was removed from heat and cooled to room temperature. The dark yellow liquid from the reactor was filtered through a silica plug with ether as the eluent. The ether was removed by rotary evaporation, and the viscous oil was dissolved into 500 mL 2M KOH. The aqueous solution was washed with chloroform (100 mL) and hexane (100 mL) and then acidified with 3M HCl solution until a pH of 2 was reached. The aqueous solution was extracted with chloroform (8 x 100 mL) and the organic extracts were combined, dried with MgSO4, and filtered. Removal of chloroform by rotary evaporation gave 19g (40 % yield, 95:5 *endo*/*exo*) of a pale yellow oil which was used without further purification. ^{19}F-NMR (282.4 MHz, $CDCl_3$, $CFCl_3$): δ –76.929 (q, 3F, CF_3), -77.775 (q, 3F, CF_3); ^{1}H NMR (300.1 MHz, $CDCl_3$): δ 1.397 (m, 1H, aliphatic), 1.675 (m, 1H, aliphatic), 2.201 (m, 1H, aliphatic) 2.527 (m, 1H, aliphatic), 2.905 (m, 1H, aliphatic), 3.512 (s, 3H, CH_3), 3.568 (s, 3H, CH_3).

(2b) 7,7-dimethoxy-3-(5-bicyclo [2.2.1] hepten-2-yl)-1,1,1-trifluoro-2-(trifluoromethyl)-2-propanol **2a** (19 g, 40.5 mmol) was combined with t-butyl alcohol (54 g, 730 mmol) and 350 mL of dry THF in a 1 L three neck round bottom flask containing a stir bar and a condenser under a N_2 atmosphere. Na (30 g, 1.3 mol), cut into small cubes, was slowly added over a 45 min period. The mixture was vigorously stirred at reflux for 48 hrs, cooled to room temperature, and filtered to remove any unreacted sodium. The filtrate was poured into ice-water (300 mL) and extracted with ether (3 x 100 mL). The organic layers were combined and washed with brine, dried with MgSO4, and filtered. Removal of ether by rotary evaporation gave 13 g (96% yield) of a white solid m.p 115 °C (98% purity by GC/MS). ^{19}F-NMR (282.4 MHz, $CDCl_3$, $CFCl_3$): δ –75.648 (q, 3F, CF_3), -78.237 (q, 3F, CF_3); ^{1}H NMR (300.1 MHz, $CDCl_3$): δ 0.512 (m, 1H, aliphatic), 1.528-1.689 (m, 2H, aliphatic), 2.087 (m, 1H, aliphatic) 2.462 (m, 1H, aliphatic), 2.645 (m, 1H, aliphatic), 2.986 (m, 1H, aliphatic), 3.060 (s, 3H, CH_3), 3.116 (s, 3H, CH_3), 5.965 (m, 1H, alkene), 6.058 (m, 1H, alkene); ^{13}C-NMR (75.5 MHz, $CDCl_3$): δ 29.509(s), 32.211(s), 33.427(s), 44.410(s), 48.896(s), 51.532(s), 76.253(m), 118.986(s), 131.527(s), 133.814(s).

(2c) 5-(3,3,3-Trifluoro-2-hydroxy-2-trifluoromethyl-propyl)-bicyclo[2.2.1]hept-2-en-7-one The acetal **2b** (0.9g, 2.7mmol) was dissolved into 20mL of 1,4-dioxane. To this solution is added 10 mL 1N HCl, and the reaction mixture is heated to 105 °C for 3hrs. After 3hrs, the solution is cooled to room temperature and poured into pentane. The aqueous layer is washed (3 x 25mL) with pentane and the organic layers are combined and dried over $MgSO_4$. Rotary evaporation of the pentane gave 0.69g of a white solid m.p. 108 °C (90% yield). Recrystallization from the slow evaporation of DCM gave crystals suitable for x-ray analysis. ^{19}F-NMR (282.4 MHz, $CDCl_3$, $CFCl_3$): δ –76.391 (q, 3F, CF_3), -78.029 (q, 3F, CF_3); ^{1}H NMR (300.1 MHz, $CDCl_3$): δ 0.757 (m, 1H, aliphatic), 1.565-1.782 (m, 2H, aliphatic), 2.164 (m, 1H, aliphatic), 2.514 (m, 1H, aliphatic), 2.710 (t, 1H, aliphatic), 2.976 (t, 1H, aliphatic), 5.526

(b, 1H, OH), 6.325 (m, 1H, alkene), 6.501 (m, 1H, alkene); ^{13}C-NMR (75.5 MHz, $CDCl_3$): δ 27.498(s), 30.404(s), 33.543(s), 46.178(s), 51.022(s), 76.146(m), 130.222(s), 134.090(s), 205.257(s).

(2d) 2-(7,7-Difluoro-bicyclo[2.2.1]hept-5-en-2-ylmethyl)-1,1,1,3,3,3-hexafluoro-propan-2-ol The procedure for the fluorination of **2c** and **2e** is identical for both the unsaturated and saturated starting material. *CAUTION—DAST has been known to explode at temperatures around 80 °C. DO NOT heat the reaction, and DO NOT expose DAST to water, it reacts EXPLOSIVELY with water.* The ketone **2c** (1.0g, 3.5 mmol) in 20 mL DCM was added to a 50 mL 3 neck round bottom flask under a nitrogen blanket and cooled to 10 °C. The solution was stirred vigorously while 1.36mL (10.35 mmol) DAST was added over a period of 10 minutes. The reaction progress was monitored by GC/MS and after 3 hrs the reaction was complete. Upon completion, methanol (5 mL) was slowly added. The reaction mixture was stirred for an additional 20 min once the methanol had been added and then slowly poured into a sepratory funnel containing ice. The aqueous layer is extracted 3 x 15mL with pentane. The organic layers are combined and rotary evaporation of the solvent gave a pale viscous liquid 0.83g (78% yield) b.p. 48-50 °C at 0.35 Torr. ^{19}F-NMR (282.4 MHz, $CDCl_3$, $CFCl_3$): δ –76.327 (q, 3F, CF_3), -78.106 (q, 3F, CF_3), -118.660 (d, 1F, CF_2), -135.529 (d, 1F, CF_2); ^{1}H NMR (300.1 MHz, $CDCl_3$): δ 0.685-2.979 (m, 7H, aliphatic), 6.052 (m, 1H, alkene), 6.190 (m, 1H, alkene); ^{13}C-NMR (75.5 MHz, $CDCl_3$): δ 28.827(s), 30.968(s), 32.920(s), 45.104(t), 49.649(t), 53.239(s), 76.260(m), 130.605(d), 134.261(d).

(2e) 2-(3,3,3-Trifluoro-2-hydroxy-2-trifluoromethyl-propyl)-bicyclo[2.2.1]heptan-7-one A solution of 8 g (28 mmol) of **2c**, 0.8g (10 wt%) Pd on carbon and 75 mL DCM were added to Parr bomb and pressurized to 100 psi with H_2 and stirred for 12 hrs. The solution is then filtered through celite and rotary evaporation of the solvent gives 7.95 g (98% yield) of white solid m.p. 105 °C. ^{19}F-NMR (282.4 MHz, $CDCl_3$, $CFCl_3$): δ –76.029 (q, 3F, CF_3), -78.2187 (q, 3F, CF_3); ^{1}H NMR (300.1 MHz, $CDCl_3$): δ 0.700-2.127 (m, 10H, aliphatic), 2.416 (m, 1H, aliphatic), 3.186 (s, 3H, CH_3), 3.197 (s, 3H, CH_3); ^{13}C-NMR (75.5 MHz, $CDCl_3$): δ 20.101(s), 27.449(s), 30.209(s), 32.197(s), 36.429(s), 37.914(s), 40.051(m), 50.033(s), 50.201(s), 114.807(s).

(2f) 2-(7,7-Difluoro-bicyclo[2.2.1]hept-2-ylmethyl)-1,1,1,3,3,3-hexafluoro-propan-2-ol The synthesis of **2f** follows the same procedure used in the fluorination of the ketone **2c**. The DAST fluorination of **2e** (4.5g, 15.63mmol) gave a pale viscous liquid 3.95g (81% yield) b.p. 45-47 °C at 0.35 Torr. ^{19}F-NMR (282.4 MHz, $CDCl_3$, $CFCl_3$): δ –76.962 (q, 3F, CF_3), -78.193 (q, 3F, CF_3), -125.892 (d, 1F, CF_2), -130.647 (d, 1F, CF_2); ^{1}H NMR (300.1 MHz, $CDCl_3$): δ 0.845-2.656 (m, 11H, aliphatic); ^{13}C-NMR (75.5 MHz, $CDCl_3$): δ 18.854(d), 26.290(d), 29.065(d), 32.109(s), 35.124(d), 38.904(t), 43.419(t), 75.901(m).

(3a) 2-one-3-(5-bicyclo [2.2.1] heptan-2-yl)-1,1,1-trifluoro-2-(trifluoromethyl)-2-propanol Diisopropyl amine (11 mL) was combined with 25 mL dry THF under a N_2 atmosphere and cooled to -78 °C. *n*-Butyl lithium (38 mL of 2M solution in hexanes) was slowly added over 20 min and the solution was warmed to room temperature and kept at that temperature for 30 min. After 30 min the room temperature LDA solution was added dropwise to a solution of norcamphor (8 g, 72 mmol) and 50 mL dry THF under a N_2 atmosphere which was cooled to -78 °C. Once the LDA solution was added, the reaction mixture was warmed to room temperature and held there for 30 min. It was then cooled to -78 °C and the brominated alcohol [10] (9 g, 35 mmol) in 10 mL dry THF was slowly added over 30 min. Once all of the alcohol was added, the reaction flask was removed from the ice bath and left stirring at room temperature over night (12 hrs). The solvent was removed by rotary evaporation and 100 mL of DCM was added. The DCM solution was acidified with 3M HCl until a pH of 2 was reached. The DCM layer was extracted and the aqueous layer was extracted (2 x 50 mL) with DCM. The organic layers were combined and washed with water, brine, dried with $MgSO_4$, filtered, and the DCM was removed by rotary evaporation to give 11.5 g of a yellow oil. Recrystallization from water/acetonitrile gave 5.5 g (56% yield) of white crystals (m.p. 115 °C) suitable for x-ray analysis. ^{19}F-NMR (282.4 MHz, $CDCl_3$, $CFCl_3$): δ –76.391 (q, 3F, CF_3), -78.029 (q, 3F, CF_3); ^{1}H NMR (300.1 MHz, $CDCl_3$): δ 0.700-2.127 (m, 10H, aliphatic), 2.416 (m, 1H, aliphatic), 3.186 (s, 3H, CH_3), 3.197 (s, 3H, CH_3); ^{13}C-NMR (75.5 MHz, $CDCl_3$): δ 27.498(s), 30.404(s), 33.543(s), 46.178(s), 51.022(s), 76.146(m), 130.222(s), 134.090(s), 205.257(s).

(3b) 2,2-Difluoro-3-(5-bicyclo [2.2.1] heptan-2-yl)-1,1,1-trifluoro-2-(trifluoromethyl)-2-propanol The synthesis of **3b** follows the same procedure used in the fluorination of the ketone **2c**. The DAST fluorination **3a** (1 g, 3.4 mmol) gave the product (480 mg, 45% yield, b.p. 42-45 °C at 0.2 Torr, 99% pure by GC/MS) as a clear oil. ^{19}F-NMR (282.4 MHz, $CDCl_3$, $CFCl_3$): δ –76.962 (q, 3F, CF_3), -78.193 (q, 3F, CF_3), -125.892 (d, 1F, CF_2), -130.647 (d, 1F, CF_2); ^{1}H NMR (300.1 MHz, $CDCl_3$): δ 0.845-2.656 (m, 11H, aliphatic); ^{13}C-NMR (75.5 MHz, $CDCl_3$): δ 18.854(d), 26.290(d), 29.065(d), 32.109(s), 35.124(d), 38.904(t), 43.419(t), 75.901(m).

(3c) 2-Fluoro-4,4-bis-trifluoromethyl-3-oxa-tricyclo[5.2.1.0^{2,6}]decane 3c was isolated by column chromatography of reaction mixture from DAST fluorination of **3a** on silica gel using pentane:DCM (1:1) as the eluent. Rotary evaporation of the eluting solvent gave **3c** (400 mg, 40% yield, b.p. 55-60 °C at 15 Torr, 99% pure by GC/MS) as a clear oil. ^{19}F-NMR (282.4 MHz, $CDCl_3$, $CFCl_3$): δ –76.029 (q, 3F, CF_3), -78.2187 (q, 3F, CF_3); ^{1}H NMR (300.1 MHz, $CDCl_3$): δ 0.700-2.127 (m, 10H, aliphatic), 2.416 (m, 1H, aliphatic), 3.186 (s, 3H, CH_3), 3.197 (s, 3H, CH_3); ^{13}C-NMR (75.5 MHz, $CDCl_3$): δ 20.101(s), 27.449(s), 30.209(s), 32.197(s), 36.429(s), 37.914(s), 40.051(m), 50.033(s), 50.201(s), 114.807(s).

(4b) 3,6-Bis-(2,2,2-trifluoro-1-hydroxy-1-trifluoromethyl-ethyl)-bicyclo[2.2.2]oct-7-ene-2,5-dione: The dione (**4a**) was synthesized by a known

literature preparation [12]. Diisopropyl amine (8.5 mL) was combined with 40 mL dry THF under a N_2 atmosphere and cooled to -78 °C. *n*-Butyl lithium (27.5 mL of 2M solution in hexanes) was slowly added over 20 min and the solution was warmed to room temperature and kept at that temperature for 30 min. After 30 min the room temperature LDA solution was added dropwise to a solution of the dione (**4a**) (3.9 g, 28.7 mmol) and 50 mL dry THF under a N_2 atmosphere which was cooled to -78 °C. Once the LDA solution was added, the reaction mixture was warmed to room temperature and held there for 30 min. It was then cooled to -78 °C and hexafluoroacetone (12 g, 72 mmol) was condensed into an addition funnel and added dropwise to the solution. Once all of the hexafluoroacetone was added, the reaction flask was removed from the ice bath and left stirring at room temperature over night (12 hrs). The THF solution was acidified with 3M HCl until a pH of 2 was reached. The organic layer was extracted and the aqueous layer was extracted (2 x 100 mL) with diethyl ether. The organic layers were combined and washed with water, brine, dried with $MgSO_4$, filtered, and the solvent was removed by rotary evaporation to give 16 g of an orange solid. Column chromatography on silica gel using hexane/ethyl acetate (2:1) as the eluent gave **4b** (11 g, 85% yield, m.p.176-182 °C). Recrystallization of **4b** from the slow evaporation of DCM gave crystals suitable for x-ray analysis. ^{19}F-NMR (282.4 MHz, $CDCl_3$, $CFCl_3$): δ –72.970 (q, 3F, CF_3), -76.055 (q, 3F, CF_3); ^{1}H NMR (300.1 MHz, $CDCl_3$): δ 3.900 (m, 2H, bridge CH), 3.306(m, 2H, aliphatic), 6.473 (m, 1H, alkene); ^{13}C-NMR (75.5 MHz, $CDCl_3$): δ 50.038(s), 60.714(s), 129.588(s), 204.876(s).

(4c) 3,6-Bis-(2,2,2-trifluoro-1-hydroxy-1-trifluoromethyl-ethyl)-bicyclo[2.2.2]octane-2,5-dione: The procedure for the hydrogenation of **4b** is identical to the procedure used to hydrogenate **2c**. **4b** is a pale yellow solid (yield 98%, m.p. 190-194 °C). ^{19}F-NMR (282.4 MHz, $CDCl_3$, $CFCl_3$): δ –72.970 (q, 3F, CF_3), -76.055 (q, 3F, CF_3); ^{1}H NMR (300.1 MHz, $CDCl_3$): δ 3.900 (m, 2H, bridge CH), 3.306(m, 2H, aliphatic), 6.473 (m, 1H, alkene); ^{13}C-NMR (75.5 MHz, $CDCl_3$): δ 50.038(s), 60.714(s), 129.588(s), 204.876(s).

(4d) 1,1,1,7,7,7-Hexafluoro-4-isopropylimino-2,6-bis-trifluoromethyl-heptane-2,6-diol: Although 4d was isolated as a by product of the LDA/hexafluoroacetone reaction with 4b, it can also be synthesized by treating LDA with hexafluoroacetone. Diisopropyl amine (3 g, 29.7 mmol) is added to 25 mL dry THF under a N_2 atmosphere and cooled to -78 °C. *n*-Butyl lithium (13.6 mL of 2.2 M solution of *n*-butyl lithium in hexanes) was slowly added over 20 min and the solution was warmed to room temperature and kept at that temperature for 30 min. After 30 min the room temperature LDA solution was cooled to -78 °C and hexafluoroacetone (12 g, 75 mmol) is condensed in a dry ice condenser and slowly added dropwise. Once all the hexafluoroacetone is added, the reaction is removed from the ice bath and stirred overnight (12 hrs) at room temperature. The solution is then poured into 1N HCl 150 mL and the organic layer is separated. The aqueous layer is washed with ether (2 x 50 mL) and the organic layers were combined and washed with water, brine, dried with $MgSO_4$, filtered, and the solvent was removed by rotary evaporation to a give 6 g mixture of **4d**

and **4e**. Recrystallization from hexane/ethyl acetate (2.5:1) gave crystals of 4d (5.3 g, yield 41%, m.p. 143-147°C) which were suitable for x-ray analysis. ^{19}F-NMR (282.4 MHz, $CDCl_3$, $CFCl_3$): δ –76.453 (s, 3F, CF_3), -77.631 (s, 3F, CF_3); ^{1}H NMR (300.1 MHz, $(CD_3)CO$): δ 1.161 (d, 6H, CH_3), 3.058 (s, 2H, CH_2), 3.152 (s, 2H, CH_2), 3.972 (hept, 1H, CH); ^{13}C-NMR (75.5 MHz, $CDCl_3$): δ 23.126(s), 32.069(s), 33.730(s), 51.791(s), 162.803(s).

Chapter 5—Condensation Polymers: Vicinal Norbornane Diols, Norbornane Cyclic Carbonates and Norbornane Epoxides

Condensation Polymers

The search for transparent resins at 157 nm surveyed the traditional photoresist polymer types: radical, addition and ROMP polymer platforms. Both radical and metathesis polymers yielded materials too strongly absorbing for use as a V-UV resist. Addition polymerization worked fine until norbornene compounds with geminal disubstitution were used, which failed to incorporate into polymers to any large extent. This led to a search for alternate polymerization methods, and led to consideration of condensation polymerization as an alternate methodology.

Polymers have traditionally been grouped into either addition or condensation polymers (Carothers 1928). The difference between the two depends on whether the polymer repeat units have the same number of atoms as the monomers. Addition polymers does contain the same number of atoms in both the polymer repeat unit and monomer; condensation polymers have fewer resulting atoms in the repeat units than the monomer, by nature of the byproducts lost during the condensation polymerization.

Unfortunately, such an easy description to encapsulate all polymer types fails when one considers that polymers that look to be addition or condensation polymers can indeed be made via ring-opening, addition or condensation methods, and be incorrectly labeled. For example, the synthesis of a polyester can be accomplished by condensation or ring-opening methods (**Figure 5.1**):

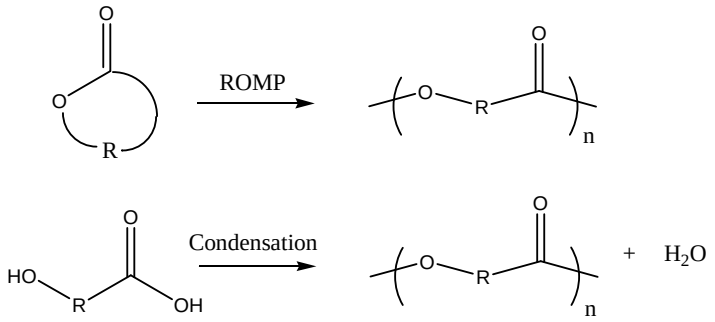

Figure 5.1: The production of polyester can occur via a ring opening or a condensation mechanism. Carothers would define the resultant polymer as either a condensation or addition polymer.

Modern polymer types are defined by the mechanism by which the polymer is produced, and there are two definitions, step-growth or chain-growth polymers. The differentiating aspect is whether polymers are formed in a stepwise method, going from unimer, dimer, trimer, tetramer—this is a step-growth polymer. Step-growth polymerizations, including condensation polymers, follow the Carothers equation (**Equation 5.1**) and degree of polymerization increases exponentially as conversion nears 90-100% (**Figure 5.2**). Those polymers made by continually adding monomers to a growing chain end are termed chain-growth polymers. Of course, ring-opening polymers can form in either chain-growth or step-growth fashion (Stevens 1999).

$$DP = \frac{1}{1-p} \qquad \textit{(5.1)}$$

Equation 5.1: The Carothers equation for step-growth polymers (p = reaction conversion; DP = degree of polymerization).

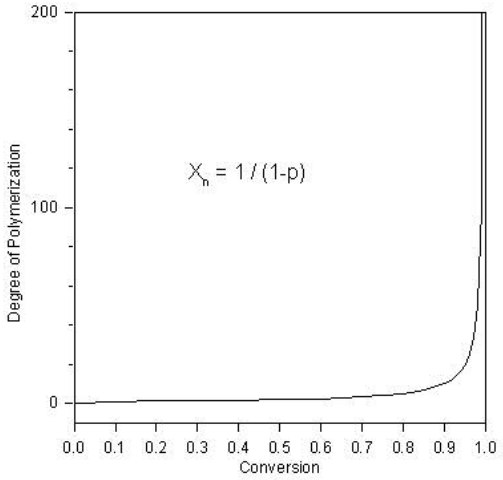

Figure 5.2: The exponential increase in degree of polymerization versus conversion for condensation polymers.

Condensation Polymers for 157 nm

The majority of photoresist polymers are of course made by chain-growth mechanisms, so considering condensation polymerization (step-growth) involved finding novel condensation monomeric materials that were transparent at 157 nm. One transformation of norbornene that would make it amenable to condensation polymerization would be to form the diol from the olefin. There are several ways to accomplish this, but two methods that were readily apparent were to dihydroxylate the olefin to yield a diol, or form the epoxynorbornane and then ring-open the epoxide to yield a diol (**Figure 5.3**). The resulting norbornane diol could be combined with either an acid dicholoride (such as phosgene) or some type of carbonate. The resulting polycarbonate might then be a way to incorporate those geminally-substituted norbornenes that polymerize poorly with addition or radical catalysts.

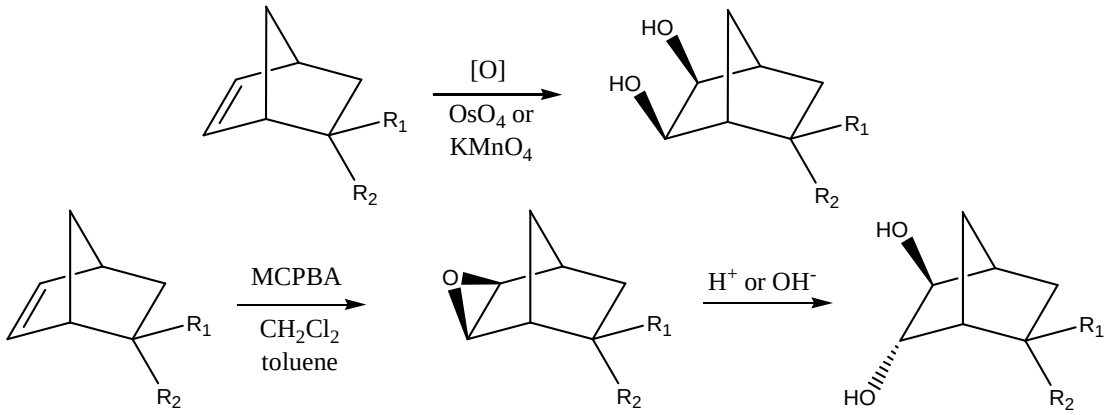

Figure 5.3: Direct oxidation of the olefin of norbornene, or by first going through an epoxy intermediate, could yield diols for condensation polymers.

This led the search for high transparency 157 nm materials to that of condensation precursor monomers, specifically targeting fluoronorbornane diols.

Norbornane Diols

Conversion began with norbornene itself. Literature precedent indicated that osmium tetroxide (OsO_4), used with N-methyl morpholine N-oxide (NMO) as the oxidizing species, gave better dihydroxylation yields on norbornene substrates. Potassium permanganate ($KMnO_4$) was decided against because of the published lower yields compared to OsO_4. The norbornene diol was recovered in good yield. Recrystallization from hexanes:ether gave pure white crystals that were resolved using X-ray. The X-ray crystallography is shown below, **Figure 5.4**.

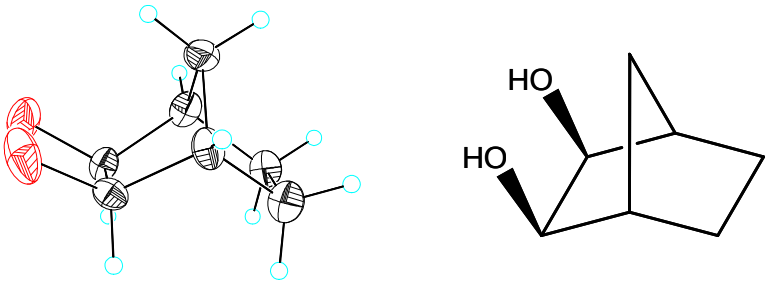

Figure 5.4: X-ray crystallography of the *cis*-diol of norbornane following oxidation with OsO_4.

When done dihydroxylation was done with a geminally disubstituted norbornene such as 2-*tert*-butyl-2-trifluoromethyl-bicyclo[2.2.1]hept-5-ene-3-carboxylate, the resulting *cis*-diol was found to be remarkably transparent in the vacuum (Chapter 2) (**Figure 5.5**).

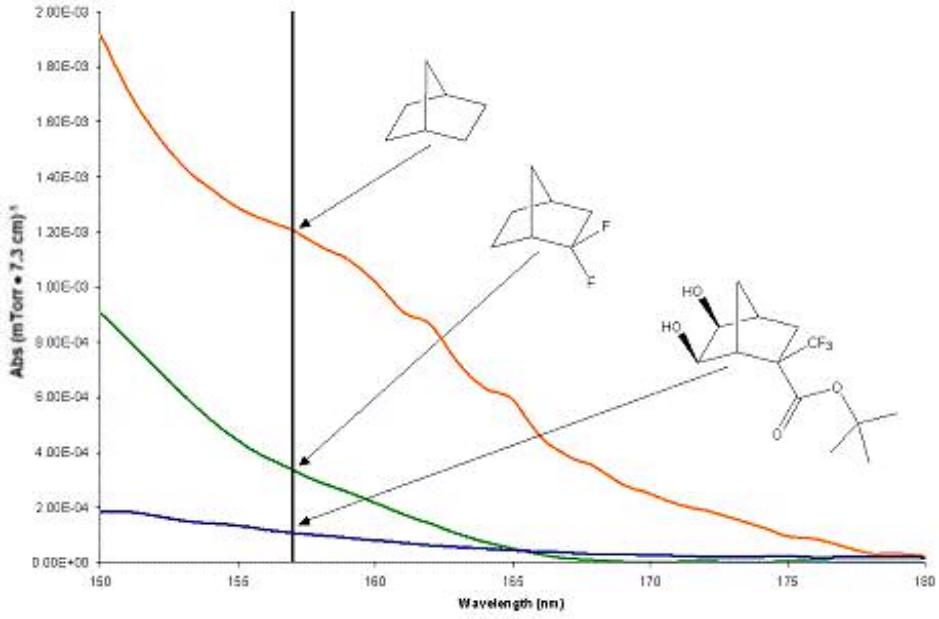

Figure 5.5: The gas phase V-UV spectra of 2-*tert*-butyl-2-trifluoromethyl-2,3-bicyclo[2.2.1]hept-5-ene-3-carboxylate diol shows high transparency, prompting studies into polycarbonates.

This low absorbance was easily one of the best results in the V-UV seen in materials screened for 157 nm materials and was found to be a consistent and repeatable gas phase result. The low absorbance rivals that of any other compound synthesized for use in 157 nm lithography in our research group. Finally, two more norbornene compounds were oxidized to the corresponding *exo*-*cis*-diols: norbornene hexafluoroisopropanol and the compound 2,2-difluoro-3-trifluoromethylnorbornen-3-ol (**Figure 5.6**).

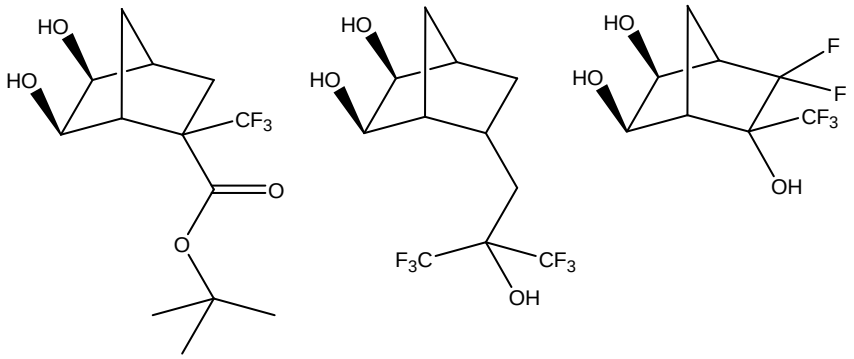

Figure 5.6: Other norbornene monomers that have been oxidized to the *cis*-diol with OsO_4.

The norbornane diol of 2-*tert*-butyl-2-trifluoromethyl-bicyclo[2.2.1]hept-5-ene-3-carboxylate was used for initial polymerization studies. A phosgene solution in toluene was used, both as an additive as well as adding the diol to the phosgene solution (**Figure 5.7**). Unfortunately, both synthetic routes formed the same product: the *exo* cyclic carbonate of the diol. This was repeated and confirmed even with the simple *exo*-*cis* diol of norbornane, and a crystal structure confirmed the final structure (**Figure 5.8**).

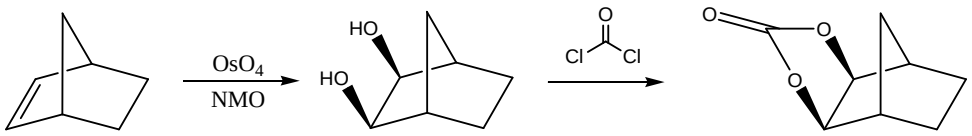

Figure 5.7: Initial attempts to form a condensation polymer instead produced a cyclic carbonate.

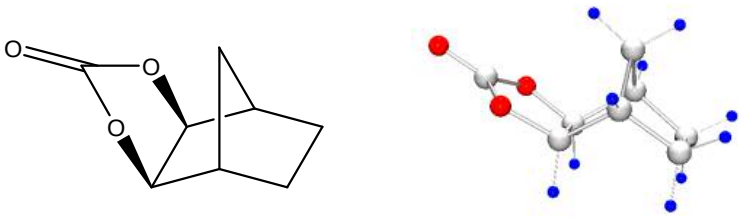

Figure 5.8: X-ray crystallography of the *exo* cyclic carbonate of norbornane.

Repeated experiments showed that the *cis* diols of norbornane, with or without functional groups, would close to form the five-member carbonate ring with little or no side reactions. One avenue of surmounting this issue would be to form the *trans* diol of norbornane and see if the increase through-space separation between the two alcohol groups would be enough to allow for polymerization. A seemingly obvious and straightforward way to synthesize a norbornane *trans* diol would be through an epoxide intermediate, opened with acid or base (**Figure 5.9**). Even isomerization of the norbornane *cis* diols with Raney nickel was considered (Heyns 1972, Taylor 1985, Taylor 1998), but all attempts to transform a norbornane *cis* diol into the corresponding *trans* diol with Raney nickel were unsuccessful.

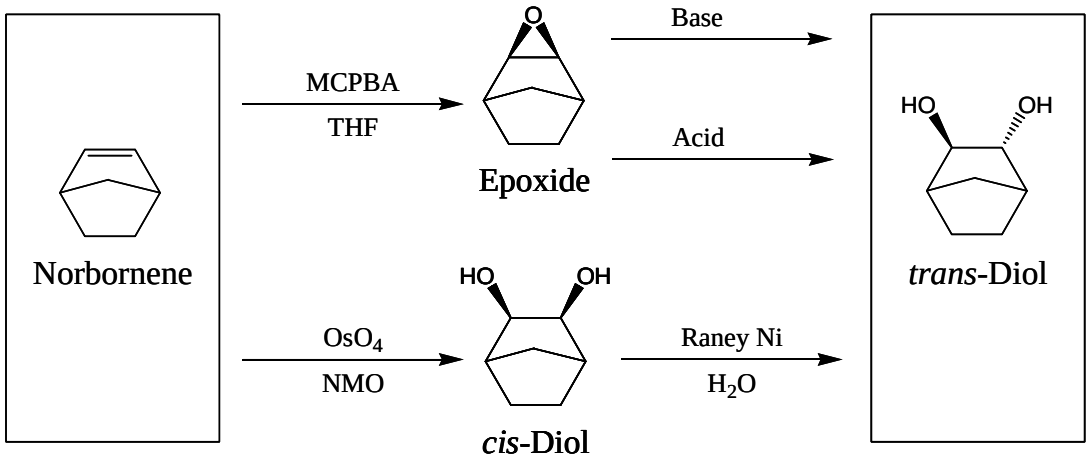

Figure 5.9: Possible ways of converting the olefin of norbornene into a *trans*-diol.

Epoxynorbornanes

Epoxides of norbornane were seen as a viable method for accessing a *trans* of norbornane. Typical ring opening of aliphatic or monocyclic epoxides proceeds in high conversion to the corresponding *trans* diol. Epoxides of a variety of fluorinated compounds were synthesized, using *meta*-chloroperbenzoic acid for ring opening reactions (**Figure 5.10**).

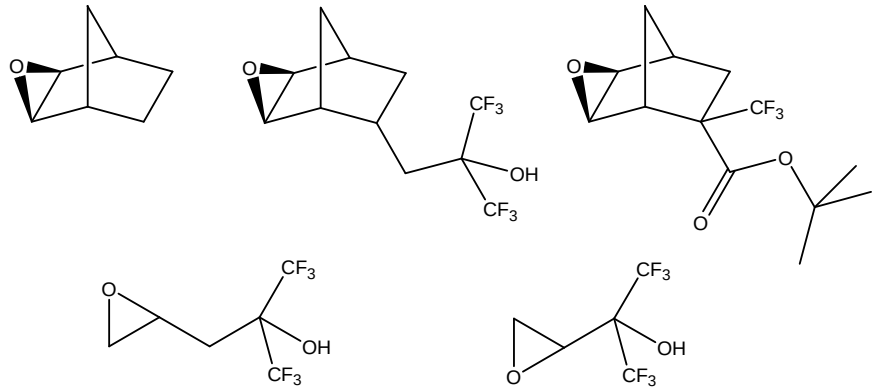

Figure 5.10: Various olefins were converted into epoxides for 157 nm materials studies.

Using a variety of reagents starting with strong acids and bases and *exo*-2,3-epoxynorbornane, attempts to ring-open the epoxide and form a *trans*-diol failed upon repeated experiments (**Figure 5.11**).

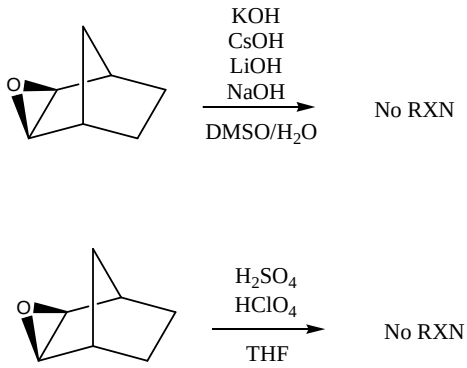

Figure 5.11: *exo*-2,3-Epoxynorbornane is resistant to a variety of acids and bases towards ring-opening reactions.

In fact, all bases used in many solvents failed to produce material other than starting material. Acid also led to an unchanged epoxide, although HCl did produce a diol, but not a *trans*-2,3-norbornane diol but rather a 2,7-norbornane diol. It is apparent that the epoxide opened on the norbornane ring, and the subsequent carbocation formed undergoes a Wagner-Meerwein rearrangement, resulting in the *cis*-2,7-substitution pattern instead of the desired 2,3-norbornane diol (**Figure 5.12**).

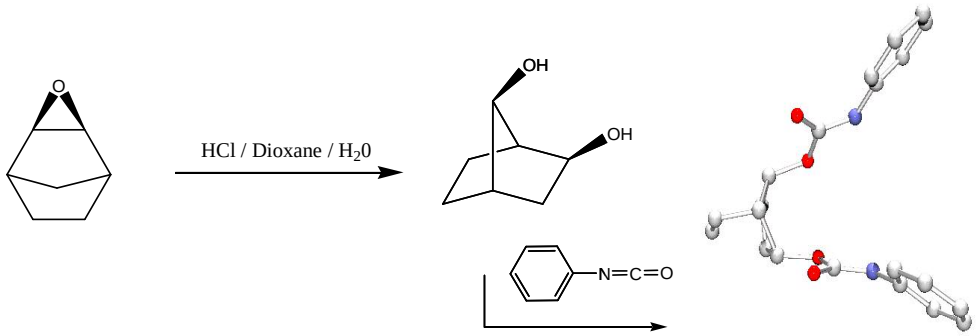

Figure 5.12: Acid-induced rearrangement of the norbornane skeleton results in a 2,7-norbornane diol.

Epoxides were formed from norbornane hexafluoroisopropanol and of 2-*tert*-butyl-2-trifluoromethyl-bicyclo[2.2.1]hept-5-ene-3-carboxylate, and ring-opening reactions were attempted again with base and acid, but to the same effect: no diol was formed. While polycarbonate could be formed from the *cis*-2,7-norbornane diol, the failure of fluorinated epoxynorbornanes to ring-open and rearrange precluded the use of (**Figure 5.13**).

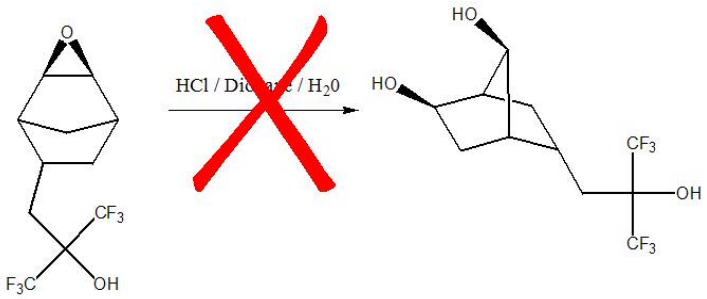

Figure 5.13: *exo*-2,3-Epoxynorbornane hexafluoroisopropanol fails to ring-open in a manner similar to *exo*-2,3-epoxynorbornane.

The inability to ring-open fluorinated epoxynorbornanes led to a search for alternate routes to polymers from these epoxides. The literature pointed to several papers by Crivello about photoinduced cationic ring opening of epoxides to produce polyethers (Crivello 1999). As epoxides of fluorinated norbornanes were readily accessible, this was seen as a viable means to access high transparency polymers for 157 nm applications. Photoinitiators used are typically sulfonium and iodonium salts, irradiated with a medium pressure mercury arc lamp, forming the epoxide through the cationic acid photoproducts (**Figure 5.14**).

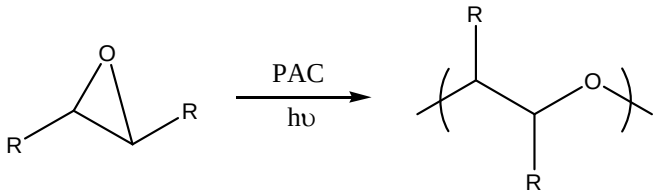

Figure 5.14: Photoinduced cationic polymerization of epoxides to form polyethers (PAC = photoactive compound).

Aliphatic and cyclic epoxides (1,2-epoxycyclohexane is a prominent example) are readily converted to polyethers, and so photoinduced cationic polymerization was attempted with the set of fluorinated norbornane epoxides synthesized. Unfortunately, only *exo*-2,3-epoxynorbornane was found to form polymer; all other attempts to cationically polymerize fluorinated alicyclic or aliphatic epoxides only resulted in starting material. The polyether of *exo*-2,3-epoxynorbornane was found to have a very strong absorbance at 157 nm, of 7.2 μm^{-1} (**Figure 5.15**).

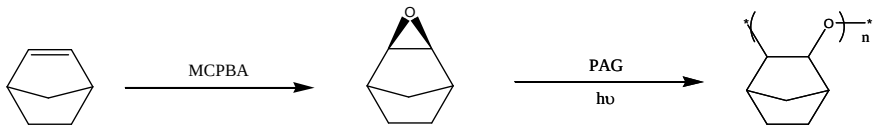

$A_{157} = 7.2$

Figure 5.15: Successful polymerization of *exo*-2,3-epoxynorbornane using a cationic photoinitiator.

Epoxides of various fluorinated materials for use in 157 nm resists were unable to be incorporated into polymers by ring opening reactions to form the corresponding *trans* diol, then reacting the diol with a carbonate or acid dichloride; the epoxide ring was observed to be strongly resistant to various strong acids and bases. Interestingly enough, hydrochloric acid did ring-open the epoxide, but the resulting norbornane rearrangement formed the *cis*-2,7-norbornane diol. While this compound could be made into a condensation polymer, no fluorinated norbornane epoxides were able to be ring opened with HCl. Alternatively, attempting to cationically open these epoxides with a photoinitiator was only successful with *exo*-2,3-epoxynorbornane, while none of the other functionalized, fluorinated epoxides could be polymerized in this manner. These results prompted studies into alternative methods for incorporating these fluorocompounds into a polymer.

Norbornane Cyclic Carbonates

Since the reaction of cis-2,3-norbornane diols to phosgene resulted only in cyclic carbonates, the literature was searched for the means to take advantage of this structure. Several possibilities arose from literature, as anionic, metal and cationic methods were

reported to successfully ring-open carbonates to form polymer (Takata 1996, Hult 2003) (**Figure 5.16)**. These different methods were applied to the cyclic carbonate of 2-*tert*-butyl-2-trifluoromethyl-bicyclo[2.2.1]hept-5-ene-3-carboxylate, but, unfortunately no polymer was recovered upon workup, only starting material.

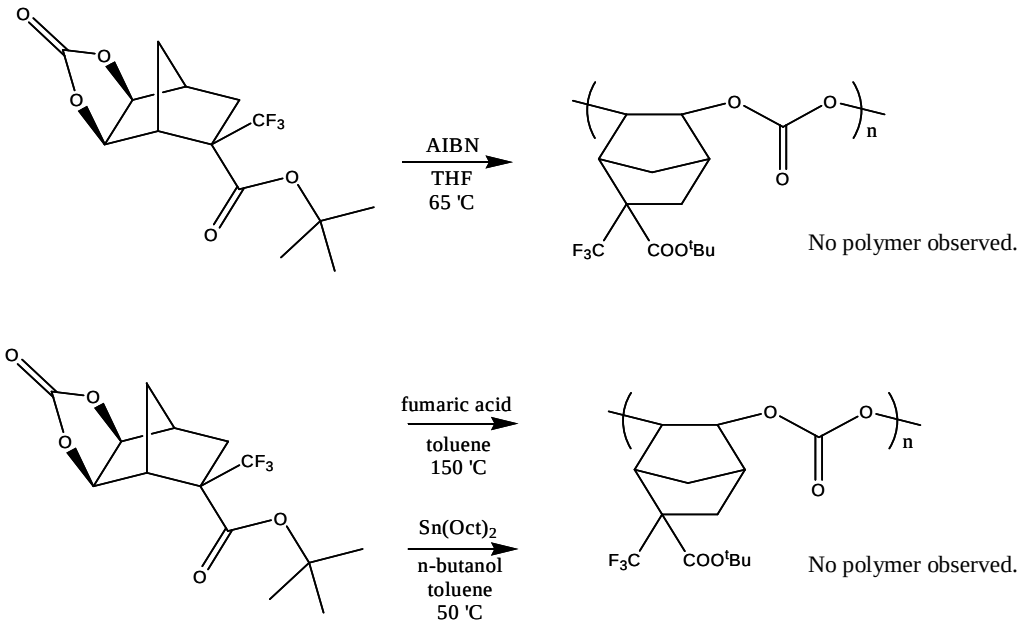

Figure 5.16: Attempts to polymerize cyclic carbonates with a variety of initiators.

Although attempts to form polycarbonates and polyethers from their respective cyclic carbonates and epoxides were largely unsuccessful, one more attempt would be made to take advantage of the propensity of *cis*-2,3-norbornane diols to readily form carbonates and ketals.

Polyketals from *cis*-Norbornane Diols

The difficulty in producing polymer from *exo*-*cis*-2,3-norbornane diols, *exo*-norbornane cyclic carbonates or from *exo*-epoxynorbornanes left fewer options available.

However, the propensity for the *cis*-norbornane diol to readily form a carbonate with phosgene was just as marked as how readily these diols would also form ketals. Acetone, when mixed in with a *cis*-norbornane diol, quickly forms a ketal (**Figure 5.17**).

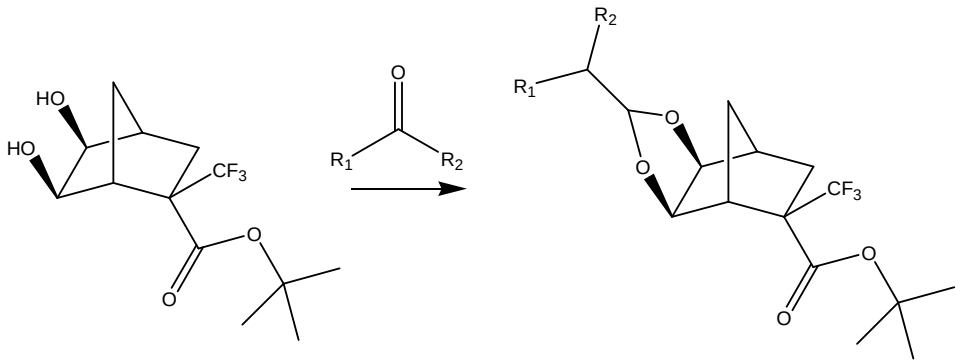

Figure 5.17: *cis*-Norbornane diol readily forms a ketal when mixed with ketones and acid.

This led to an idea of using this propensity for ketal formation to form a polymer backbone constructed by ketal linkages. By functionalizing a fluorinated norbornane diol with a pendant ketone, such a polymer might be feasibly synthesized. To this end, the *cis*-diol of norbornane hexafluoroisopropanol would be modified to include a methyl ketone at vicinal to the hexafluoroisopropanol group (**Figure 5.18**). An attempt would then be made to polymerize this compound under acidic conditions, and see what resulted, and if such a polymer could actually be realized.

Synthesis of a Polyketal Monomer

The synthesis of 1-[5,6-Dihydroxy-3-(3,3,3-trifluoro-2-hydroxy-2-trifluoromethyl-propyl)-bicyclo[2.2.1]hept-2-yl]-ethanone (**1**) was accomplished in a six-

step process from readily available starting material (**Scheme 5.1**). The preparation of **1c** closely followed a known literature preparation with only slight modification. The synthesis of **1d**, **1e** and **1** represents original syntheses conducted in our group and the first ever synthesis of an **AB** monomer with a hexafluoroisopropyl alcohol functionality incorporated into it.

Synthesis of 1-[5,6-Dihydroxy-3-(3,3,3-trifluoro-2-hydroxy-2-trifluoromethyl-propyl)-bicyclo[2.2.1]hept-2-yl]-ethanone (1)

The benzoylate (**1a**) was formed from the esterification of benzoyl chloride and 4-penten-2-ol. Treatment of **1a** with hexafluoroacetone resulted in an "*ene*" reaction, which gave the alcohol (**1b**) in high yield. Saponification of **1b** with NaOH resulted in the diol (**1c**). Selective oxidation of the secondary alcohol with Jones-reagent gave the *alpha-beta* unsaturated ketone (**1d**), which readily undergoes a Diels-Alder cyclization with cyclopentadiene to give the 2,3-substituted norbornene (**1e**). Osmium tetroxide was used to convert the olefin to the vicinal *cis*-diol (**1**).

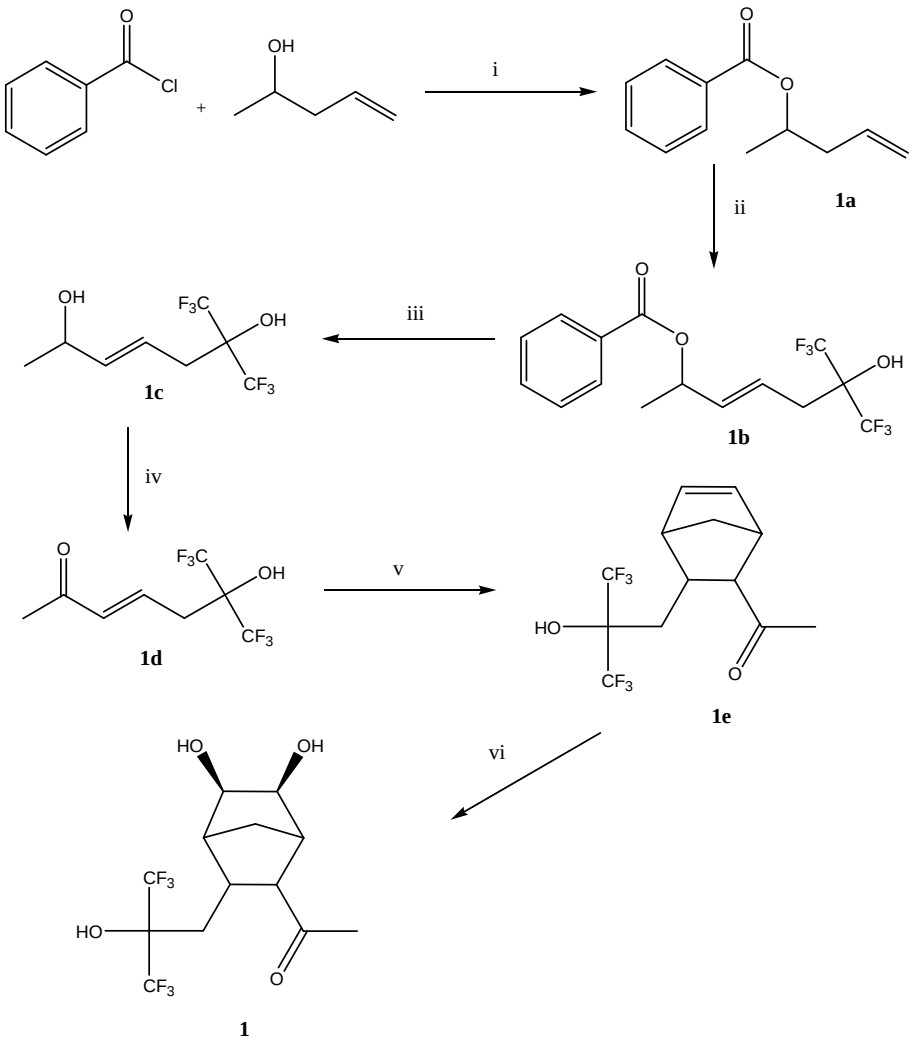

Scheme 5.1: (i) Py, DCM; (ii) hexafluoroacetone, 150 °C; (iii) NaOH; (iv) Jones reagent; (v) cyclopentadiene 60 °C; (vi) OsO_4/NMO.

The synthesis of **1** was accomplished from the starting material (benzoylchloride and 4-penten-2-ol). Steps i-v were relatively high yielding steps, and only the yield in last step (vi) dropped below 60%. The isolation of all intermediates could readily be accomplished through simple distillation (**1a-d**) or flash chromatography (**1e**). Isolation of **1** was problematic because distillation was not a viable route due to the high boiling point of the compound (>150 °C), and because of its propensity to adhere to the silica

column during chromatography. Final isolation was accomplished through a dual chromatography process. Initial flash chromatography through a plug with ethyl acetate as the eluent removed the osmium tetroxide from the product and resulted in a green/brown oil. Chromatography on a silica column with pentane/DCM (1:1) as the eluent gave **1** in 97% purity (by GC/MS).

Polyketal Synthesis

Once the monomer (**1**) was synthesized, its application towards homopolymer synthesis was investigated. The first attempt at polymerization was successful, albeit the resulting polymer was of low molecular weight (1000 amu) and its absorbance at 157 nm was much higher than expected (A_{157} = 3.7 μm^{-1}). The polymer was formed through a condensation pathway using benzene as a solvent, and tosic acid as the catalyst. Workup consisted of removal of benzene by rotary evaporation and precipitation of the polymer into a methanol/water mixture (2:1 respectively). The results from this "first pass" were both positive and negative in that the successful synthesis from monomer to polymer was accomplished, but that the resulting characteristics of the polymer formed were not ideal for 157 nm applications. Reproduction of monomer synthesis with careful attention to intermediate isolation and purification was initiated, and the homopolymerization was repeated in an analogous manner as before with only slight modification. The acid catalyst used initially was tosic acid, and investigation into alternative catalysts occurred. The results indicated that successful polymerization occurred when a sample of **1** (in benzene) was refluxed with a Dean-Stark to remove water. The acid catalyst used was Amberlyst® 15. This resin is an ion-exchange resin, which is strongly acid due to its

macroreticular structure and the sulfonic acid functionality contained therein. The resulting homopolymer (**2**) was approximately 2000 amu in mass, and had a much lower absorbance (A_{157} = 2.2 μm^{-1}) than its predecessor (**Figure 5.18**).

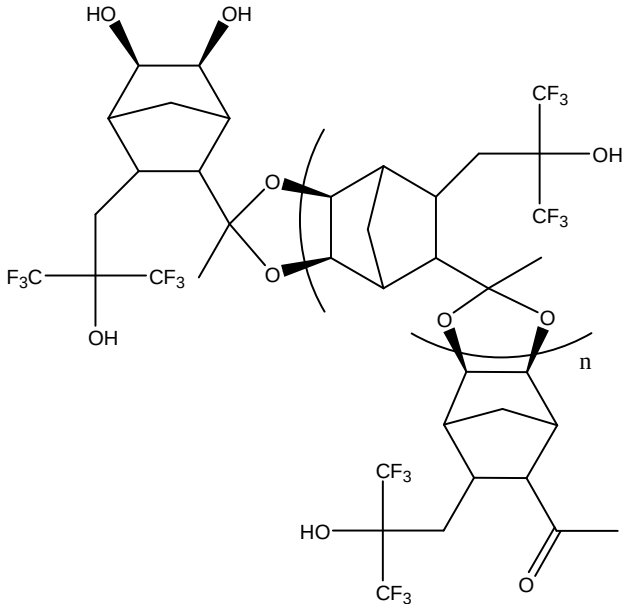

Figure 5.18: The homopolymer of 1. (M_w = 2000, A_{157} = 2.2 μm^{-1}).

The "second pass" polymer was a marked improvement in comparison to the initial work done in this area. The absorbance data obtained for this polymer is still high when compared to the homopolymer of NBHFA [ref]. This is most likely due to the low molecular weight of the polymer (**Figure 2**), which "amplifies" the effect on absorbance due to the end groups. This is rationalized by the ratio of end group functionality compared to chain length (*n*). When *n* is a low (dimer, trimer, tetramer,…etc.) the effect of the end groups is increased because they represent (by weight) a significant portion of the polymer. When n becomes large then their percent composition is drastically reduced, and their influence on the molecule is essentially negated. In terms of influence it is easy to see that repeat units that are 2, 3, and 4 monomers away from the end groups

will "know" they are there and chemically behave accordingly. When the distance from incorporated monomer to end group increases beyond 3-4 monomer units, the monomers do not chemically notice the end group species. Therefore, by increasing the polymer chain length (*n*) of 2, it is believed the corresponding absorbance values will drop substantially.

Experimental

Materials Nitrogen was purified by passage through KOH, NaOH and Drierite $CaSO_4$. All solvents were dried by the standard methods. All manipulations and polymerizations with air-sensitive materials were performed in a helium-filled drybox or using standard Schlenk vacuum line techniques under argon. All starting materials were procured from Aldrich except (2-trifluoromethyl)acrylic acid (Honeywell Int., Inc.), and were used as received unless noted otherwise.

Instruments and Equipment Nuclear magnetic resonance (NMR) spectra were obtained using either a Bruker AMX300 or a Varian *Unity Plus 300* spectrometer (^{1}H: 300 MHz, ^{13}C: 75 MHz, ^{19}F: 282 MHz). Shifts for NMR spectra are reported in ppm relative to TMS (for ^{19}F, $CFCl_3$) or to the chemical shift of the solvent. Infrared spectra were recorded on a Nicolet *Avatar 360* IR spectrometer. Melting points are uncorrected. Mass spectra were measured on a Finnigan *MAT TSQ-700* spectrometer. Molecular weights (M_w) and polydispersity indices (PDI) were measured from THF solutions using a Viscotek GPC equipped with a set of two 5 mm crosslinked polystyrene columns (linear mix and 100 Å) from American Polymer Standards and are reported relative to polystyrene standards. Polymers containing acidic functional groups were pretreated with either diazomethane or iodomethane/DBU before GPC measurement, unless noted otherwise. Differential scanning calorimetry (DSC) measurements and thermal gravimetric analysis (TGA) were performed on a Perkin Elmer *Series-7* thermal analysis system. Gas chromatographs were recorded on a Hewlett Packard *5890 Series II* with an *HP-5* (crosslinked 5% PH ME siloxane) capillary column and flame ionization detector (FID).

General Dihydroxylation Procedure with OsO_4 Typical dihydroxylation conditions are as follows: the olefin and *N*-methyl morpholine *N*-oxide (NMO) were added to a 100 mL round bottom flask placed in a water bath. Then, enough of a 90:10 mixture of THF:water was added to make a *ca.* 0.7 M solution. Osmium tetroxide (OsO_4), 2.5 wt. % in isopropyl alcohol, was added via syringe through the septum. The reaction mixture was stirred overnight in the water bath. Workup involves rotary

evaporating off the THF:water solvent, diluting in ethyl acetate and running the solution through a 1" silica plug and washing with excess ethyl acetate. Rotary evaporation followed by high vacuum removes virtually all solvent from the system, leaving the crude product, typically a crystalline solid. The solids can be recrystallized from various nonpolar organic solvents; here a 1:1 mixture of hexanes and diethyl ether was used for the recrystallization.

Dihydroxylation of Bicyclo[2.2.1]hept-2-ene Norbornene (1.0 g, 11 mmol), NMO (1.5 g, 13 mmol), OsO_4 (0.02 g, 0.085 μmol) and 33 mL THF:water were added to a 100 mL round bottom flask as described in the procedure above. The resulting crude solid had a light green color, upon recrystallization from hexanes:diethyl ether, white crystals were observed (1.8 g, 90%). ^{1}H NMR ($CDCl_3$, 300 MHz, ppm): δ 1.0-1.2 (3H), 1.4-1.5 (2H), 1.7-1.8 (1H), 2.1-2.2 (2H -OH), 3.6-3.7 (2H). IR (NaCl, cm^{-1}): 3398, 3252, 2950, 2868, 1457, 1342, 1148, 1069. GC (RT, min): 7.29 (95%). Crystal structure obtained (**Figure 5.4**).

Dihydroxylation of 2-*tert*-Butyl-2-trifluoromethyl-bicyclo[2.2.1]hept-5-ene carboxylate

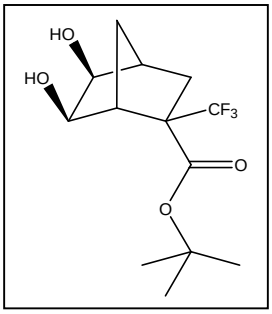

2-*tert*-Butyl-2-trifluoromethyl-bicyclo[2.2.1]hept-5-ene-3-carboxylate (1.0 g, 4 mmol), NMO (0.5 g, 4 mmol), OsO_4 (0.08 g, 0.03 mmol) and 15 mL THF:water were added to a 100 mL round bottom flask as described in the procedure above. The solution turned a dark brown immediately, but after an hour of stirring at room temperature turned to an orange color. The resulting crude solid had a dark brown to black color to it. Recrystallization from 1:1 hexanes:diethyl ether yielded a white solid. GC (RT, min): 11.2 (96%). ^{1}H NMR ($CDCl_3$, 300 MHz, ppm): δ 0.6-1.0 (m, 2H), 1.2-1.4 (m, 2H), 1.6-1.7 (m, 2H), 2.0-2.2 (m, 9H, *t*-Bu), 3.3-3.4 (d, 1H), 3.8 (m, 1H), 4.5 (m, 1H), 5.2-5.3 (d, 1H). No olefinic peaks observed. IR (NaCl, cm^{-1}): 3426, 3242 (-OH), 2969, 1735 (C=O), 1294, 1142, 1084, 1048, 1027, 842.

Dihydroxylation of 3-(5-Bicyclo[2.2.1]hepten-2-yl)-1,1,1-trifluoro-2-(trifluoromethyl)-2-propanol

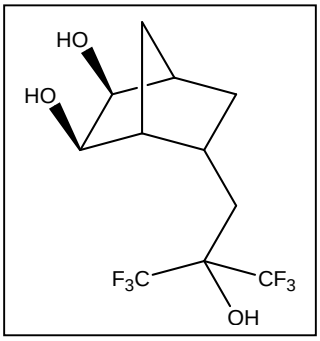

3-(5-Bicyclo[2.2.1]hepten-2-yl)-1,1,1-trifluoro-2-(trifluoromethyl)-2-propanol (1.0 g, 4 mmol), NMO (0.5 g, 4 mmol), OsO_4 (0.008 g, 0.003 mmol) and 15 mL THF:water were added to a 100 mL round bottom flask as described in the procedure above. The solution turned a dark green-yellow color upon addition of OsO_4, after stirring overnight at room temperature; the mixture has a light green color. This compound was worked up as described in the procedure above, and white crystals were formed in the evacuated flask. Recrystallization from dichloromethane yields a white solid. GC (RT, min): 10.4 (96%). ^{1}H NMR ($CDCl_3$, 300 MHz, ppm): δ 1.4-1.5 (d, 2H), 1.5-1.6 (m, 1H), 1.6-1.7 (m, 2H), 1.8-1.9 (m, 1H), 2.3-2.4 (m, 1H), 2.6-2.7 (d, 1H), 2.7-2.8 (m, 1H), 3.3-3.4 (m, 3H), 3.9 (m, 1H), 4.0-4.1 (m, 1H). No olefinic peaks observed.

General Epoxidation Prodecure (Reference: *Org. Syn. V*, **1973**, 467 and *Org. Syn. VI*, **1988**, 39) A typical epoxidation procedure is as follows: a 100 mL three-neck round bottom flask was charged with the olefin and fitted with a reflux condenser and 50 mL addition funnel under a N_2 blanket. To a solution of *meta*-chloroperbenzoic acid (MCPBA, 75% solution in water) was added THF to make an overall 0.5 M solution. This solution was added to the olefin over a period of 2 h. Alternatively, the olefin can be diluted into toluene to make a 3 M solution, and the MCPBA taken up enough into dichloromethane to make a 0.4 M solution, which was similarly added dropwise to the olefin solution over a period of 2 h. The reaction mixture was stirred overnight at reflux. After workup (NaOH or $Na_2S_2O_5$, 5% $NaHCO_3$, brine), solvent was removed via rotary evaporation and the product can typically be distilled to purify the product.

Synthesis of *tert*-butyl *exo-cis*-2,3-epoxy-5-trifluoromethyl-5-bicyclo[2.2.1]heptane carboxylate

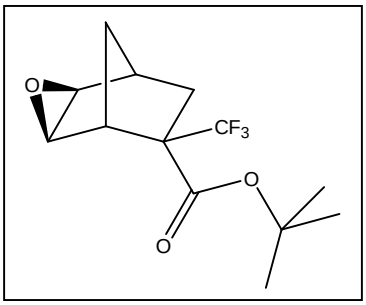

To a 100 mL three-neck round bottom flask was added 2-*tert*-butyl-2-trifluoromethyl-bicyclo[2.2.1]hept-5-ene-3-carboxylate ($NBCF_3TBE$) (3.0 g, 11 mmol). MCPBA (2.4 g, 14 mmol) in 50 mL THF was added per the above procedure. The solution was washed once with 25 mL $Na_2S_2O_5$, three times with 100 mL 5% $NaHCO_3$ and with 100 mL saturated NaCl, dried over $MgSO_4$, filtered and the THF removed by rotary evaporation. Fractional vacuum distillation yielded the product (65-67 °C @ 5 Torr) as a clear liquid, 9.5 g (45% yield). ^{1}H NMR ($CDCl_3$, 300 MHz, ppm): δ 1.4-1.5 (s, 9H, *t*-Bu), 1.8-1.9 (m, 2H), 2.8 (m, 1H), 2.9 (m, 1H), 3.0-3.1 (m, 1H), 3.2-3.3 (m, 1H).

Synthesis of *exo-cis*-2,3-epoxy-5-(3,3,3-trifluoro-2-trifuoromethyl-2-hydroxypropyl) bicyclo[2.2.1]heptane

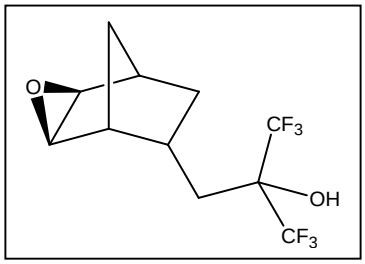

To a 100 mL three-neck round bottom flask was added 2-(3,3,3-trifluoro-2-trifuoromethyl-2-hydroxypropyl) bicyclo[2.2.1]heptane-5-ene (NBHFA) (10.0 g, 36 mmol) and 15 mL toluene. MCPBA (6.6 g, 38 mmol) in 10 mL CH_2Cl_2 was added per the above procedure. The solution was washed five times with 100 mL of 5% $NaHCO_3$, once with 100 mL saturated NaCl and with 100 mL H_2O, dried over $MgSO_4$, filtered and the solvents removed by rotary evaporation. This afforded 4.4 g of a white solid (42% yield). GC (RT, min): 8.1 (95%). ^{1}H NMR ($CDCl_3$, 300 MHz, ppm): δ 1.4-1.5 (m, 2H), 1.5-1.6 (m, 2H), 1.7-1.8 (m, 2H), 2.6-2.7 (m, 2H), 2.7-2.8 (m, 1H), 3.0-3.1, (m, 2H), 4.5 (s, 1H).

Synthesis of *n*-1,2-epoxy-4-trifluoromethyl-5,5,5-trifluoropentanol

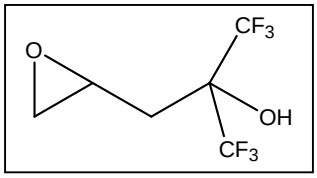

To a 100 mL three-neck round bottom flask was added allyl hexafluoroisopropanol (10.0 g, 48 mmol) and 15 mL toluene. MCPBA (6.6 g, 38 mmol) in 10 mL CH_2Cl_2 was added per the above procedure. The solution was washed five times with 100 mL of 5% $NaHCO_3$, once with 100 mL saturated NaCl and with 100 mL H_2O, dried over $MgSO_4$, filtered and the solvents removed by rotary evaporation. This afforded a light yellow liquid that darkened over time to an orange color (9.5 g, 89% yield). GC (RT, min): 4.1, 4.2 (99+%). ^{1}H NMR ($CDCl_3$, 300 MHz, ppm): δ 2.2-2.4 (m, 2H), 2.4-2.5 (m, 2H), 3.0-3.1 (d, 1H), 4.6-4.7 (s, 1H).

Typical Acid Hydrolysis of *exo*-2,3-Epoxynorbornanes *exo*-2,3-Epoxynorbornane (2.0 g, 18 mmol), perchloric acid (8.5 mL, 70% solution, 21 mmol) and 100 mL THF were combined in a 250 mL round bottom flask and stirred overnight under a N_2 blanket. The solution was diluted with 150 mL H_2O, extracted four times with 100 mL diethyl ether, dried with $MgSO_4$, filtered and the solvent removed by rotary evaporation. White solids were recovered and recrystallized with 10 mL of 1:1 ether:methanol mixture. In all cases studied here ($HClO_4$, H_2SO_4), GC and IR showed only starting material.

Typical Base Hydrolysis of *exo*-2,3-Epoxynorbornanes *exo*-2,3-Epoxynorbornane (2.0 g, 18 mmol), potassium hydroxide solution (2.75 mL, 4M solution, 11 mmol) and 40 mL DMSO were combined in a 100 mL round bottom flask, heated to reflux and stirred overnight under a N_2 blanket. The solution was washed twice with 50 mL DCM. The organic layer was washed twice with 100 mL 5% $NaHCO_3$ and twice with 100 mL of brine solution. The organic solution was dried over $MgSO_4$, filtered and the solvent (*ca.* 100 mL DCM) removed by rotary evaporation. In all cases studied here (NaOH, KOH, KOtBu, KOAc, NaOMe), GC and IR show only starting material.

Raney Nickel Isomerization of *cis*-Norbornane Diols (Reference: Taylor, J.E., *Synthesis*, **1985**, 1142-44.) Raney nickel, a slurry in water, pore size 50 μm (1.0 mL) was added to 5-*tert*-butyl-5-trifluoromethyl-2,3-bicyclo[2.2.1]heptandiol carboxylate with 20 mL water. The reaction was stirred for 72 h under N_2. The resulting slurry solution was filtered through Celite to remove the nickel catalyst. The aqueous solution was rotary evaporated to remove all but approximately 50 mL of water. To this solution was added

50 mL CH_2Cl_2 and the solution was stirred for 12 h to extract out the norbornane diol. After 12 h, the CH_2Cl_2 was separated and another 50 mL CH_2Cl_2 added. This cycle of extraction continued for 48 h. The organic fractions were combined, dried over $MgSO_4$, and the solvent removed by rotary evaporation. All functionalized norbornane diols were unaffected by this isomerization, only starting material was observed by GC and IR.

Polyketal Synthesis

Compounds **1a-d** were synthesized according to known literature procedures (Nagai 1989). All spectral and physical data match published data.

(1e) 1-[3-(3,3,3-Trifluoro-2-hydroxy-2-trifluoromethyl-propyl)-bicyclo[2.2.1]hept-5-en-2-yl]-ethanone **1d** (2 g, 8 mmol) was combined with freshly distilled cyclopentadiene and 30 mL benzene in a Parr reactor and heated to 100 °C for 24 hrs. After 24 hrs, the reaction mixture was removed from the Parr reactor and the solvent was removed by rotary evaporation. Column chromatography on silica gel with hexane/ethyl acetate (5:1) gave **1e** (1 g, 40% yield, 99% pure by GC/MS, white solid m.p. 125-130 °C). ^{19}F-NMR (282.4 MHz, $CDCl_3$, $CFCl_3$): δ –77.289 (q, 3F, CF_3), -78.881 (q, 3F, CF_3); ^{1}H NMR (300.1 MHz, $CDCl_3$): δ 1.566 (m, 2H, CH_2), 2.193 (s, 3H, CH_3) 2.264 (m, 2H, CH)2.645 (m, 2H, bridge CH), 6.052 (m, 1H, alkene), 6.313 (m, 1H, alkene); ^{13}C-NMR (75.5 MHz, $CDCl_3$): δ 28.488(s), 35.888(s), 45.967(s), 47.009(s), 49.915(s), 62.106(s), 132.677(s), 139.515(s), 204.876(s).

(1) 1-[5,6-Dihydroxy-3-(3,3,3-trifluoro-2-hydroxy-2-trifluoromethyl-propyl)-bicyclo[2.2.1]hept-2-yl]-ethanone **1e** (2.6 g, 8 mmol) was combined with N-methylmorpholine oxide (NMO) (1.2 g, 10 mmol) in 60 mL THF/H_2O (9:1). Osmium tetroxide (0.8 mL, 6.5 e^{-5} mmol) was added and the mixture was stirred at room temperature for 12 hrs. After 12 hrs, the solvent was removed via rotary evaporation and the residue was washed through a silica gel plug with ethyl acetate as the eluent. The eluent was removed by rotary evaporation and the 3.75 g brown oil was chromatographed on a silica gel column to give **1** (1.5 g, 53% yield). ^{19}F-NMR (282.4 MHz, $CDCl_3$, $CFCl_3$): δ –76.321 (q, 3F, CF_3), -77.543 (q, 3F, CF_3); ^{1}H NMR (300.1 MHz, $CDCl_3$): δ 1.2-2.2 (m, 7H, aliphatic), 2.8-3.6 (m, 6H, aliphatic), 4.01(bs, 2H, OH); ^{13}C-NMR (75.5 MHz, $CDCl_3$): δ 23.702(s), 28.020(s), 36.432(s), 38.212(s), 42.982(s), 49.333s), 59.136(s), 71.557(s), 72.435(s), 210.476(s).

Homopolymer of 1: poly-1-[5,6-Dihydroxy-3-(3,3,3-trifluoro-2-hydroxy-2-trifluoromethyl-propyl)-bicyclo[2.2.1]hept-2-yl]-ethanone 4 mL of a 0.7 M solution of **1** in benzene was placed into a round bottom flask with 100 mg of Amberlyst® 15 and heated to reflux with a Dean-Stark trap attached. After 36 h at reflux, the solution was cooled and filtered to remove the Amberlyst® beads. Rotary evaporation was used to remove the benzene, and the polymer was then dissolved into 2 mL DCM and precipitated into cold (-78 °C) hexanes. M_w = 2000, A_{157} = 2.2 μm^{-1}.

Chapter 6— Imaging and Materials Development for 157 nm Photolithography

Photoresist Evaluation at 157 nm

The screening of materials for good lithographic performance at 157 nm had to adhere to the same requirements as that of any photoresist. A high performance resist must satisfy the following provisions: transparency at the exposure wavelength, high T_g, photosensitivity, high contrast and good etch resistance. The difficulty in surveying materials at 157 nm, as evidenced by the preceding chapters, is the high absorbance of most organic compounds at this short wavelength. The search for increasingly transparent polymers for use at 157 nm became representative of the difficulty in finding materials with low absorbance at 157 with which to formulate high-resolution photoresists. Vacuum ultraviolet spectroscopic screening and evaluation of various hydrogenated monomers aided in the search for high transparency materials for 157 nm.

Materials Development of 157 nm Photoresists

One of the ultimate goals for 157 nm resist materials was to produce well-defined, high-resolution features with the most transparent resins available. This was a significant challenge considering that the majority of polymers produced for resists used were strongly absorbing, usually having an absorbance between 2-4 μm^{-1} at 157 nm. The aim was to begin with a polymer resin that had an absorbance below 2 μm^{-1} or optimally, below 1 μm^{-1}. The absorbance and performance impact of the photoacid generator (PAG) and dissolution inhibitors was also taken into account. This narrowed the materials options as well as presented new challenges. These interesting issues were

resolved using innovative methods during imaging and helped our understanding of the and new properties associated with the resist materials that were studied.

Controlling the dissolution rate of resist is a matter of much discussion that has been reported on elsewhere in detail (Burns 2002). The basic challenge in positive tone lithography systems is to assure that in the unexposed regions, the resist has as low a dissolution rate as possible. Conversely, when the photoresist is irradiated, it is desirable to have the resist dissolution rate be as high as possible. The difference in exposed and unexposed dissolution rates leads to what is known as *contrast* (**Figure 6.1**), represented by γ (**Eqn 6.1**). Contrast is an important indicator of the resolving power of a photoresist. Many polymers and dissolution modifiers were designed and synthesized in order to streamline and maximize optimum imaging performance.

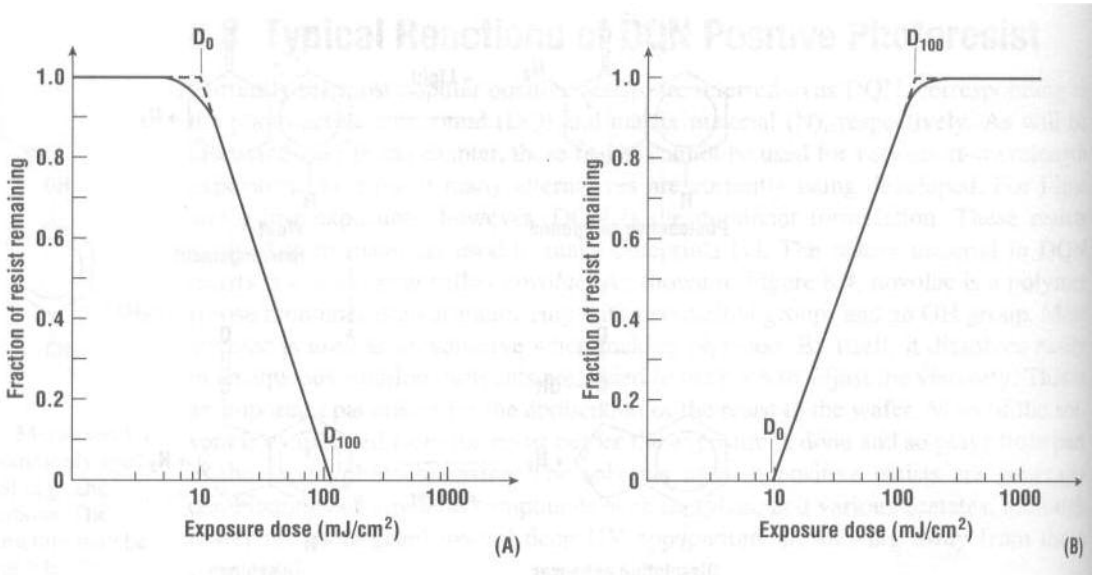

Figure 8.7 Contrast curves for idealized resists: (A) postitive tone and (B) negative tone.

Figure 6.1: Contrast curves for positive and negative tone photoresists (Campbell 2001).

$$\gamma = \frac{1}{\log_{10}(D_{100} / D_0)} \qquad \textbf{(6.1)}$$

Equation 6.1: Resist contrast is defined as the rate of change of resist thickness with increasing dose.

The targeted imaging goal was to successfully print 100 nm dense lines and spaces (100 nm wide lines with a 100 nm space between each line), at a minimum resist thickness of 300 nm. The primary concern in accomplishing this goal was finding a resist transparent enough and with high enough contrast to accomplish this task.

Radical Copolymers

Many photoresists used today in the semiconductor industry are made by a free radical process; this includes acrylate and norbornene systems, as well as the so-called COMA (Cyclic Olefin Maleic Anhydride) alternating copolymer systems (ref). One advantage of the free radical copolymers was the ability to incorporate geminally disubstituted norbornene monomers into a polymer, something not achievable with metal catalysts.

Analogous polymers were made to emulate those used at 193 nm, although these low molecular weight copolymers were found to be strongly absorbing at 157 nm. In fact, compared to polymers prepared by metal catalyzed addition methods, free radical polymers were usually found to be an order of magnitude more absorbing. Although it is possible to image such radical polymers at 157 nm (**Figure 6.2**), this high absorbance precluded their use as a resin for attempting 100 nm printing.

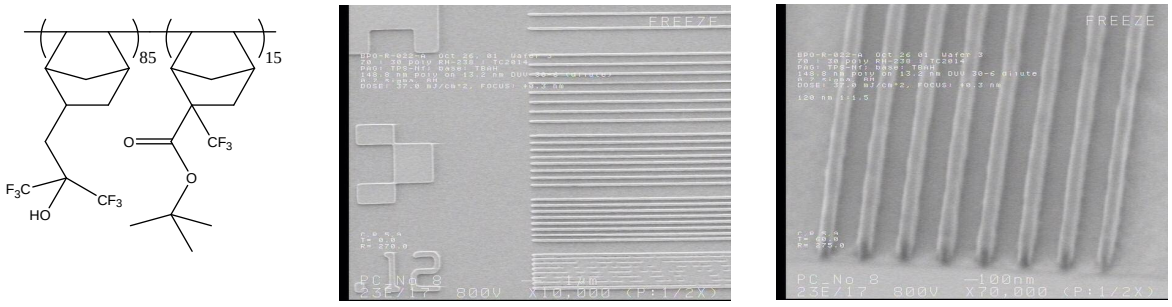

Figure 6.2: Imaging of the free radical copolymer poly(NBHFA-*co*-CF3NBtBE) at 157 nm.

Alternative Polymer Platforms

Copolymers synthesized via ring opening metathesis polymerization (ROMP) that have been described previously (Chapter 3). These polymers suffered from high absorbance at 157 nm, again ruling out their use as a high performance 157 nm resist material. Tricyclononene-based polymers were also used with success for high resolution imaging at 157 nm (Chapter 4). However, even these robust polymers displayed an absorbance that was still above 1 μm^{-1}, and so alternative addition polymers were investigated. Condensation polymer synthesis had only just begun while final imaging experiments were carried out, and no polymers have yet been synthesized with transparency that rivals the addition polymers, although may likely change in the very near future. Siloxane and silsesquioxane modified polymers have been reported previously (Tran 2002).

Carbon Monoxide Copolymers

The carbon monoxide copolymer oligomers shown below (**Figure 6.3**) were synthesized using Drent's catalyst and have been well characterized and reported

previously (Trinque 2002). These compounds were evaluated for use as a 157 nm resin material, despite relatively high absorbance of a variety carbon monoxide copolymers (Hung 2000).

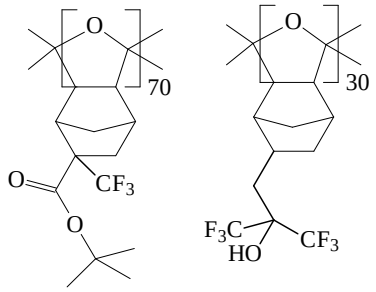

Figure 6.3: Carbon monoxide copolymers that were able to incorporate geminally disubstituted norbornenes; high absorbance of the copolymers (2.7 to 3.6 μm^{-1})relegated these materials to use as dissolution inhibitors.

Mixed with a photoacid generator (PAG), triphenylsulfonium nonflate (TPS-Nf) and a small amount of base, tetrabutylammonium hydroxide (TBAH) to quench undesired acid migration into the unexposed areas, this resist was imaged at 157 nm. The resist images are shown below (**Figure 6.4**) and indicate a great deal of roughness everywhere along the resist, thus making this system a poor candidate for a 157 nm resin. These CO copolymers would find better use as dissolution inhibitors for the many addition polymers of norbornene hexafluoroisopropanol.

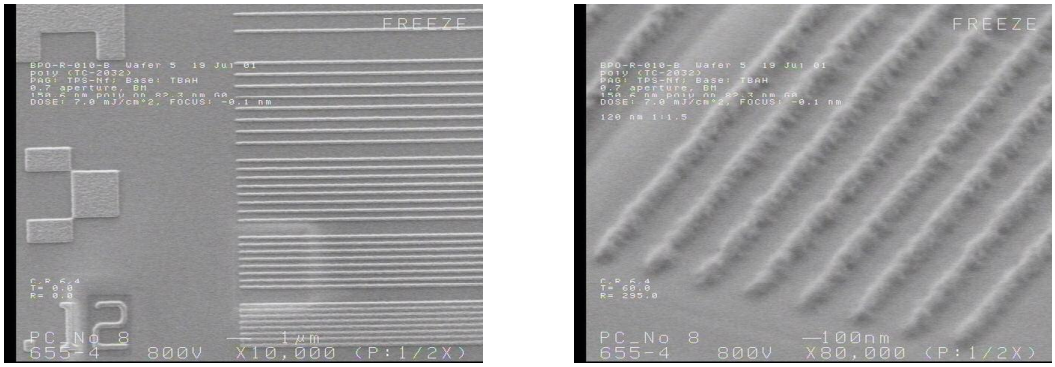

Figure 6.4: Carbon monoxide copolymer system at 157 nm; high absorbance (2.7 μm^{-1}) and roughness of the polymer precludes the use of this material as a 157 nm resin.

PNBHFA: An Ideal Candidate for Addition Copolymers

The homopolymer of (3-(bicyclo[2.2.1]hept-5-en-2-yl)-1,1,1-trifluoro-2-(trifluoromethyl)propan-2-ol) (NBHFA), synthesized via addition polymerization, is very transparent at 157 nm. Its synthesis and characterization is well known (Tran 2002). The catalyst used is a transition allyl palladium chloride dimer, and polymers made by this method were found to be more transparent than those made by radical processes. Since purity is such a critical aspect of material syntheses for 157 nm, batch-to-batch variation was quite common. Various polymer workup methods were used to try to clean the polymer, improving the transparency of the material. The cleanest batch of PNBHFA made in our research group had an absorbance of 1.15 μm^{-1} at 157 nm (**Figure 6.5**) (Hung 2000).

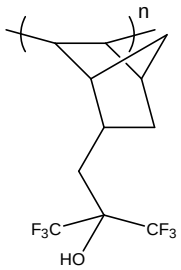

Figure 6.5: Addition norbornene hexafluoroisopropanol polymer (PNBHFA), A_{157} = 1.15 μm^{-1}.

Addition PNBHFA Copolymer Systems

The low absorbance of PNBHFA made it an ideal material for a series of copolymers with which to attempt high aspect ratio imaging experiments at 157 nm. One of the very first copolymer systems examined at 157 nm was the addition polymer of norbornene hexafluoroisopropanol and norbornene t-butyl ester, as indicated below (**Figure 6.6**).

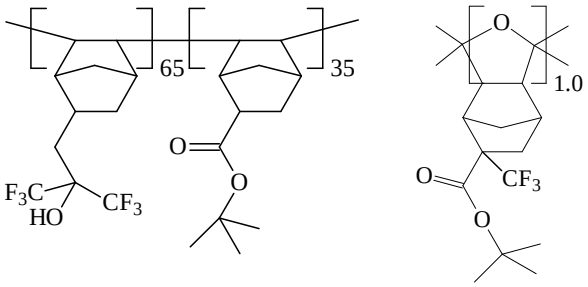

Figure 6.6: Addition norbornene hexafluoroalcohol-co-norbornene tert-butyl ester, with the carbon monoxide copolymer as the dissolution inhibitor.

This copolymer has no geminal disubstitution on either monomer, and so can be polymerized using the conventional Pd^{+2} addition polymerization method. The resist formulation also incorporated the carbon monoxide copolymer as a dissolution inhibitor, which added contrast to the system. Unfortunately, the inclusion of the norbornene t-

butyl ester monomer, which has no fluorination, greatly increased the absorbance of the final polymer. At 157 nm, this polymer has an absorbance of 2.7 μm^{-1} (Hung 2001). Initial imaging experiments using this polymer were carried out at a thickness of approximately 150 nm to optimize processing conditions, in order to yield the best profile. This produced the images seen below (**Figure 6.7**), which showed promising initial results.

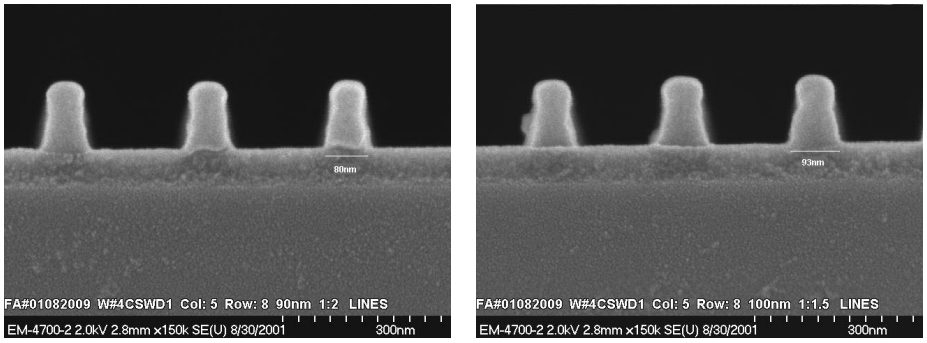

Figure 6.7: Imaging the poly(NBHFA-co-NBTBE) platform at 90 and 100 nm feature sizes.

Increasing the Poly(NBHFA-co-NBTBE) Resist Thickness to 200 nm

The following experiment increased the same poly(NBHFA-*co*-NBTBE) resist formulation to a film thickness of 200 nm and examined the resulting image profiles. The best images, exposed using a phase shift mask, are shown below (**Figure 6.8**). As can be seen from the SEM images, there is severe erosion of the feature profile, known as top loss, and the subsequent film thickness is much lower than 200 nm. The significant absorbance impact is seen as well, leading to the trapezoid-like shape to the resist shape.

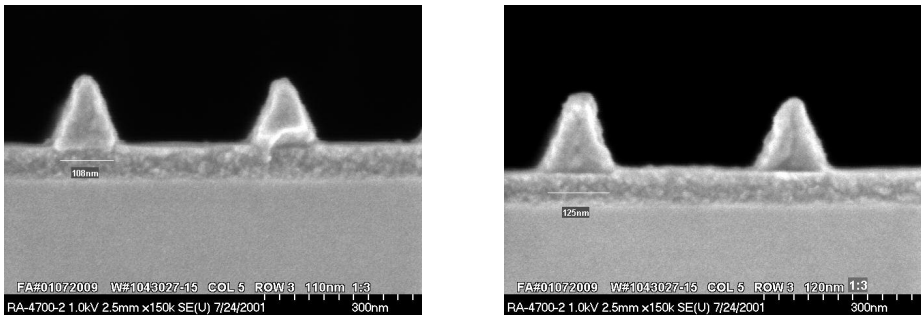

Figure 6.8: 110 nm and 120 nm 1:3 images of the poly(NBHFA-co-NBTBE) platform starting at an initial resist thickness of 200 nm. Note the trapezoidal resist profile shape, resulting from the high absorbance of the resist at 157 nm.

The formulated resist has an absorbance of 3.4 μm^{-1} at 157 nm, beginning with a base polymer absorbance of 2.7 μm^{-1}. The resist profile is markedly different than when imaged at an initial 150 nm film thickness. Nearly all of the images using this addition copolymer formulation suffered from significant resist top loss, and the impact of its high absorbance. There simply are not enough photons making it through the resist film.

This gives some indication to the severity of the absorbance problem faced regarding polymer synthesis for 157 nm applications. Whereas the base polymer can have a reasonably favorable absorbance of between 2-3 μm^{-1}, the fully formulated resist will often have a final absorbance of approximately 2.5 to 4.0 μm^{-1}, which gives an order of magnitude more absorbance to the photoresist. This limits the ability to print images much thicker than 150 nm.

PNBHFA-*co*-PNBHFABOC Copolymer Imaging Studies

One of the promising addition copolymer platforms we examined at 157 nm imaging experiments was the poly(NBHFA-*co*-NBHFABOC), an attractive platform

because of the polymer's low base absorbance at 157 nm (2.0 μm^{-1}), which should aid the imaging profile greatly. At first, a polymer with 30% *t*-BOC protection was used in conjunction with a carbon monoxide dissolution inhibitor (**Figure 6.9**).

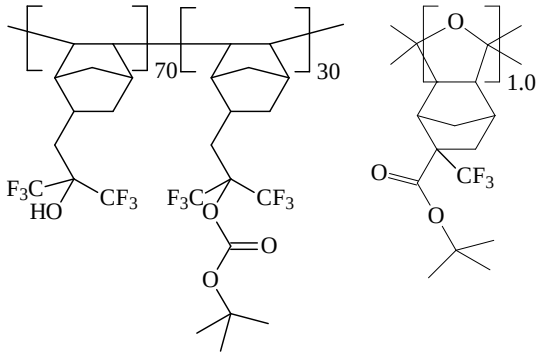

Figure 6.9: A formulation of poly(NBHFA-co-NBHFA t-BOC) with 30% t-BOC protection, and a carbon monoxide dissolution inhibitor, blended at a ratio of 70:30.

As can be seen, the 70:30 blend of the poly(NBHFA-*co*-NBHFABOC) copolymer was found to be too absorbing, due to the amount of dissolution inhibitor used (Hung 2001). The resultant images for the 70:30 blend are shown below (**Figures 6.10**). As shown, there is significant top loss of resist as well as poor contrast. The final resist absorbance at 157 nm was found to be 2.1 μm^{-1}, a relatively small increase in absorbance, compared to the earlier formulations studied.

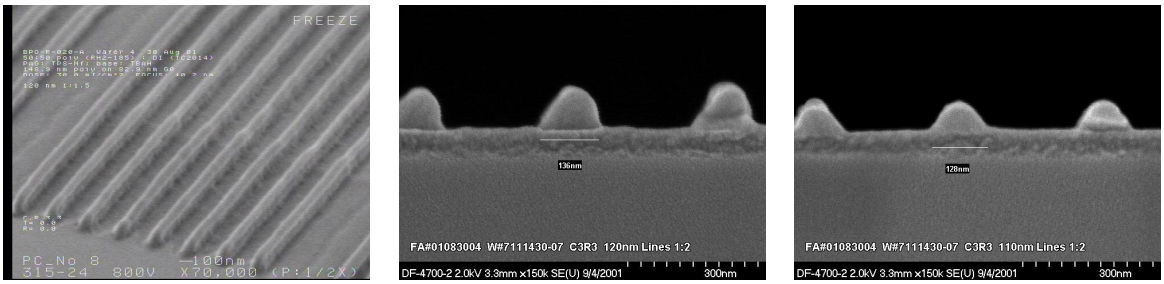

Figure 6.10: Initial poly(NBHFA-*co*-NBHFA *t*-BOC) imaging at 157 nm.

Ultimately it was found that less *t*-BOC protection of the copolymer, which led to a lower absorbance at 157 nm, led to better imaging performance. Using the same formulation but with lower *t*-BOC protection of the base polymer, high resolution images were achieved that were superior to the 30% *t*-BOC-protected polymer (**Figure 6.11**).

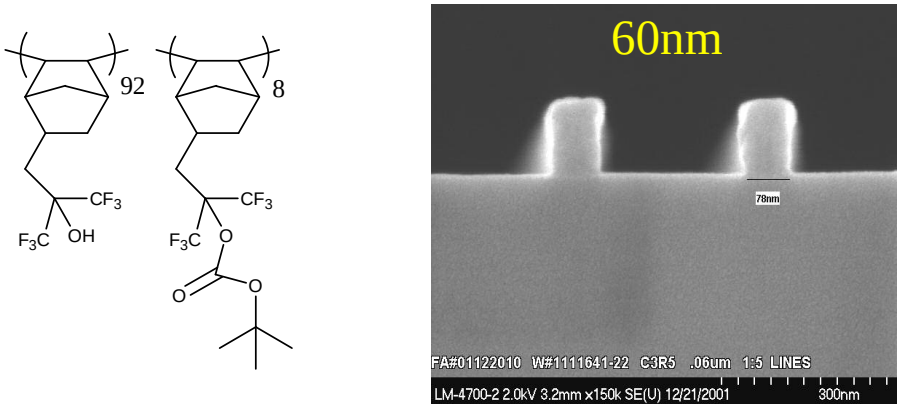

Figure 6.11: Optimum imaging with the poly(NBHFA-*co*-NBHFA *t*-BOC) system, using less protection and therefore a more transparent resin.

Unfortunately again, difficulty arose when trying to image this formulation at film thickness of 200 nm or higher. However, the reduced amount of protection leading to a lower absorbance in the PNBHFA system would lead to a different approach to solving the high aspect ratio 157 nm imaging challenge.

The PNBHFA Homopolymer

The PNBHFA homopolymer has the highest transparency of any addition polymers synthesized during the 157 nm project (Chapter 2), and so was an ideal candidate to use as the base resist resin. Incredibly, one of the most important findings during the materials evaluation for 157 nm resists was that certain dissolution modifiers could have drastic effects on the homopolymer of NBHFA. Simply adding relatively small amount of even traditional dissolution inhibitors (DIs) such as TDQ (tetracyclododecanequinone) can have a drastic effect on both the exposed and unexposed dissolution rates of PNBHFA (Trinque 2002).

This finding is important because this greatly simplifies the approach to optimizing a resist formulation, in much the same manner as TDQ had on novolac systems used at 365 nm to great effect. The fact that the dissolution properties of the homopolymer of PNBHFA are that sensitive to dissolution modifiers keeps the overall absorbance of the resist lower than that of other polymers, PNBHFA copolymers or the highly absorbing carbon monoxide copolymers. To this end, a variety of transparent dissolution modifiers were mixed with PNBHFA in order to find an optimum mixture of base polymer resin and a highly effective dissolution modifier.

A variety of different DI types were surveyed, including the carbon monoxide copolymers, radical copolymer oligomers, sulfone copolymers, all of which were found to have significant processing problems. These problems included high absorbance, phase separation from the PNBHFA polymer and poor contrast (Chambers 2003).

The one set of dissolution modifiers that did work quite well with the homopolymer of PNBHFA were oligomers of PNBHFA. These oligomers were typically composed of dimers, trimers, tetramers and sometimes pentamers. The polymers were easy to modify, protecting the hexafluoroisopropanol groups with *t*-butyl ester groups or *t*-BOC groups. Phase separation was not seen and the resulting absorbance was smaller when compared to the analogous carbon monoxide copolymers. The contrast of PNBHFA polymer and PNBHFA oligomer DI systems was found to be much higher (**Figure 6.12**).

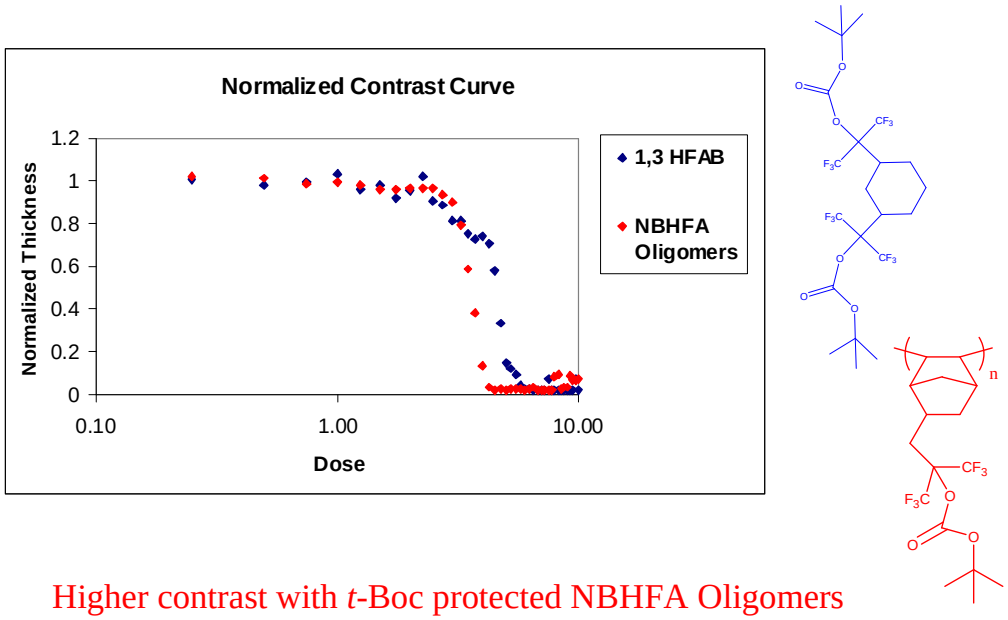

Figure 6.12: Increased contrast (resist performance) is observed when using PNBHFA oligomers instead of molecular-based dissolution modifiers such as 1,3-HFAB.

Imaging performance of the PNBHFA polymer with a DI was very promising, enabling resolving power superior to that of the systems using carbon monoxide

copolymers as dissolution modifiers (**Figure 6.13**). Unfortunately, the homopolymer PNBHFA system suffered from an absorbance that was still too high to make it reasonable to attempt 300 nm thick imaging at 157 nm. Attention then turned to an alternate polymer resin that had a superior transparency at 157 nm, but using the lessons learned using the PNBHFA oligomers with the PNBHFA homopolymer.

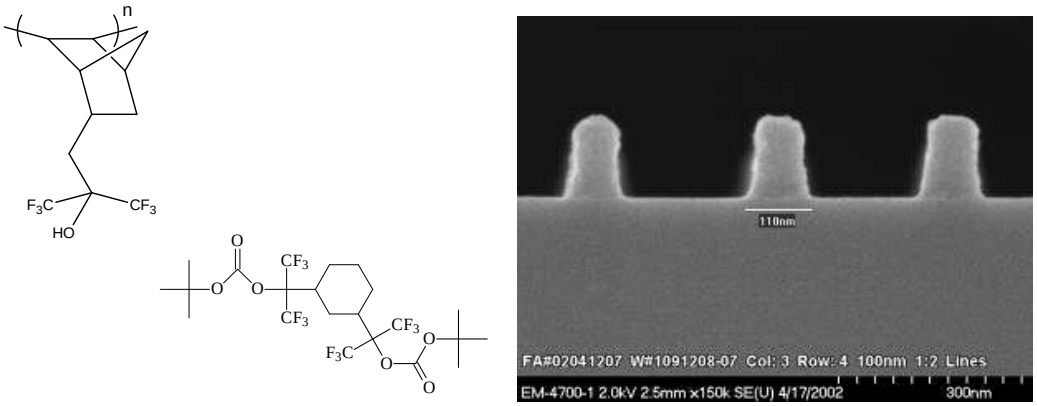

Figure 6.13: A 85:15 blend of PNBHFA and 15% 1,3 bis-BOC-HFAB DI imaged at 157 nm.

The Asahi Cyclopolymer

The majority of polymers screened at 157 nm did not have the requisite transparency for thicker resist exposures. However, one polymer, developed by the Japanese company Asahi Glass, was found to be highly transparent at 157 nm, having an absorbance of approximately 0.5 μm^{-1}. The Asahi Glass polymer is a product of radically initiated ring-closing polymerization, with a highly fluorinated backbone and strongly acidic alcohol off the ring (**Figure 6.14**).

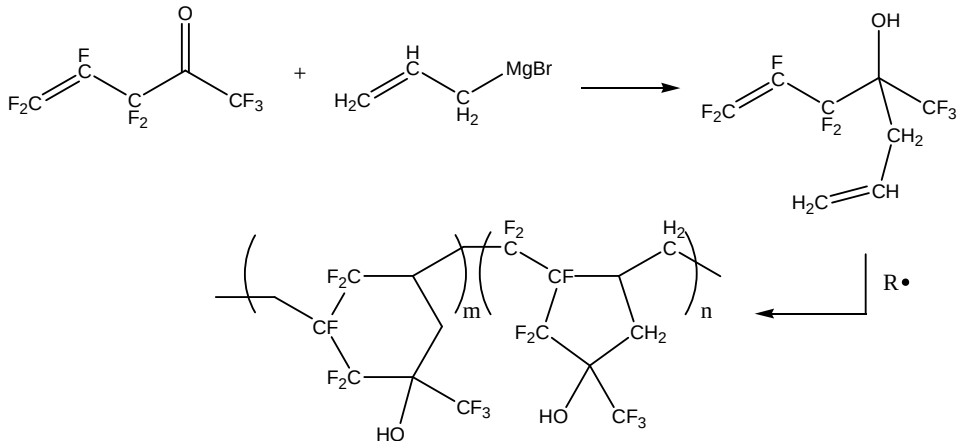

Figure 6.14: The commercial synthesis of the Asahi Glass cyclopolymer through radical ring closing polymerization produces six- and five-member rings.

The primary drawback for this polymer is its low T_g, measured to be 107 °C with 20% methylmethoxy acetal protection (**Figure 6.15**) (Ito 2004). This amount of protection is necessary to halt the dissolution of the polymer in standard 0.26 N TMAH. Without the protecting groups, this polymer has an absorbance of 0.39 μm^{-1} at 157 nm. This polymer also suffers from a much lower etch resistance relative to the various polynorbornene platforms discussed thus far.

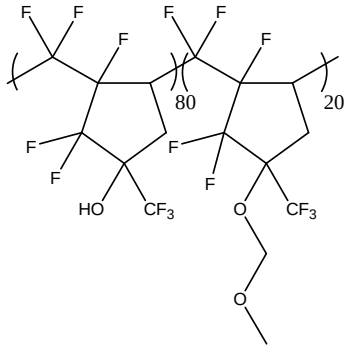

Figure 6.15: The Asahi Glass polymer, which has an extremely low absorbance at 157 nm of 0.5 μm^{-1} with 20% MOM protection.

Dissolution Inhibitors and the Asahi Polymer

The Asahi Glass polymer by itself can be imaged by itself with a photoacid generator; however, the result is a photoresist that still suffers from low etch resistance. Combining the etch resistance of norbornene systems while keeping the Asahi polymer as the base resin, it was hoped that the overall resist etch resistance could be increased. The work done in our research group on dissolution inhibitors covered many different types of dissolution inhibitors, all of which initially were used with the PNBHFA homopolymers and copolymers. The intention was to take advantage of the low absorbance of the Asahi Glass polymer, coupled with the high contrast oligomer dissolution modifiers in an attempt to print 300 nm tall 100 nm 1:1 images at 157 nm.

Asahi Polymer and PNBHFA Oligomers

The Asahi Glass cyclopolymer suffers from a low T_g, low etch resistance and also poor contrast during imaging experiments. The PNBHFA oligomers were seen as a way to both improve the etch resistance of the Asahi polymer resist, as bicyclic olefin polymers have higher etch resistance compared to other alicyclic systems (Ohnishi 1983). Further, the high activation energy-protecting group on the oligomers would aid in increasing the contrast of the resist system. The oligomers were good dissolution modifiers, requiring as little as 2-10% incorporation into a formulation to affect dissolution rate and contrast of 20% MOM-protected Asahi cyclopolymer.

Oligomers with a t-BOC protecting group were examined in the survey of materials to use with the Asahi resin, and very good contrast was observed, followed by good imaging performance at 157 nm (**Figure 6.16**).

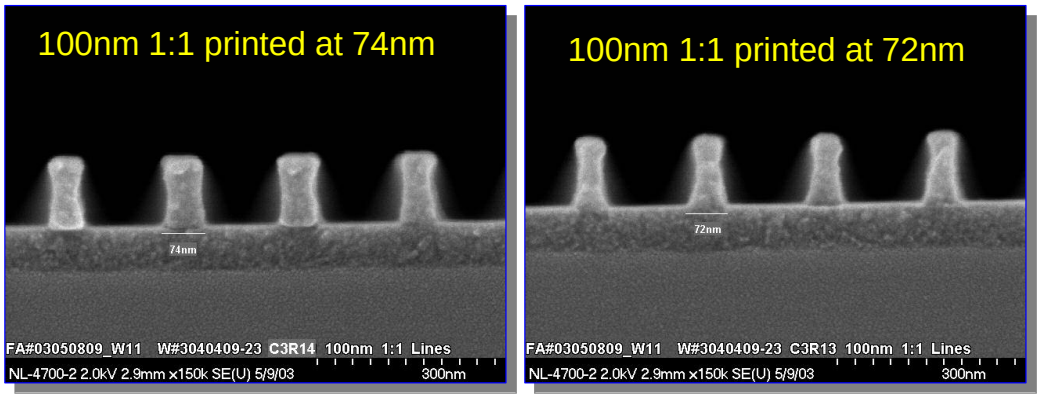

Figure 6.16: Asahi Glass cyclopolymer and t-BOC PNBHFA oligomers imaged at 157 nm.

Modified PNBHFA oligomers with a t-butyl ester protecting group were also used in conjunction with the Asahi polymer. Again, high contrast, high resolution images at typical film thickness of 150 nm were achieved (**Figure 6.17**).

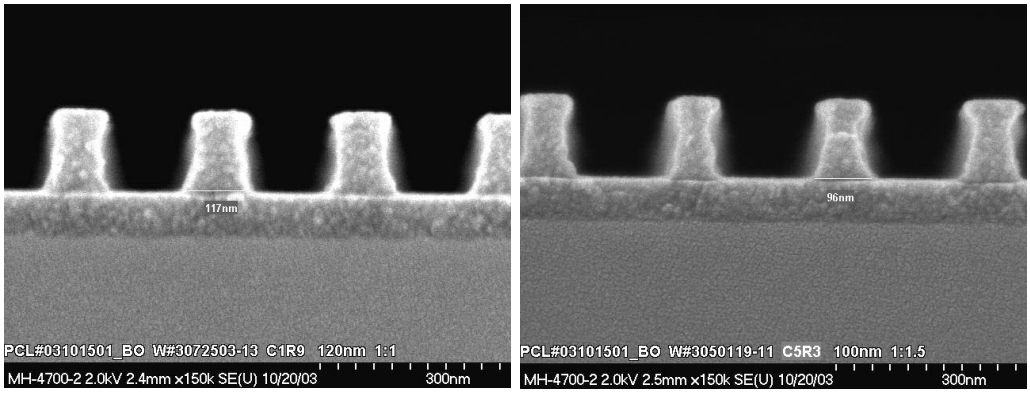

Figure 6.17: Asahi Glass cyclopolymer and *t*-butyl ester PNBHFA oligomers imaged at 157 nm.

The final absorbance of these systems was between 0.8 to 0.9 μm^{-1}, at 157 nm, due to the impact of the oligomer absorbance. While highly transparent, this lack of transparency for 157 nm resists continued to plague the imaging of thick films. This

problem would be largely resolved upon observation of an advantageous property of the Asahi polymer.

Inhibiting PAGs with the Asahi Polymer

It was seen that there was a strong inhibition effect on the PNBHFA homopolymer, one that was superior to the effect TDQ had on the novolac polymer. What was also interesting was that there was a similar inhibition effect with the Asahi Glass cyclopolymer. While not as strong an inhibition effect as that seen with the PNBHFA homopolymer, it was an effect that could be taken advantage of, when it was discovered that not only did the cyclopolymer respond to dissolution modifiers, but even to a photoacid generator (PAG) as well. In fact, as little as *2%* of the PAG tri(*p*-methoxyphenyl)sulfonium triflate (TMOPS-Tf) can completely halt the dissolution of the Asahi polymer in TMAH (Chambers 2004).

This was an added advantage when taking the absorbance impact of the PAG into account. In earlier formulations, the loss of transparency due to added PAG was not taken heavily into account. Typically up to 6% of TPS-Nf was used as the photoactive component of 157 nm resist formulations. As can be seen from the VASE measurements of increasing amounts of PAG in the Asahi polymer, even 4% of TPS-Nf raised the base absorbance of the cyclopolymer to almost 1.0 μm^{-1} at 157 nm. Using 6% TPS-Nf and no dissolution inhibitors, the absorbance of the Asahi system is already 1.1 μm^{-1} at 157 nm (**Figure 6.18**).

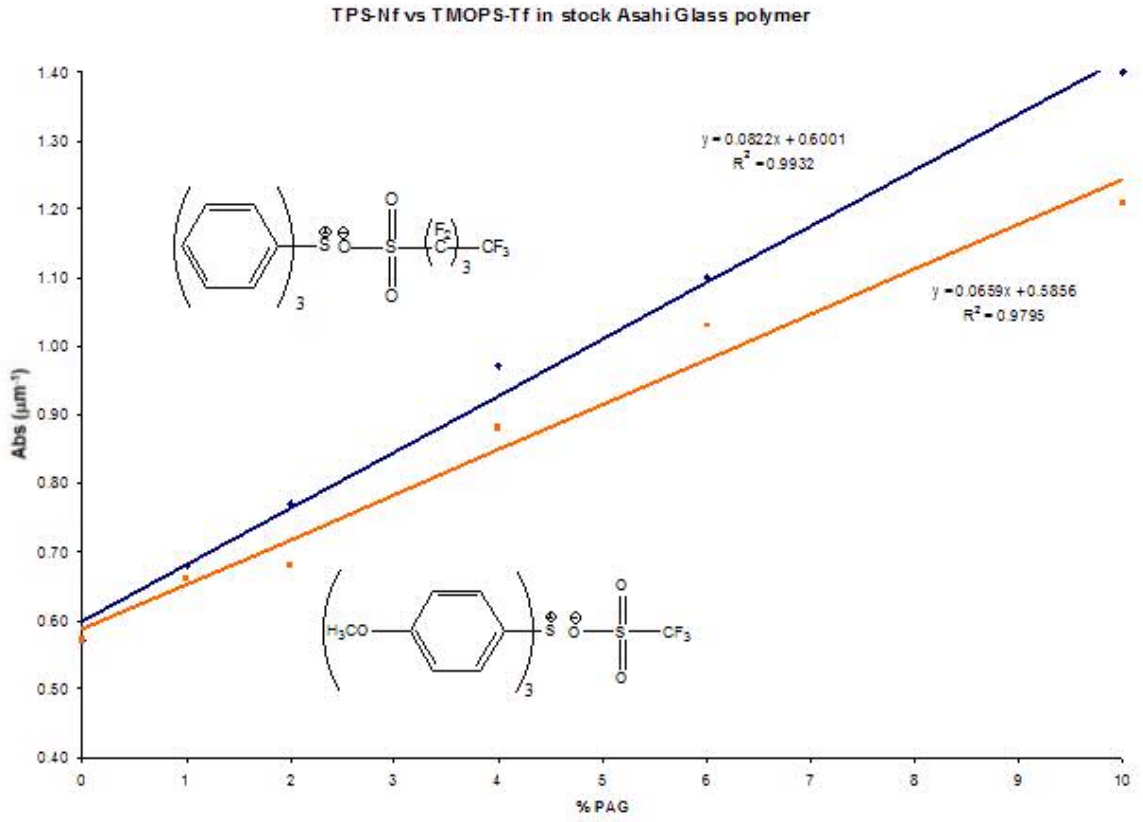

Figure 6.18: The absorbance impact of photoacid generators (PAGs) in the Asahi Glass cyclopolymer at 157 nm.

The TMOPS-Tf PAG not only had a strong inhibiting effect on the Asahi polymer, it was also less absorbing at 157 nm than TPS-Nf. With 2% of TMOPS-Tf combined with the Asahi polymer, not only was polymer dissolution nearly completely halted, but also the impact on absorbance of polymer and PAG amounts to approximately 0.67 μm^{-1}. This led to a formulation that took advantage of the inhibition and transparency of the TMOPS-Tf PAG. The results of using an inhibiting PAG at low weight loadings in the Asahi cyclopolymer are shown below (**Figure 6.19**).

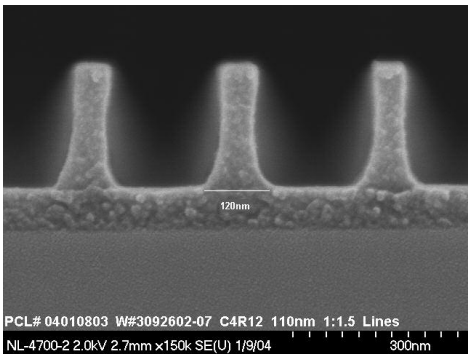

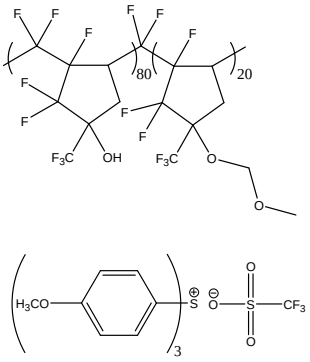

0.7 σ, binary mask	220 nm thick resist on DUV-30 ARC
Asahi polymer	PAB 90 °C/90 s
2% TMOPS-Tf	Dose: 30 mJ/cm^2 Focus: +0.25
0.3% TBAH	PEB 90 °C/90s, 30 s develop

Figure 6.19: Initial imaging of the Asahi polymer and TMOPS-Tf.

The initial results with TMOPS-Tf were encouraging. However, when attempting to reproduce these results, a few incongruities appeared. Phase incompatibility and scumming were observed, and adding PNBHFA oligomers did not improve the situation at all. In some cases, the scum increased, to the point where features were not resolved. Interaction with the antireflective coating (ARC), general phase incompatibilities or unusual interaction between oligomer and TMOPS-Tf were possible causes.

These issues were temporarily resolved by using TPS-Nf once again to do thick film printing, resulting in our final formulation for attempting high aspect ratio, high resolution imaging (**Table 6.1**). The imaging results are shown below (**Figure 6.20**).

Photoresist Component	Structure	Relative Amount	Actual Formulation
Asahi Glass cyclopolymer	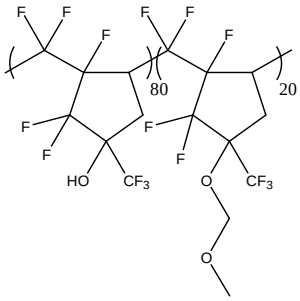	-	0.197 g
t-Butyl ester PNBHA oligomer	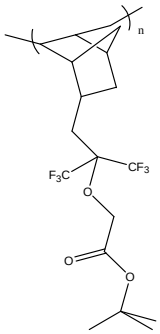	3 wt% of polymer	0.003 g
TPS-Nf	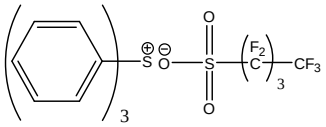	6 wt% of polymer	1.28 x 10^{-2} g
Tetrabutylammonium hydroxide	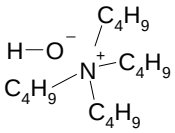	0.3 wt% of polymer	6.41 x 10^{-4} g
PGMEA	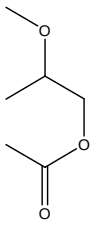	9 x polymer	1.8 g

Table 6.1: The final optimized photoresist formulation recipe for 157 nm imaging.

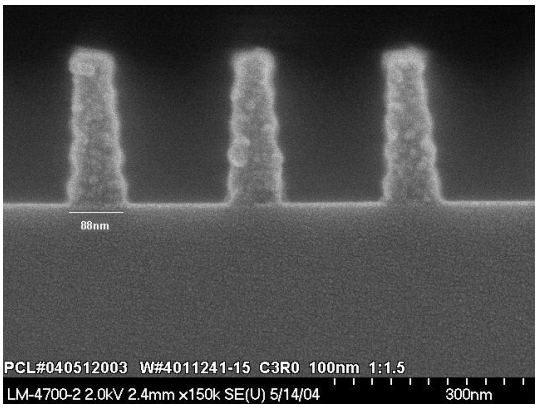

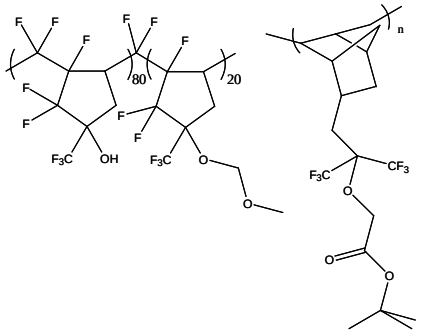

0.3 σ, phase shift mask	250 nm final thickness on HMDS Si
97:3 stock Asahi : oligomer	PAB 90 °C / 90 s
6% TPS-Tf	Dose: 58.0 mJ/cm^2 Focus: -0.15
0.3% TBAH	PEB 90 °C / 90 s, 30 s develop

- Initial results on HMDS-primed Si
- Top loss observed
- 2.8 aspect ratio, first pass
- Standing waves due to lack of ARC
- 3:1 aspect ratio 100 nm 1:1 within reach

Figure 6.20: Cross sections of the final 157 nm formulated resist for high aspect ratio imaging.

These images were the final attempts to achieve 300 nm tall features and it is clear that with more formulation optimization and imaging experiments, high resolution, high aspect ratio lithographic imaging at 157 nm would certainly have been achieved.

Experimental

Instrumentation

All 157 nm imaging work was performed on an Exitech 157 nm small field (1.5 x 1.5 mm^2) mini-stepper (0.6 NA) using either a binary mask (σ 0.7) or phase-shift mask (σ 0.3) at International SEMATECH in Austin, TX. Scanning electron micrographs were collected on a JEOL *JWS-7550* or KLA-Tencor 8100 XT on-wafer inspection tool, and cross-sectional data were collected on a Hitachi *4500* microscope. Coating, baking, and

development of resist films were performed using an FSI *Polaris 2000* track. Thickness measurements were made on a Prometrix or Rudolph interferometer. A typical resist formulation was prepared by mixing the polymer with 6 wt% (relative to polymer) photoacid generator (triphenylsulfonium nonaflate) and 0.3 wt% tetrabutylammonium hydroxide (TBAH) as the base to control acid diffusion and reduce T-topping. Dissolution inhibitors were mixed with the polymer to the desired ratio. The entire mixture was dissolved into PGMEA to provide a viscosity that provides resist thickness of approximately 100-300 nm after spinning the resist at 1500-3000 rpm onto a silicon wafer that had been previously coated with ~80 nm BARC (bottom anti-reflective coating, Shipley AR19). The post-apply bake was 140°C for 60 s and the post-exposure bake was 130°C for 90 s, unless stated otherwise. The exposed resists were developed in the industry-standard 0.26 *N* tetramethylammonium hydroxide (TMAH) developer.

Bibliography

Adamo, C.; Scuseria, G. E.; Barone, V. *J. Chem. Phys.* **1999**, *111*, 2889.

Allen, R. D.; Wallraff, G. M.; Hofer, D. C.; Kunz, R. R. *IBM J. Res. Develop.* **1997**, *41*, 95.

Ando, S.; Fujigaya, T.; Ueda, M. *J. Photopolym. Sci. Technol.* **2002**, *15(4)*, 559-568.

Bae, Y. C.; Douki, K.; Yu, T.; Dai, J.; Schmaljohann, D.; Koerner, H.; Ober, C. K.; Conley, W. *Chem. Mat.* **2002**, *14(3)*, 1306-1313.

Barten, J. A.; Kadyrov, A. A.; Lork, E.; Röschenthaler, G. V. *J. Fluorine Chem*. 2002, *116*, 87-92.

Bauernschmitt, R.; Ahlrichs, R. *Chem. Phys. Lett.* **1996**, *256*, 454.

Bauernschmitt, R.; Häser, M.; Treutler, O.; Ahlrichs, R. *Chem. Phys. Lett.* **1997**, *264*, 573.

Becke, A. D. *J. Chem. Phys.* **1993**, *98*, 5648.

Bensel N.; Fréchet, J.M.J. **2003**, *UC Berkeley*, private communication.

Blomquist, A. T.; Meinwald, Y. C. *J. Am. Chem. Soc.* **1959**, *81*, 667-672.

Bott, G.; Field, L. D.; Sternhell, S. *J. Am. Chem. Soc.* **1980**, *102*, 5618-5626.

Braedlin, H. P.; Zielinski, A. Z.; McBee, E. T. *J. Am. Chem. Soc.* **1962**, *84*, 2109-2112.

Breunig, S.; Risse, W. *Makromol. Chem.* **1992**, *193*, 2915-2927.

Brodsky, C.; Byers, J.; Conley, W.; Hung, R.; Yamada, S.; Patterson, K.; Somervell, M.; Trinque, B.; Tran, H. V.; Cho, S.; Chiba, T.; Lin, S-H.; Jamieson, A.; Johnson, H.; Vander Heyden, T.; Willson, C. G. *J. Vac. Sci. Technol. B.* **2000**, *18*, 3396-3401.

Burns, S. D.; Schmid, G. M.; Tsiartas, P. C.; Willson, C. G.; Flanagin, L. *J. Vac. Sci. Technol., B* **2002**, *20(2)*, 537-543.

Carothers, W. H. *J. Am. Chem. Soc.*, **1929**, *51*, 2548.

Casida, M. E.; Casida, K. C.; Salahub, D. R. *Int. J. Quantum Chem.* **1998**, *70*, 933.

Casida, M. E.; Jamorski, C.; Casida, K. C.; Salahub, D. R. *J. Chem. Phys.* **1998**, *108*, 4439.

Chambers, C. R.; Kusumoto, S.; Lee, G. S.; Vasudev, A.; Walthal, L.; Osborn, B. P.; Zimmerman, P.A.; Conley, W.; Willson, C. G. *Proc. SPIE-Int. Soc. Opt. Eng.* **2003**, *5039*, 93-102.

Chambers, C. R.; Kusumoto, S.; Osborn, B. P.; Vasudev, A.; Ootani, M.; Walthal, L.; McMichael, H.; Zimmerman, P. A.; Conley, W. E.; Willson, C. G. *Proc. SPIE-Int. Soc. Opt. Eng.* **2004**, *5376*, 360-368.

Chambers, C.R.; Kusumoto, S.; Lee, G.S.; Vasudev, A.; Walthal, L.; Osborn, B.P.; Zimmerman, P.; Conley, W.; Willson, C.G. *Proc. SPIE-Int. Soc. Opt. Eng.* **2003**, *5039*, 93-102.

Chiba, T.; Hung, R. J.; Yamada, S.; Trinque, B.; Yamachika, M.; Brodsky, C.; Patterson, K.; Vander Heyden, A.; Jamison, A.; Lin, S. H.; Somervell, M.; Byers, J.; Conley, W.; Willson, C. G. *J. Photopolymer Sci. Technol.* **2000**, *13*, 657-664.

Chong, D. P., "Recent Advances in Density Functional Methods," World Scientific, Singapore, **1995**.

Conley, W.; Miller, D. A.; Chambers, C. R.; Osborn, B. P.; Hung, R. J.-P.; Tran, H. V.; Trinque, B. C.; Pinnow, M. J.; Chiba, T.; McDonald, S.; Zimmerman, P.; Dammel, R. R.; Romano, A. R.; Willson, C. G. *Proc. SPIE-Int. Soc. Opt. Eng.* **2002**, *4690*, 69-75.

Connor, E. F.; Younkin, T. R.; Henderson, J. I.; Hwang, S.; Grubbs, R. H.; Roberts, W. P.; Litzau, J. J. *J. Polym. Sci., Part A: Polym. Chem.* **2002**, *40(16)*, 2842-2854.

Connor, E. F; Younkin, T. R; Henderson, J. I.; Waltman, A. W.; Grubbs, R. H. *Chem. Commun.* **2003**, *18*, 2272-3.

Cookson, R. C.; Dance, J.; Hudec, J. *J. Chem. Soc.* **1964**, 5416-5422.

Cossee, P. J. *J. Catal.* **1964**, 3, 80.

Crandall, J. K. *J. Am. Chem. Soc.* **1964**, *29*, 2830-33.

Crivello, J. V., Ahn J., *J. Polym. Sci., Part A: Polym. Chem.* **2003**, *41*, 2570-2587.

Crivello, J. V.; *J. Polym. Sci., Part A: Polym. Chem.* **1999**, *37*, 4241-54.

Crivello, J. V.; Lam, J. H. W. *J. Polym. Sci. Polym. Chem. Ed.* **1980**, *18*, 2677.

Crivello, J. V.; Liu, S. *J. Polym. Sci., Part A: Polym. Chem.* **1999**, *38*, 2570-2587.

Crivello, J. V.; Liu, S. *J. Polym. Sci., Part A: Polym. Chem.* **2000**, *38*, 389-401.

Crivello, J. V.; Ortiz, R. A. *J. Polym. Sci., Part A: Polym. Chem.* **2001**, *39*, 2385-95.

Dabbagh, G.; Bertz, S.H. *J. Am. Chem. Soc.* **1981**, *103*, 5932-5934.

Dunning, T. H. *J. Chem. Phys.* **1989**, *90*, 1007.

Eleuterio, DE-B *Chem. Abstr.* **1961**, *55*, 16005.

Frechet, J. M. J.; Eichler, E.; Ito, H.; Willson, C. G. *Polymer*, **1983**, *24*, 995.

French, R. H.; Whelan, R. C.; Jones, D. J.; Hilfiker, J. N.; Synowicki, R. A.; Zumsteg, F. C.; Feldman, J.; Feiring, A. E. *Proc. SPIE-Int. Soc. Opt. Eng.* **2000**, *4000*, 1491-1502.

Frisch, M. J., *et al* Gaussian 98, Revision A.7, Gaussian, Inc., Pittsburgh PA, **1998**.

Fürstner, A. *Angew. Chem., Int. Ed.* **2000**, *39(17)*, 3012-3043.

Gastinger, R. G.; Anderson, B. B.; Klabunde, K. J. *J. Am. Chem. Soc.* **1980**, *102*, 4959-4966.

Gleason, W. B.; Ojala, C. R.; Ojala, W. H. *Acta. Cryst.* **1998**, *C54*, 60-63.

Gleason, W. B.; Ojala, C. R.; Ojala, W. H.; Pennamon, S.Y. *Acta. Cryst.* **1998**, *C54*, 57-60.

Godbout, N., Salahub, D. R., Andzelm, J., Wimmer, E. *Can. J. Chem.* **1992**, *70*, 560.

Gokan H.; Esho, S.; Ohnishi, Y. *J. Electrochem. Soc.* **1983**, *130*, 143.

Goodall, B. L.; Benedikt, G. M.; McIntosh, L. H.; Barnes, D. A. *US Pat. 5,468,819*, **1995**.

Goodall, B. L.; Risse, W.; Mathew, J. P. *US Pat. 5,705,503*, **1998.**

Görling, A.; Heinze, J. H.; Ruzankin, S. P.; Staufer, M.; Rösch, N. *J. Chem. Phys.* **1999**, *110*, 2785.

Grandler, J. R.; Jencks, W. P. *J. Am. Chem. Soc.* **1982**, *104*, 1937-1951.

Grushin, V. V.; Marshall, W. J.; Halliday, G. A.; Davidson, F.; Petrov, V. A. *J. Fluorine Chem*. **2002**, *117*, 121-129.

Hall, H. K.; Jr. *J. Org. Chem.* **1960**, *25*, 42-44.

Handy, N. C.; Tozer, D.J. *J. Comput. Chem.* **1999**, *20*, 106.

Haselwander, T. F. A.; Heitz, W.; Krugel, S. A.; Wendorff, J. H. *Macromol. Chem. Phys.* **1996**, *197*, 3435-3453.

Heinz, B. S.; Alt, F. P.; Heitz, W. *Macromol. Rapid. Commun.* **1998**, *19*, 251-256.

Hennis, A. D.; Polley, J. D.; Long, G. S.; Sen, A. *Organometallics* **2001**, *20*, 2802-2812.

Hennis, A. D.; Polly, J. D.; Long, G. S.; Sen, A.; Yandulov, D.; Lipian, J.; Benedikt, G. M.; Rhodes, L. F.; Huffman, J. *Organometallics* **2001**, *20*, 2802-2812 and references therein.

Hennis, A. D.; Sen, A. *Polym. Prepr.* **2000**, *41*, 1933-194.

Heyns, K.; Rudiger, G.; Paulsen, H. *Chem. Ber.* **1972**, *105*, 1019-27.

Hohenberg, P., Kohn, W. *Phys. Rev. B* **1964**, *136*, 864; Kohn, W., Sham, L., *J. Phys. Rev. A* **1965**, *140*, 1133.

Hughes, R. P.; Powell, J. *J. Organometal. Chem.* **1973**, *60*, 387.

Hult, A. *Royal Institute of Technology, Stockholm, Sweden,* **2003**, personal communications.

Hung, R. J.-P.; Tran, H. V.; Trinque, B. C.; Chiba, T.; Yamada, S.; Sanders, D. P.; Connor, E. F.; Grubbs, R. H.; Klopp, J. M.; Frechet, J. M. J.; Thomas, B. H.; Shafer, G. J.; DesMarteau, D. D.; Conley, W.; Willson, C. G. *Proc. SPIE-Int. Soc. Opt. Eng.* **2001**, *4345*, 385-395.

Hung, R. J-P. "Organic materials for microelectronics: 157 nm photoresists and electrooptic liquid crystals." *Ph.D. Thesis.* Univ. of Texas, Austin, TX, USA. **2001**, 230 pp.

Ito, H. *IBM Corp.*, Alamaden Research Center, San Jose, CA, USA, personal communications.

Ito, H., Reichmanis, E., Nalamasu, O., Ueno, T., Eds. *ACS Symposium Series*; American Chemical Society: Washington, DC, **1998,** 208-223.

Ito, H.; Willson, C. G.; Frechet, J. M. J. "New UV Resists with Negative or Positive tone," Digest of Technical Papers of 1982 Symposium on VLSI Technology, **1982**, 86-87.

Ivin, K. J.; Mol, J.C. "Olefin Metathesis and Metathesis Polymerization," Academic Press, San Diego, California, **1997**.

Johs, B.; French, R. H.; Kalk, F. D.; McGahan, W. A.; Woollam, J. A. *Proc. SPIE-Int. Soc. Opt. Eng.* **1994**, *2253*, 1098-1106.

Kaufmann, T. H.; Baumeister, W.; Jungen, M. *J. Phys. B* **1989**, *22*, 2223.

Kawabe, Y., Tan, S., Nishiyama, F., Sakaguchi, S., Kokubo, T., Blakeney, A. J. and Ferreira, L. *Proc. SPIE-Int. Soc. Opt. Eng.* **1996**, 2724, 420-437.

Kinkead, E.R.; Wolfe, R.E.; Salins, S.A.; Grabau J.H.; Mantech Environmental Technology Inc., Dayton, OH, **1993**.

Knunyants, I. L.; Zeifman, Y. V.; Lushnikova, T. V.; Rokhlin, E. M.; Abduganiev, Y. G.; Utebaev, U. *J. Fluorine Chem.* **1975**, *6*, 227-241.

Kraus, C. A.; Brown, E. H. *J. Am. Chem. Soc.* **1929**, *51*, 2690-2696.

Kunz, R. R. *Proc. SPIE-Int. Soc. Opt. Eng.* **1999**, *13*, 3678.

Kunz, R. R.; Bloomstein, T. M.; Hardy, D. E.; Goodman, R. B.; Downs, D. K.; Curtin, J. E. *J. Photopolym. Sci. Technol.* **1999**, *12*, 561.

Kunz, R.R.; Bloomstein, T.M.; Hardy, D.E.; Goodman, R.B.; Downs, D.K.; Curtin, J.E. *J. Vac. Sci. Technol. B* **1999**, *17*, 3267-3272.

Kunz, R.R.; Bloomstein, T.M.; Hardy, D.E.; Goodman, R.B.; Downs, D.K.; Curtin, J.E. *J. Photopolym. Sci. Technol.* **1999**, *12*, 561-570.

Lautens, M.; Edwards, L. G.; Tam, W.; Lough, A. J. *J. Am. Chem. Soc.* **1995**, *117*, 10276-10291 and references therein.

Lautens, M.; Tam, W.; Lautens, J. C.; Edwards, L. G.; Crudden, C. M.; Smith, A. C. *J. Am. Chem. Soc.* **1995**, *117*, 6863-6879.

Lee, C.; Yang, W.; Parr, R. G. *Phys. Rev. B* **1988**, *37*, 785.

Leroy, J.; Fischer, N.; Wakselman, C. *J. Chem. Soc. Perkin Trans. I* **1990**, 1281-1287.

Lightner, D. A.; Paquette, L. A.; Chayangkoon, P.; Lin, H. S.; Peterson, J.R. *J. Org. Chem.*, **1988**, *53(9)*, 1969-1973.

Lin, S-T.; Narske, R. N.; Klablunde, K. J. *Organometallics* **1985**, *4*, 571-574.

Lipian, J. H.; Rhodes, L. F.; Goodall, B. L.; Bell, A.; Mimna, R. A.; Fondran, J. C.; Hennis, A. D.; Elia, C. N.; Polley, J. D.; Sen, A.; Saikumar, J. *PCT Int. Appl. WO 0020472*, **2000**.

Mack, C.A. "Inside Prolith: A complete Guide to Optical Lithography," FINLE Technologies, Inc., Austin, Texas, **1997**, 75.

Mathew, J. P.; Reinmuth, A.; Melia, J.; Swords, N.; Risse, W. *Macromolecules* **1996**, *29*, 2755-2763.

Matsuzawa, N. N.; Ishitani, A.; Dixon, D. A.; Uda, T. *J. Phys. Chem. A* **2001**, *105(20)*, 4953-4962.

Matsuzawa, N. N.; Ishitani, A.; Dixon, D. A.; Uda, T. *Proc. SPIE-Int. Soc. Opt. Eng.* **2001**, 4345, 396-405.

Matsuzawa, N. N.; Mori, S.; Yano, E.; Okasaki, S.; Ishitani, A.; Dixon, D. A. *Proc. SPIE-Int. Soc. Opt. Eng.* **2000**, *3999*, 375-384.

Mayr, H.; Koschinsky, R.; Will, E.; Bauml, E. *J. Org. Chem.* **1987**, *52*, 1342-44.

McBee, E. T.; Hsu, C. G.; Roberts, C. W. *J. Am. Chem. Soc.* **1956**, *78*, 3389-3392.

McBee, E. T.; Hsu, C. G.; Roberts, C. W. *J. Am. Chem. Soc.* **1956**, *78*, 3393-3394.

McBee, E. T.; Keogh, M. J.; Levek, R. P.; Wesseler, E. P. *J. Org. Chem.* **1973**, *38*, 632-636.

Moore, G. E. *Electronics* **1965**, *38(8)*.

Moore, G. E. *Proc. SPIE-Int. Soc. Opt. Eng.* **1994**, *2438*, 2.

Natta, G.; Dall'Asta, G.; Mazzanti, G. *Angew. Chem.* **1964**, *76*, 765-722.

Nagai, T. *Chem. and Pharm. Bull.* **1989**, *37(1)*, 177-183.

Niu, Q. J.; Frechet, J. M. J. *Angew. Chem. Int. Ed.* **1998**, *37*, 667-670.

Noyori, R.; Umeda, I.; Kawauchi, H.; Takaya, H. *J. Am. Chem. Soc.* **1975**, *97*, 812-820.

Okoroanyanwu, U.; Shimokawa, T.; Byers, J.; Medeiros, D.; Willson, C. G.; Niu, Q. J.; Frechet, J. M. J.; Allen, R. *Proc. SPIE-Int. Soc. Opt. Eng.* **1997**, *3049*, 92-103.

Parr, R. G., Yang, W. "Density-Functional Theory of Atoms and Molecules," Oxford, Univ. Press, Oxford, **1989**.

Partridge, R. H. *J. Chem. Phys.* **1966**, *45 (5)*, 1685-90.

Patterson, K. W. "Design, Synthesis, and Optimization of Materials for 193 nm and 157 nm Photoresists," *Ph.D. Thesis.* Univ. of Texas, Austin, TX, USA. **2000**, 184 pp.

Patterson, K.; Yamachika, M.; Hung, R.J.; Brodsky, C.J.; Yamada, S.; Somervell, M. H.; Osborn, B.; Hall, D.; Dukovic, G.; Byers, J.; Conley, W.; Willson, C.G. *Proc. SPIE-Int. Soc. Opt. Eng.* **2000**, *3999*, 365-374.

Patterson, K. *Proc. SPIE-Int. Soc. Opt. Eng.* **2000**, *3999*, 365-374, and all references therein.

Pinnow, M. J.; Noyes, B. F.; Tran, H. V.; Tattersall, P. I.; Cho, S.; Klopp, J.M.; Bensel, N.; Fréchet, J. M. J.; Sanders, D. P.; Grubbs, R. H.; Willson, C. G. *Polym. Mater. Sci. Eng.* **2002**, *87*, 403-404.

Prinzbach, H. *Pure Appl. Chem.* **1968**, *16*, 17-46.

Prinzbach, H; Rivier, J. *Angew. Chem., Int. Ed. Engl.* **1967**, *6*, 1069-1070.

Reinmuth, A.; Mathew, J. P.; Melia, J., Risse, W. *Macromol. Rapid Commun.* **1996**, *17*, 173-180.

Rhodes, L. F; Bell, A.; Saikumar, J.; Lipian, J. H.; Goodall, B. L.; Shick, R. A. *US Pat. 6,232,417*, **2001**.

Rieber, N.; Alberts, J.; Lipsky, J. A.; Lemal, D. M. *J. Am. Chem. Soc.* **1969**, *91*, 5668-5669.

Safir, A. L.; Novak, B. M. *Macromolecules* **1995**, *28*, 5396-5398.

Salakhov, M. S.; Bagmanova, M. I. *Russ. J. Org. Chem.* **2000**, *38(2)*, 265-8.

Sanders, D. P.; Connor, E. F.; Grubbs, R. H.; Hung, R. J.-P.; Osborn, B. P.; Chiba, T.; MacDonald, S. A.; Willson, C. G.; Conley, W. *Macromol.* **2003**, *36(5)*, 1534-1542.

Schlosser, M.; Keller, H. *Liebigs Ann.* **1995**, 1587-1589.

Schmid, G. M.; Stewart, M. D.; Singh, V. K.; Willson, C. G. *J. Vac. Sci. Technol., B* **2002,** *20(1)*, 185-190.

Schrauzer, G. N.; Glockner, P. *Chem. Ber.* **1964**, *97*, 2451-2462.

Sen, A.; Lai, T-W.; Thomas, R. R. *J. Organomet. Chem.* **1988**, *358*, 567-588.

Six C.; Beck, K; Wegner A.; Leitner, W. *Organometallics*, **2000**, *19(22)*, 4639-42.

Smith, C. D. *J. Am. Chem. Soc.* **1966**, *88*, 4273-4274.

Somervell, M. H.; Fryer, D. S.; Osborn, B. P.; Patterson, K.; Byers, J.; Willson, C. G. *J. Vac. Sci. Technol., B* **2000**, *18(5)*, 2551-2559.

Stevens, M. P. *Polymer Chemistry*, Oxford University Press, **1999**.

Stewart, M.; Somervell, M.; Tran, H. V.; Postnikov, S.; and Willson, C. G. *Proc. SPIE-Int. Soc. Opt. Eng.* **2000**, *3999*, 665-674.

Stratmann, R. E.; Scuseria, G. E.; Frisch, M. J. *J. Chem. Phys.* **1998**, *109*, 8218.

Tabushi, I.; Yamamura, K.; Yoshida, Z. *J. Am. Chem. Soc.* **1972**, *94*, 787-792.

Takata, T.; Kanamaru, M.; Endo, T. *Macromolecules* **1996**, *29*, 2315-17.

Taylor, J. E. *Synth. Commun.* **1985**, 1142-4.

Taylor, J. E.; Janini, T. E.; Elmer, O. C. *Org. Process Res. Dev.* **1998**, *2*, 147-150.

Toriumi, M.; Satou, I.; Itani, T. *J. Vac. Sci. Technol. B* **2000**, *18*, 3328-3331.

Tozer, D. J.; Handy, N. C. *J. Chem. Phys.* **1998**, *109*, 10180.

Tran, H. V.; Hung, R. J.; Chiba, T.; Yamada, S.; Mrozek, T.; Hsieh, Y.-T.; Chambers, C. R.; Osborn, B. P.; Trinque, B. C.; Pinnow, M. J.; Sanders, D. P.; Connor, E. F.; Grubbs, R. H.; Conley, W.; MacDonald, S. A.; Willson, C. G. *J. Photopolym. Sci. Technol.* **2001**, *14(4)*, 669-674.

Tran, H. V.; Hung, R. J.-P.; Chiba, T.; Yamada, S.; Mrozek, T.; Hsieh, Y. T.; Chambers, C. R.; Osborn, B. P.; Trinque, B. C.; Pinnow, M.J.; MacDonald, S. A.; Willson, C. G.; Sanders, D. P.; Connor, E. F.; Grubbs, R. H.; Conley, W. *Macromol.* **2002**, *35(17)*, 6539-6549.

Tran, H.V. “Materials for advanced microlithography: polymers for 157 nm lithography and acid diffusion measurements,” *Ph.D. Thesis,* Univ. of Texas, Austin, TX, USA, **2002,** 251 pp.

Trinque, B. C.; Chambers, C. R.; Osborn, B. P.; Callahan, R. P.; Lee, G. S.; Kusumoto, S.; Sanders, D. P.; Grubbs, R. H.; Conley, W. E.; Willson, C. G. *J. Fluorine Chem.* **2003**, *122(1)*, 17-26.

Trinque, B. C.; Chiba, T.; Hung, R. J.; Chambers, C. R.; Pinnow, M. J.; Osborn, B. P.; Tran, H.V.; Wunderlich, J.; Hsieh, Y.-T.; Thomas, B. H.; Shafer, G.; DesMarteau, D. D.; Conley, W.; Willson, C. G. *J. Vac. Sci. Technol., B* **2002**, *20(2)*, 531-536.

Trinque, T. C.; Osborn, B. P.; Chambers, C. R.; Hsieh, Y. T.; Corry, S.; Chiba, T.; Hung, R. J.; Tran, H. V.; Zimmerman, P.; Miller, D.; Conley, W.; Willson, C. G. *Proc. SPIE-Int. Soc. Opt. Eng.* **2002**, *4690*, 58-68.

Truett, W. L.; Johnson, D. R.; Robinson, I. M.; Montague, B. A. *J. Am. Chem. Soc.* **1960**, *82*, 2337-2340.

Ullman, E. F. *Chem. Ind. (London)* **1958**, 1171-1174.

Vosko, S.H., Wilk L., Nusair M., *Canadian J. Phys.* **1980**, *58*, 1200.

Wan, J.; Meller, J.; Hada, M.; Ehara, M.; Nakatsuji, H. *J. Chem. Phys.* **2000**, *113*, 7853, and references therein.

Wiberg, K. B., Stratmann, R.E.; Frisch, M. *J. Chem. Phys. Lett.* **1998**, *297*, 60.

Wiberg, K. B.; Saegebarth, K. A. *J. Am. Chem. Soc.* **1956**, *79*, 2822-24.

Willson, C. G. *157 nm Technical Data Review* (Waltham, MA, November 17-19, 1999, organized by International SEMATECH), p. 535.

Willson, C. G.; Ito, H.; Frechet, J. M. J.; Tessier, T. G.; Houlihan, F. M.; *J. Electrochem. Soc.* **1986**, *133*, 181.

Willson, C.G.; Bowden, M. J., Eds. “Introduction to Microlithography,” 2nd Edition, American Chemical Society, Washington, D.C., **1994**, Chapter 3.

Yamada, S. “Design and Study of Advanced Photoresist Materials: Positive Tone Photoresists with Reduced Environmental Impact and Materials for 157 nm Lithography,” *Ph.D. Thesis,* The University of Texas at Austin, **2000**, 276 pp.

Zhan, C.-G., Dixon, D. A. *J. Mol. Spectrosc.* **2002**, *81*, 216.

VITA

Brian Philip Osborn was born in Carswell Air Force Base, Fort Worth, Texas on September 1, 1974, the son of Robert A. and Elia S. Osborn, and brother to Michael J. Osborn. After graduating from Crockett High School, Austin, Texas in May 1992, he entered the United States Air Force Academy in Colorado Springs, Colorado, in June 1992. He enrolled at the University of Texas at Austin in August of 1993 and received the degree of Bachelor of Science in Chemistry in May 1999. In August 1999, he enrolled at the Georgia Institute of Technology and received the degree of Master of Science in Chemistry in August 2000. In August 2000, he entered the Graduate School of the University of Texas at Austin, working in the Department of Chemistry, Organic Division under the supervision of Professor C. Grant Willson.

Permanent Address: 7111 Wishing Well DR, Austin, TX 78745

This dissertation was typed by the author.